FUNCTIONAL CHARACTERIZATION OF TWO POTENTIAL BREAST CANCER RELATED GENES

A THESIS SUBMITTED TO
THE GRADUATE SCHOOL OF NATURAL AND APPLIED SCIENCES
OF
MIDDLE EAST TECHNICAL UNIVERSITY

BY

SHIVA AKHAVANTABASI

IN PARTIAL FULFILLMENT OF THE REQUIREMENTS
FOR
THE DEGREE OF DOCTOR OF PHILOSOPHY
IN
BIOLOGY

MARCH 2012

Approval of the thesis:

FUNCTIONAL CHARACTERIZATION OF TWO POTENTIAL BREAST CANCER RELATED GENES

Submitted by **SHIVA AKHAVANTABASI** in partial fulfillment of the requirements for the degree of **Doctor of Philosophy in Biology Department, Middle East Technical University** by,

Prof. Dr. Canan ÖZGEN _____
Dean, Graduate School of **Natural and Applied Sciences**

Prof. Dr. Musa DOĞAN _____
Head of Department, **Biological Sciences**

Assist. Prof. Dr. A.Elif ERSON BENSAN _____
Supervisor, **Biological Sciences Dept., METU**

Examining Committee Members:

Assoc. Prof. Dr. M. Cengiz YAKICIER _____
Medical Biology Dept., Acibadem University

Assist. Prof. Dr. A.Elif ERSON BENSAN _____
Biological Sciences Dept., METU

Assoc. Prof. Dr. Mayda GÜRSEL _____
Biological Sciences Dept., METU

Assoc. Prof. Dr. Mesut MUYAN _____
Biological Sciences Dept., METU

Assist. Prof. Dr. Sreeparna BANERJEE _____
Biological Sciences Dept., METU

Date: _____

I hereby declare that all information in this document has been obtained and presented in accordance with academic rules and ethical conduct. I also declare that, as required by these rules and conduct, I have fully cited and referenced all material and results that are not original to this work.

Name, Last name: Shiva AKHAVANTABASI

Signature:

ABSTRACT

FUNCTIONAL CHARACTERIZATION OF TWO POTENTIAL BREAST CANCER RELATED GENES

Akhavantabasi, Shiva

Ph.D., Department of Biological Sciences

Supervisor: Assist. Prof. Dr. A. Elif Erson Bensan

March 2012, 183 pages

Cancer may arise as a result of deregulation of oncogenes and/or tumor suppressors. Although much progress has been made for the identification of such cancer related genes, our understanding of the complex tumorigenesis pathways is still not complete. Therefore, to improve our understanding of how certain basic mechanisms work in normal and in cancer cells, we aimed to characterize two different breast cancer related genes. First part of the study focused on subcellular localization USP32 (Ubiquitin Specific Protease 32) to help understand the function of this uncharacterized gene. USP32 is a member of deubiquitinating enzymes (DUBs) and the gene maps to a gene rich region on 17q23. Genes on 17q23 are known to undergo amplification and overexpression in a subset of breast cancer cells and tumors. DUBs are known to be implicated in a variety of cellular functions including protein degradation, receptor endocytosis and vesicle trafficking. Therefore to elucidate the function of *USP32*, we localized the full length USP32 protein fused to GFP, in HeLa cells, using Fluorescence Protease

Protection (FPP) assay and confocal microscopy. Results suggested a Golgi localization for USP32 as confirmed by co-localization study via BODIPY-TR, a Golgi specific marker. Additional investigations to find the role of USP32 in Golgi will further clarify the function of this candidate oncogene. Second part of the study focused on a potential tumor suppressor. For this purpose, we functionally characterized miR-125b, a microRNA gene as a potential tumor suppressor in breast cancer. microRNAs are regulators of gene expression and their deregulation is detected in cancer cells. miR-125b is reported as a down regulated microRNA in breast cancers. In this study, we investigated the expression, function and possible targets of miR-125b in breast cancer cell lines (BCCLs). Our results revealed a dramatic down regulation of miR-125b in a panel of BCCLs. Restoring the expression of miR-125b in low miR-125b expressing cells decreased the cell proliferation and migration as well as cytoplasmic protrusions, detected by staining of actin filaments. While connection of miR-125b and cell motility based on ERBB2 targeting has been reported earlier, here we present data on ERBB2 independent effects of miR-125b on cell migration in non-ERBB2 overexpressing breast cancer cells. Our results showed involvement of a miR-125b target, *ARID3B*, in cell motility and migration. Our findings showed miR-125b to be an important regulator of cell proliferation and migration in ERBB2 negative breast cancer cells, possibly through regulating multiple targets.

Keywords: USP32, DUBs, localization, miR-125b, cell migration, *ARID3B.*

ÖZ

MEME KANSERİ İLE İLİŞKİLİ İKİ GENİN FONKSİYONEL KARAKTERİZASYONU

Akhavantabasi, Shiva
Doktora, Biyoloji Bölümü
Tez Yöneticisi: Yrd. Doç. Dr. A. Elif Erson Bensan

Mart 2012, 183 sayfa

Kanser; onkogen ve/veya tümör baskılayıcı genlerin deregülasyonu sonucu ortaya çıkmaktadır. Her ne kadar kanserle ilişikili genlerin bulunması ile ilgili birçok çalışma olsa da, tümör oluşumuna neden olan komplike yolaklar henüz tam olarak anlaşılamamıştır. Bu çalışmada normal ve kanser hücrelerindeki bu temel mekanizmaları anlayabilmek amacıyla, meme kanseriyle ilişkili iki geni karakterize etmeyi amaçladık. Çalışmamınızın ilk kısmında henüz karakterize edilmemiş *USP32* (Ubiquitin Specific Protease 32) geninin hücredeki lokalizasyonunu anlamaya yönelik çalışmalara odaklandık. *USP32*, gen açısından zengin 17q23 bölgesinde yeralan bir gendir ve deubikitinaz enzim ailesindendir (DUBs) . 17q23 üzerinde yer alan genlerin meme kanserinde ve tümörlerde amplifiye olduğu ve aşırı ifade edildikleri bilinmektedir. DUB'ların protein yıkımı, reseptör endositozisi ve vesikül trafiği gibi birçok hücresel fonksiyonda rol oynadıkları bilinmektedir. Bu nedenle USP32'nin fonksiyonunu daha iyi anlayabilmek amacıyla, GFP bağlanmış tam uzunluktaki USP32 proteinini Floresan Proteaz Koruma (FPP) deneyi ve

konfokal mikroskop ile HeLa hücrelerindeki konumunu inceledik. Golgi'ye özgül bir belirteç olan BODIPY-TR ile yapılan örtüşenlokalizasyon çalışmaları sonucu USP32'nin Golgi'de olduğuna dair bulgular elde ettik. Ileride USP32'nin Golgi'deki rolünü anlamaya yönelik yapılacak çalışmalar, bu onkogenin fonksiyonunu netleştirecektir. Çalışmamızın ikinci kısmında potansiyel bir tümör baskılayıcı gen üzerinde yoğunlaştık. Bu amaçla, meme kanserinde tümör baskılayıcı olduğu düşünülen miRmiR-125b'yi fonksiyonel olarak karakterize ettik. mikroRNAların kanser hücrelerinde deregülasyona uğradıkları ve gen ifadesini kontrol ettikleri bilinmektedir. miR-125b'nin ifadesinin meme bazı meme kanseri hastalarında azaldığı gösterilmiştir. Bu çalışmada ise, meme kanseri hücre hatlarındamiR-125b'nin ifadesini, fonksiyonunu ve hedeflediği genleri araştırdık. Sonuçlarımız göstermiştir ki, miR-125b meme kanseri hücre hatlarında da ciddi oranda azalmaktadır. Bu tip hücrelerde miR-125b'nin ifadesinin tekrar sağlandığı çalışmalar yapıldığında, bu hücrelerin çoğalmasında ve göçünde azalma gözlemlenmiştir. Bunun yanı sıra miR-125b ifadesi sağlanan hücrelerde aktin filamentleri boyandığında sitoplazmik uzantıların azaldığı gözlemlenmiştir. Daha önceki çalışmalar, miR-125b'nin hücre hareketliliğine etkisinin *ERBB2* genini hedeflemesi ile ilgili olduğunu işaret etmekle beraber, Sonuçlarımız miR-125b'nin hedeflediği *ARID3B* geninin hücre hareketliliği ve göçü ile ilgili olduğunu göstermektedir. Sonuçlarımız ERBB2 negatif meme kanseri hücre hatlarında miR-125b'nin birden fazla geni hedefleyerek hücre çoğalması ve göçünde rol oynayan önemli bir regülator olduğunu göstermektedir.

Anahtar kelimeler: USP32, DUBs, lokalizasyon, miR-125b, hücre hareketi, *ARID3B.*

To

AORKAMM

ACKNOWLEDGEMENTS

First of all, I would like to express my deepest gratitude to my supervisor Assist. Prof. Dr. A. Elif ERSON BENSAN for her guidance, encouragement and support throughout my graduate study.

I would like to thank my thesis committee members: Assoc. Prof. Dr. M. Cengiz YAKICIER, Assist. Prof. Dr. Sreeparna BANERJEE, Assoc. Prof. Dr. Mayda GÜRSEL and Assoc. Prof. Dr. Mesut MUYAN for their critics and suggestions.

I would like to thank all the previous and current members of our lab, for their friendship and supports.

I am grateful to Dr. Can ÖZEN and Fatma GÜL, from METU Central laboratory for their help with the microscopy.

I would like to thank Dr. Volkan SEYRANTEPE for pEGFPC1 and pEGFPN1 vectors and Dr. Uygar. H. TAZEBAY and Dr. I.YULUG for the breast cancer cell lines they shared with us. I would also kindly thank Dr. Sreeparna Banerjee and her laboratory for sharing materials and resources with us.

I would like to express my great appreciation to my family members for their endless love, trust and support. I would also like to thank my husband for his endless love and support not only during this study, but also in my life.

This thesis project was financially supported by TÜBİTAK project No: 104S241, No: 108S408 and No: 108S381.

TABLE OF CONTENTS

ABSTRACT IV

ÖZ VI

ACKNOWLEDGEMENTS IX

TABLE OF CONTENTS X

LIST OF TABLES XIV

LIST OF FIGURES XV

LIST OF SYMBOLS AND ABBREVIATIONS XX

CHAPTERS

1 INTRODUCTION 1

1.1 Localization of USP32, as a Potential Oncogene Candidate 1

1.1.1 Cancer 1

1.1.2 Gene Amplification and Cancer 2

1.1.3 USP32 Gene and Protein 9

1.1.4 Protein ubiquitination and DUBs: 13

1.1.5 Subcellular Localization of USP32 20

1.1.6 Fluorescence Protease Protection (FPP) Assay 21

1.2 microRNA-125b as a Potential Tumor Suppressor 24

1.2.1 microRNAs: Biogenesis and Function 24

1.2.2 MicroRNAs in Cancer 27

1.2.3 microRNA-125 Family and Cancer 35

1.3 Aim of the study 40

2 MATERIALS AND METHODS 41

2.1 Localization of USP32 41

2.1.1 Cell Culture and Growing Conditions 41
2.1.2 Polymerase Chain Reactions (PCRs) and Agarose Gel Electrophoresis41
2.1.2.1 Colony PCR 41
2.1.2.2 Agarose Gel Electrophoresis 42
2.1.2.3 DNA Extraction from Agarose Gels 42
2.1.3 Bioinformatics Tools for Predicting the Subcellular Localization of USP32 42
2.1.4 Cloning and Ligation Reactions 43
2.1.5 Cloning of USP32 Gene into pEGFPN1 and pEGFPC1 vectors 43
2.1.5.1 Cloning of USP32-full Length and USP32-I into pEGFPN1 44
2.1.5.2 Blunt End Cloning of USP32-II and USP32-III into pEGFPC1 .. 44
2.1.6 Preparation of Competent E. coli Cells 44
2.1.7 Transformation of Competent E.coli Cells 45
2.1.8 Storage of Bacterial Cultures 45
2.1.9 Transfection of Mammalian Cells with USP32 Constructs 46
2.2 Characterization of miR-125b 46
2.2.1 Cell Culture and Growing Conditions 46
2.2.2 Three-Dimensional (3D) Cell culture and Growing Conditions 47
2.2.3 RNA Isolation, DNase treatment and cDNA synthesis 47
2.2.4 Polymerase Chain Reactions (PCRs) 49
2.2.4.1 RT-PCRs 49
2.2.4.2 Quantitative RT-PCRs for Mature miRNA Detection 50
2.2.5 Phalloidin and DAPI Staining 50
2.2.6 Transfection of Mammalian Cells 51
2.2.7 Functional Assays 52
2.2.7.1 Cell Proliferation Assay (MTT) 52
2.2.7.2 Migration Assay 52
2.2.8 Protein Isolation 54
2.2.9 Western Blotting 54

2.2.10 Bioinformatics Tools for Prediction of miR-125 Targets 55
2.2.11 miR-125b's Predicted Target Cloning 56
2.2.12 Dual Luciferase Reporter (DLR) Assay 56
3 RESULTS 57
3.1 Subcellular Localization of USP32 Protein 57
3.1.1 Predictions for Subcellular Localization of USP32 Protein 57
3.1.2 Cloning of USP32 into Reporter Plasmids 59
3.1.2.1 Sticky End Cloning of Full Length USP32 and USP32- I Coding Sequences into pEGFPN1 Vector 61
3.1.2.2 Blunt End Cloning of USP32-II and USP32-III Coding Sequences into pEGFPC1 vector 65
3.1.3 Subcellular Localization of USP32- Full- EGFPN1 Fusion Protein 69
3.1.4 Subcellular Localization of USP32- I –EGFP, EGFP- USP32- II and EGFP- USP32- III fusion proteins 75
3.2 Functional Characterization of miR-125b 87
3.2.1 Expression of miR-125a and miR-125b in Human BCCLs 87
3.2.2 Generation of Breast Cancer Model Systems to Study the Role of miR-125b-1. 89
3.2.3 Functional Assays for miR-125b Expressing Cells 93
3.2.3.1 Cell Proliferation Assay (MTT) 93
3.2.3.2 Effect of miR-125b Expression on Cell Motility/Migration 98
3.2.4 Morphological Changes Due to miR-125b Expression 102
3.2.5 The Distribution of Actin Filaments in MCF7 Cells, Expressing miR-125b 104
3.2.6 ARID3B: a Target of miR-125b 106
3.2.7 Investigating mRNA Targets of miR-125b 115
3.2.7.1 pmiR-3'-UTR Cloning of miR-125 Potential Targets 119
3.2.7.2 Luciferase assay for miR-125 targets 125
4 CONCLUSION 131

REFERENCES 138

APPENDICES

A PRIMERS 166

B VECTORS 167

C BACTERIAL CULTURE AND MEDIA 174

D DNA AND PROTEIN MARKERS 176

CURRICULUM VITAE 179

LIST OF TABLES

TABLES

Table 1.1 Location and sizes of 24 independent amplicons detected from 14 BCCLs, using CGH microarray (Hyman et al. 2002)……..……..4

Table 1.2 The involvement of key microRNAs in cancer. Table is taken from (Lujambio and Lowe 2012)……..33

Table 3.1 Predictions for subcellular localization of USP32 protein obtained from bioinformatics tools……..58

Table A.1 List of primers……..166

LIST OF FIGURES

FIGURES

Figure 1.1 The halmarks of cancer.. 2
Figure 1.2 The physical map of 17q23 chromosomal band 6
Figure 1.3 The location of USP32 and its neighbor genes on 17q23 chromosomal band 10
Figure 1.4 The mRNA expression level of *USP32* in high, moderate and no 17q23 amplification tumor groups, detected by qRT-PCR 11
Figure 1.5 The structure of USP32 transcript 12
Figure 1.6 The domains of USP32 protein. 12
Figure 1.7 Protein ubiquitination. 15
Figure 1.8 The structure of catalytic domains of 5 DUBs family members. proteases). 17
Figure 1.9 The schematic of Fluorescence Protease Protection (FPP) assay 23
Figure 1.10 The general microRNA processing pathway 26
Figure 1.11 Illustration for the contribution of microRNAs to cancer. 30
Figure 1.12 microRNA regulation of cancer pathways. 32
Figure 1.13 The stem-loop structure of the members of miR-125 family. 36
Figure 2.1 The position of primers for PCR amplification of full length (1604 aa) and partial fragments of USP32 (I: USP32-I. II, USP32-II and III, USP32-III)..... 43
Figure 3.1 Position of the domains of USP32 protein..... 60
Figure 3.2 Double digestion of USP32-Full-TOPO and pEGFPN1 vectors with Xho1 and Apa1 restriction enzymes. 62
Figure 3.3 Confirmation of cloning for USP32-Full-pEGFPN1 construct. 63
Figure 3.4 A. Double digestion of USP32-I-TOPO construct with Xho1 and Apa1 restriction enzymes, resulted with 4 digested fragments of 104, 1307, 1388 bp and

2200 bp. B. Double digestion of pEGFPN1 vector with Xho1 and Apa1 restriction enzymes generated sticky ends..... 64
Figure 3.5 Digestion of USP32- II- pGEX-4T-2 and USP32- III- pGEX-4T-2 constructs and pEGFPC1 vector with restriction enzymes. 66
Figure 3.6 Colony PCR for confirming the cloning of USP32-II and USP32-III fragments into pEGFPC1 vector.. 67
Figure 3.7 Restriction digestion for confirming the cloning of USP32-II and USP32-III fragments into pEGFPC1 vector..... 68
Figure 3.8 Fluorescence protease protection assay for USP32-Full-pEGFP fusion protein in HeLa cells.. 71
Figure 3.9 Localization of USP32-EGFP fusion protein (USP32-Full) in HeLa cells……...73
Figure 3.10 BODIPY-TR staining of HeLa cells, expressing USP32-EGFP for detecting the location of Golgi. 74
Figure 3.11 Fluorescence protection assay for USP32-I-EGFP fusion protein.A. .. 77
Figure 3.12 Localization of USP32-I-EGFP fusion protein in HeLa cells.. 78
Figure 3.13 Fluorescence protection assay for EGFP-USP32-II fusion protein. 81
Figure 3.14 Localization of EGFP-USP32-II fusion proteins in HeLa cells. 82
Figure 3.15 Fluorescence protection assay for EGFP-USP32-III fusion protein..... 84
Figure 3.16 Localization of EGFP- USP32-III fusion proteins in HeLa cells. 85
Figure 3.17 Taqman miRNA assay to detect the mature miR-125b and miR-125a levels. 88
Figure 3.18 PCR Amplification of miR-125b-1 from stably transfected T47D cells from genomic DNA..... 90
Figure 3.19 RT-PCR for detecting the expression of precursor miR-125b-1. 91
Figure 3.20 Taqman miRNA assay for detecting the expression of mature miR-125 in T47D-125 (polyclonal 3) and T47D-EV cells. 92
Figure 3.21 Cell proliferation detected by MTT. 94

Figure 3.22 The mature sequences for hsa-miR-125a, hsa-miR-125b-1 and hsa-miR-125b-2. 96
Figure 3.23 Predicted conserved binding sites of miR-125a and miR-125b on the 3'-UTR of ETS1 mRNA by TargetScan program. 97
Figure 3.24 Transwell migration assay in MCF7-EV and MCF7-125 cells.. 99
Figure 3.25 Transwell migration assay in MCF7-125 cells, transfected with miR-125b and control oligos.. 100
Figure 3.26 Sequences of 2'-O-methyl anti-miR-125a and anti-miR-125b oligos and their alignments with mature hsa-miR-125a and hsa-miR-125b..... 101
Figure 3.27 Morphology of MCF7-EV and MCF7-125 cells, grown on 3 D culture for 24 h. 103
Figure 3.28 Staining of actin filaments (green) and nucleus (blue) of MCF7 cells……105
Figure 3.29 Western blot detecting the level of ARID3B protein in MCF10A, MCF7, MCF7-EV and MCF7-125 cells.. 107
Figure 3.30 Effect of miR-125a/b on ARID3B protein levels. 108
Figure 3.31 Effect of anti-125b on ARID3B in T47D cells. 109
Figure 3.32 Western blot for detecting the silencing of ARID3B in MCF7 cells.. 110
Figure 3.33 MTT assay for MCF7 cells to detect cell proliferation rate after silencing ARID3B. 111
Figure 3.34 Migration assay for MCF7 cells transfected with ARID3B shRNA. . 113
Figure 3.35 Taqman assay and western blot for detecting the expression of miR-125 and ARID3B. 114
Figure 3.36 Western blot indicating the level of ERBB2 and pERK1/2 in SKBR3 (ERBB2 overexpressing positive control cell line),MCF7-EV and MCF7-125b cells..... 116
Figure 3.37 Transwell migration assay to determine the effect of AG825 on A. MCF7 and B. SKBR3 cells' migration.. 117

Figure 3.38 A. Alignment of HOXB7-3'UTR and predicted binding site of miR-125b. B. *HindIII* and *SacI* digestion for confirming the cloning of 3'-UTR of *HOXB7*. 121
Figure 3.39 A. Alignment of FBI1-3'UTR (C1 and C2) and predicted binding sites of miR-125b. B. HindIII and SacI digestion for confirming the cloning of 3'-UTR of FBI1-C1 and FBI1-C2. 123
Figure 3.40 Alignment of ETS1-3'UTR (C1 and C2) and predicted binding sites of miR-125b. B. HindIII and SacI digestion for confirming the cloning of 3'-UTR of ETS1-C1 and ETS1-C2……..125
Figure 3.41 Dual luciferase assay for predicted targets of miR-125b in MCF7 cells…..... 126
Figure 3.42 Dual luciferase assay in MDA-MB-231 cells for ETS1-C1-PMIR, ETS1-C2-PMIR, HOXB7-PMIR, FBI1-C1-PMIR and FBI1-C2-PMIR constructs…..... 127
Figure 3.43 Dual luciferase assay for miR-125b targets in MDA-MB-231 cells transfected with anti-miR-125b and control oligos..... 129
Figure B. 1 The map and multiple cloning site of PCR ® 8/GW/TOPO®TA (Invitrogen) vector……..168
Figure B. 2 The map and multiple cloning site of pEGFPN1(Clontech) vector.....169
Figure B. 3 The map and multiple cloning site of pEGFPC1(Clontech) vector..170
Figure B. 4 The map of pSUPER.retro.neo+GFP (Invitrogen) vector…….171
Figure B. 5 The map of pMIR-REPORT Luciferase (Ambion) vector…….172
Figure B. 6 The map of PhRL-TK (Promega) vector…….....173
Figure D. 1 GeneRuler 100 bp Plus DNA Ladder (Fermentas, catalog #:SM0321/2/3)…….....176
Figure D. 2 MassRuler DNA Ladder Mix, ready-to-use, 80-10,000 bp (Fermentas, catalog #: R0491)…….....177

Figure D. 3 PageRuler™ Plus Prestained Protein Ladder, (Fermentas, catalog # SM1811)…….178

LIST OF SYMBOLS AND ABBREVIATIONS

3D	3 Dimensional
aa	amino acid
BCCLs	Breast Cancer Cell Lines
bp	base pair
CDS	Coding sequence
CGH	Comparative Genome Hybridization
DMSO	Dimethyl sulfoxide
dNTP	Deoxyribonucleotide triphosphate
DUBs	Deubiquitinating enzymes
ECM	Extra Cellular Matrix
EGFP	Enhanced Green Fluorescent Protein
EHS	Engelberth-Holm-Swarm
EMT	Epithelial-Mesenchymal Transition
EtBr	Ethidium bromide
FBS	Fetal bovine serum
FPP	Fluorescence Protease Protection
GFP	Green Fluorescent Protein
HA	Hemagglutinin
kDa	Kilodalton
LOH	Loss of heterozygosity
lrECM	laminin-rich ECM
miR	microRNA
miRNA	microRNA
MTT	Methylthiazol tetrazolium
nt	nucleotide
PBS	Phosphate Buffered Saline

Rb	Retinoblastoma
RFP	Red Fluorescent Protein
SDS	Sodium Dodecyl Sulfate
shRNA	short hairpin RNA
TBE	Tris Buffered Saline
Ub	Ubiquitin
USP	Ubiquitin Specific Protease
UTR	untranslated region
YFP	Yellow Fluorescent Protein

CHAPTER 1

INTRODUCTION

1.1 Localization of USP32, as a Potential Oncogene Candidate

1.1.1 Cancer

Tumorigenesis is a multistep process in which normal cells undergo various genetic alterations and turn into neoplastic cells. Cancer cells generally have six hallmark characteristics, necessary for their malignant growth as illustrated in Figure 1.1. These characteristics are: self-sufficiency for growth signals, irresponsiveness to anti-growth signals, evading apoptosis, infinitive replication and immortality, induction of angiogenesis, invasion and metastasis. Two other important properties of cancer cells are now considered as additional hallmarks of cancers: reprogramming of energy metabolism and evading from immune destruction. All of the mentioned characteristics should also be considered within the tumor microenvironment context (Hanahan and Weinberg 2000, 2011).

Cancers generally arise due to alterations of two groups of genes: proto-oncogenes and tumor suppressors. Deregulation of proto-oncogenes results in a gain-of-function and their activation contributes to cancer development. For tumor suppressors, loss of function is the result of various genetic and epigenetic changes which contribute to tumor promotion.

Malignant cells suffer from genomic instability, making the genome susceptible to undergo further genetic changes such as point mutations, chromosomal translocations, aneuploidy, small or large deletions, and gene amplifications as well as epigenetic modifications, consequently altering gene expression. The mentioned abnormalities could play significant roles in deregulation of tumor suppressors and oncogenes and contribute to abnormal growth and survival of cancer cells.

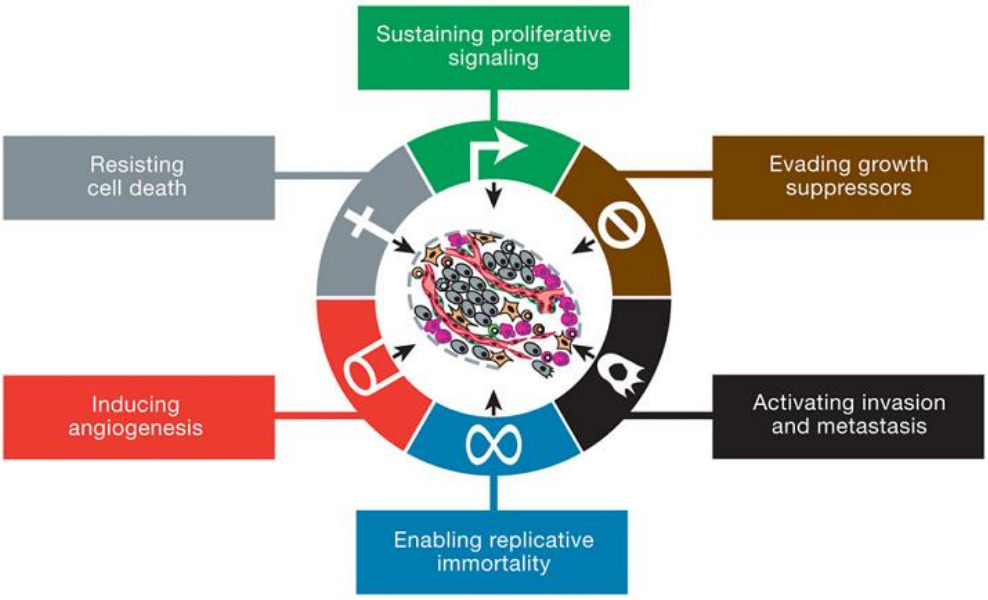

Figure 1. 1 The halmarks of cancer. Figure is taken from Hanahan and Weinberg 2011.

1.1.2 Gene Amplification and Cancer

A large number of comparative genomic hybridization (CGH) studies revealed copy number alterations in various cancers. Genetic alterations could be a source of cancer specific gene expression changes that lead to tumor progression.

Gene amplification is an increase in DNA copy number in restricted chromosomal regions called amplicons. DNA amplification widely occurs in different tumors. Telomere dysfunction, deficiency in DNA replication, aneuploidy and chromosomal fragile sites are factors which possibly support gene amplification (Albertson 2006).

Amplicons contain several copies of DNA sequences and are usually 0.5-12 Mb spanning regions (Hyman et al. 2002; Lengauer et al. 1998). Consequently, DNA amplification may result with the overexpression of the genes, within the amplicon (Myllykangas and Knuutila 2006). Based on the results of a study performed to determine the relation between amplification and gene expression of 13,824 genes on 24 independent amplicons in breast cancer, 44% of highly amplified genes revealed overexpression and 10.5% of highly overexpressed genes had amplification (Hyman et al. 2002; Parssinen et al. 2007). Many other CGH studies provided valuable information on cancer related chromosomal regions.

CGH studies in human neoplasms revealed the chromosomal regions harboring amplicons on lp22-p3l, 1p32-p36, lq, 2p13-p16, 2p23-p25, 2q31-q33, 3q, 5p, 6p12-pter, 7p12-p13, 7q11.2, 7q21-q22, 8pll-pl2, 8q, 2q13-q14, 12p, 12ql3-q21, 13q14,13q22-qter, 14ql3-q21, 15q24-qter, 17p11.2-p12, 17ql2-q21, 17q22-qter, 18q, 19pl3.2-pter, 19cen-q13.3, 20p11.2-pI2, 20q, Xpll.2-p21, and Xpll-q13 (Hyman et al. 2002; Knuutila et al. 1998).

Another study performed in 14 Breast Cancer Cell Lines (BCCLs) demonstrated the existence of 24 different amplicons (Table 1.1). One of these amplicons maps to the chromosomal band 17q23 which has been shown to be frequently amplified and associated with tumor progression and poor prognosis in breast cancer (Andersen et al. 2002; Isola et al. 1995).

Table 1. 1 Location and sizes of 24 independent amplicons detected from 14 BCCLs, using CGH microarray (Hyman et al. 2002).

Location	Start (Mb)	End (Mb)	Size (Mb)
1p13	132.79	132.94	0.2
1q21	173.92	177.25	3.3
1q22	179.28	179.57	0.3
3p14	71.94	74.66	2.7
7p12.1–7p11.2	55.62	60.95	5.3
7q31	125.73	130.96	5.2
7q32	140.01	140.68	0.7
8q21.11–8q21.13	86.45	92.46	6.0
8q21.3	98.45	103.05	4.6
8q23.3–8q24.14	129.88	142.15	12.3
8q24.22	151.21	152.16	1.0
9p13	38.65	39.25	0.6
13q22–q31	77.15	81.38	4.2
16q22	86.70	87.62	0.9
17q11	29.30	30.85	1.6
17q12–q21.2	39.79	42.80	3.0
17q21.32–q21.33	52.47	55.80	3.3
17q22–q23.3	63.81	69.70	5.9
17q23.3–q24.3	69.93	74.99	5.1
19q13	40.63	41.40	0.8
20q11.22	34.59	35.85	1.3
20q13.12	44.00	45.62	1.6
20q13.12–q13.13	46.45	49.43	3.0
20q13.2–q13.32	51.32	59.12	7.8

The first study for detecting amplification on 17q23 revealed a 19% amplification of 17q22-q24 in primary breast tumors (Kallioniemi et al. 1994). Subsequently, several groups revealed the amplification of 17q23 in different types of breast cancer and numerous studies focused on 17q23 amplicon in breast cancer due to its gene rich nature (Erson et al. 2001; Sinclair et al. 2003). Interestingly, 17q23 amplicon was not continuous and harbored multiple amplification regions,

suggesting the presence of multiple proto oncogenes independently amplified in the region during tumor development (Barlund et al. 1997; Erson et al. 2001; Monni et al. 2001; Sinclair et al. 2003). Later on, 50 known or hypothetical genes were predicted to be located on 17q23 (Sinclair et al. 2003). The location of 29 known genes on 17q23 is shown in Figure 1. 2. Southern blotting and FISH studies in MCF7 and BT474 breast cancer cell lines revealed the existence of 6 independent amplification peaks at 17q23, resulted with amplification of 7 genes*: RPS6KB1, TBX2, PAT1, Hs.88845, POPX1, BRIP* and *RAD51C*, located at amplification maxima (Wu et al. 2001).

Parssinen et al, performed quantitative real time reverse transcriptase polymerase chain reaction (qRT-PCR) for 29 known genes on 17q23 in 26 primary breast tumors (with no, moderate and high 17q23 amplification). Their results revealed that high level amplification groups showed higher gene expression levels for eleven genes, compared to non- amplified group (Parssinen et al. 2007). According to the amplification and overexpression data of 17q23 in breast cancer, *RPS6KB1* (ribosomal S6-kinase gene), was one of the first genes with a potential oncogenic role in this region (Barlund et al. 2000a; Couch et al. 1999). *FAM33A, DHX40, CLTC, PTRH2, TMEM49, TUBD1, ABC1, USP32, PPM1D, PAT1, SIGMA1B, RAD51C* and *TBX2* were also shown to have a good correlation between their amplification and overexpression in breast cancer (Barlund et al. 2000b; Lambros et al. 2010; Parssinen et al. 2007; Sinclair et al. 2003). Together, these studies reveal an association between amplification and overexpression of a number of genes on this region in breast cancer (Barlund et al. 2000b; Hyman et al. 2002; Lengauer et al. 1998; Monni et al. 2001).

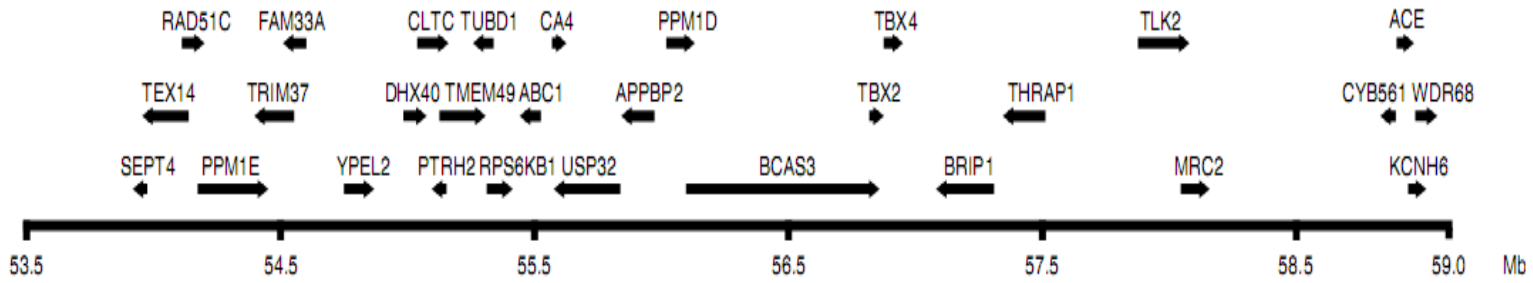

Figure 1. 2 The physical map of 17q23 chromosomal band, indicating the location of 29 known genes on this region (Parssinen et al. 2007). *SEPT4*: Peanut-like protein 2, *TEX14*: Testis expressed sequence 14, *RAD51C*: DNA repair protein RAD51 homolog, *PPM1E*: p53-induced phosphatase 1, *TRIM37*: Tripartite motif-containing 37 protein, *FAM33A*: Family with sequence similarity 33, member A, *YPEL2*: Yippee-like 2 protein, *DHX40*: *DEAH* (Asp-Glu-Ala-His) box polypeptide, *CLTC*: Clathrin heavy chain, *PTRH2*: Peptidyl-tRNA hydrolase 2, *TMEM49* Transmembrane protein 49, *TUBD1*: Tubulin δ chain, *RPS6KB1*: Ribosomal protein S6 kinase, *ABC1*: Amplified in breast cancer, *CA4*: Carbonic anhydrase IV precursor, *USP32*: Ubiquitin C-terminal hydrolase 32, *APPBP2*: Amyloid β precursor protein binding protein 2, *PPM1D*: Protein phosphatase 2C δ isoform, magnesium-dependent, *BCAS3*: Breast carcinoma amplified sequence 3, *TBX2*: T-box transcription factor *TBX2, TBX4*: T-box transcription factor *TBX4, BRIP1: BRCA1* interacting protein C-terminal helicase 1, *THRAP1*: Thyroid hormone receptor-associated protein, *TLK2:* Serine/threonine-protein kinase tousled-like 2, *MRC2:* Mannose receptor, C type 2, *CYB561:* Cytochrome b561,ACE: Angiotensin-converting enzyme, somatic isoform precursor, *KCNH6:* Potassium voltage-gated channel, subfamily H, member 6, *WRD68:* WD-repeat protein 68.

In conclusion, comprehensive analysis of the 17q23 amplicon showed a number of overexpressed genes at that region. This may consequently suggest the involvement of those genes in aggressive tumor progression, detected in breast cancer patients with 17q23 amplification.

Given the high level amplification and general overexpression of these candidate oncogenes, functional studies were done for the 3 potential oncogenes: *RPS6KB1, TBX-2* and *PPM1D*, located at or near the independent amplification peaks on 17q23, in order to investigate the mechanism by which cells gain a growth advantage.

RPS6KB1 codes for a mitogen- activated protein kinase (p70S6 kinase protein). Studies revealed that this protein phosphorylates the protein S6 of the 40S ribosome subunit (Erikson and Maller 1985) and is also activated through PI3K pathway. PI3K signaling induces Akt oncoprotein followed by activation of mTOR and consequently phosphorylation of RPS6KB1 (Aoki et al. 2001; Gonzalez-Garcia et al. 2002). RPS6KB1 protein investigation revealed its role in cell cycle control (by upregulating cyclin D3, causing phosphorylation of pRB and E2F dependent cell proliferation) (Feng et al. 2000), protein synthesis (by selective translation of cell proliferation related mRNAs) (Dufner and Thomas 1999) and cell migration (via association with Rac1 and Cdc42, 2 regulators of actin polymerization and cell migration) (Lambert et al. 2002). These findings suggest a strong potential oncogenic role for this gene to be involved in tumor progression.

TBX-2 (T box transcription factor-2), another candidate oncogene on 17q23: codes for a transcription factor associated with differentiation and development and contains transcriptional activator and repressor domains (Paxton et al. 2002). This protein is implicated with nasal mesenchyme development (Firnberg and Neubuser 2002). In

addition, the mouse homolog of human, Tbx2 in bmi$^{-/-}$ mouse embryo fibroblast cells (MEFs), lead to cellular immortalization due to downregulating Cdkn2a (P19/ARF) and bypassing p19 and p53 regulated senescence (Jacobs et al. 2000; Lingbeek et al. 2002). Furthermore, studies showed that overexpression of Tbx-2 in combination with MYC in MEFs enhanced the proliferation effect of MYC in these cells (Jacobs et al. 2000). In addition, ectopic expression of TBX-2 caused polyploidy (a condition, associated with malignancy and poor prognosis) and resistance to cisplatin in human lung fibroblast cell lines (Davis et al. 2008). These findings also reveal a more robust possible oncogenic role for *TBX-2*.

PPM1D oncogene candidate was also investigated for its function in cancer. *PPM1D*: the human wild type p53-induced phosphatase 1, encodes for type 2C protein phosphatase (PP2C). This protein was shown to have potential binding sites for NF-κB, c-Jun and E2F1 transcription factors and was revealed to be localized in the nucleus. Dephosphorylation of p38 MAPK was reported to be one of the functions of this protein (Bulavin et al. 2002). Following this event, consequently, p53 phosphorylation and p53 dependent transcription is inhibited, which further block the apoptosis and cell cycle arrest in response to DNA damage (Takekawa et al. 2000), suggesting an oncogenic role for this protein to be further investigated.

Interestingly, due to the gene rich structure and the fact that none of the oncogene candidates were found to be potent oncogenes by themselves, it seems likely that the overexpression of several genes might contribute to the neoplastic phenotype. In that context, it is crucial to understand and characterize genes and as of yet unannotated ESTs as well as hypothetical genes mapping to this interesting chromosomal band.

1.1.3 USP32 Gene and Protein

USP32 (Ubiquitin Specific Protease 32) gene (Accession number: NM_032582.3), spanning ~212 kb, maps to the 17q23 amplicon (chromosomal band 17q23.3) and codes for a hypothetical protein. The position of *USP32* and its neighboring genes on this chromosomal band are shown in Figure 1.3. *USP32* is located just adjacent to *RPS6KB1*, an already known potential oncogene candidate with its roles in tumor progression, which is located on one of the 6 determined discontinuous amplification regions on 17q23.

In order to find the correlation between amplification and overexpression, quantitative real time reverse transcriptase polymerase chain reaction (qRT-PCR) studies for *USP32* revealed that the overexpression of this gene was correlated with its high copy number in primary breast tumors, as shown in Figure 1.4 (Parssinen et al. 2007). Given these findings and the fact that USP32 was not as of yet identified, we wanted to further characterize this hypothetical gene to elucidate its function and its possible contribution to tumorigenesis, as a result of its overexpression in breast cancer.

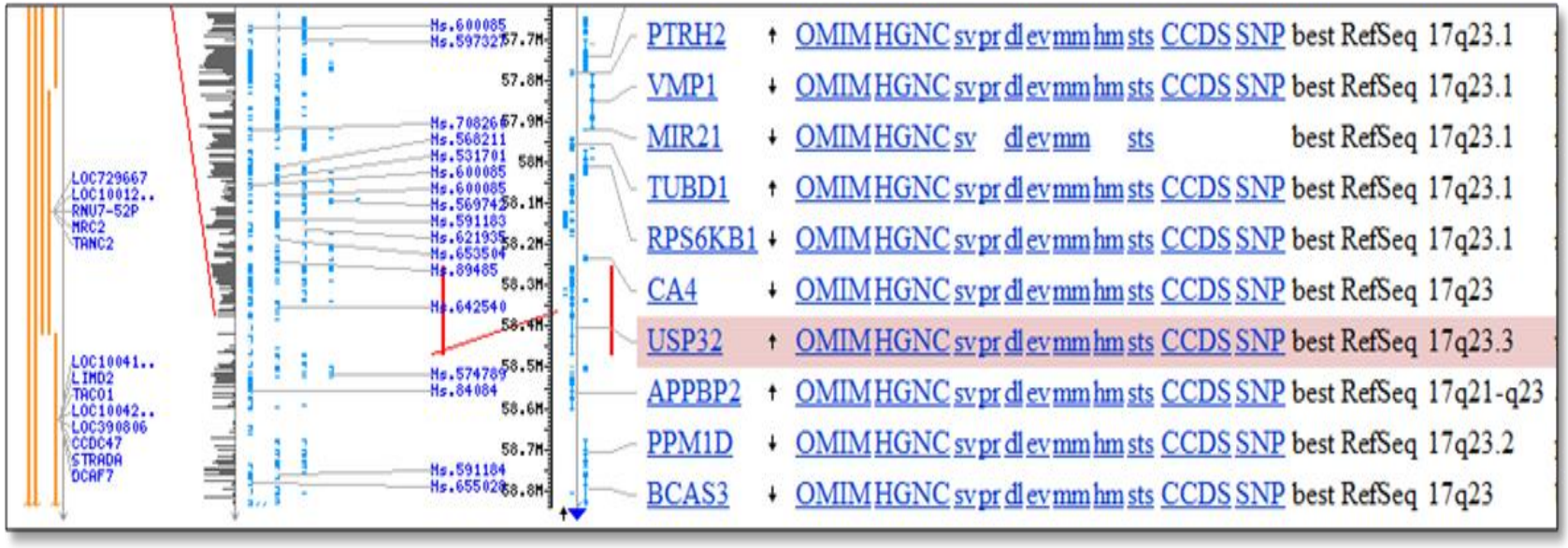

Figure 1. 3 The location of USP32 and its neighbor genes on 17q23 chromosomal band, (according to Map Viewer, NCBI database).

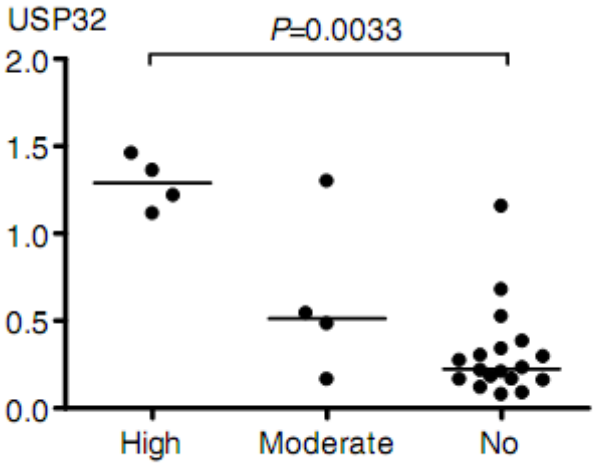

Figure 1. 4 The mRNA expression level of *USP32* in high, moderate and no 17q23 amplification tumor groups, by qRT-PCR method in 26 primary breast tumors Figure is taken from (Parssinen et al. 2007).

USP32 is composed of 34 exons (as predicted *in silico* by the Spidey alignment tool, as well as by the University of California Santa Cruz (UCSC) and National Center for Biotechnology Information (NCBI) databases). The mRNA structure of *USP32* is shown in Figure 1.5. *USP32* gene codes for USP32 protein (Accession number: NP_115971.2), which is 1604 aa long and contains 6 predicted domains as shown in Figure 1.6.

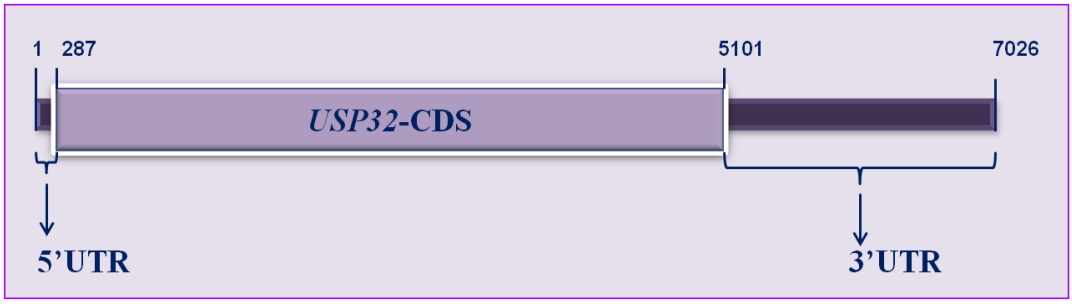

Figure 1. 5 The structure of the *USP32* transcript and CDS (coding sequence) (Accession number: NM_032582.3), according to NCBI database. UTR: untranslated region.

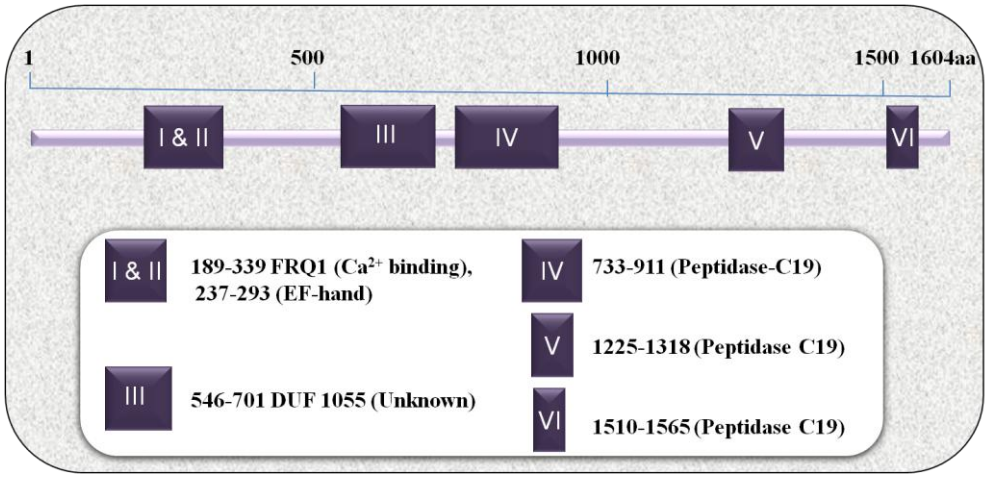

Figure 1. 6 The domains of USP32 protein. The information for domains was obtained from NCBI, using the conserved domain database.

USP32 protein is a predicted member of the Ubiquitin Specific Protease (USP) family of deubiquitinating enzymes (DUBs), with a suggested role for deubiquitination and possibly other unknown roles due to the existence of Ca^{2+}-binding and EF hand domains as well as a domain with unknown function (DUF).

1.1.4 Protein ubiquitination and DUBs:

Ubiquitination is a posttranslational modification through which, Ubiquitin (Ub), a highly conserved small 76 aa protein (8 kDa), covalently attaches to substrate proteins and has significant regulatory roles in eukaryotic cellular pathways such as protein degradation, protein trafficking, protein localization, DNA repair, cell cycle progression, transcription and apoptosis (Liu and Walters 2010). Ubiquitination of a protein could remodel the surface of target protein and affect its stability, activity and interaction with other proteins or even change its cellular localization (Mukhopadhyay and Riezman 2007; Pickart and Eddins 2004; Salmena and Pandolfi 2007; Weissman 2001).

Ubiquitin, binds to a lysine residue of the substrate protein with its C-terminal glycine (Gly76 residue) (Harper and Schulman 2006), which is activated in an ATP dependent manner (Ciechanover and Ben-Saadon 2004). Ub contains 7 lysine residues: consequently Ub molecules can bind and form poly-Ub chains. Ub chains with same or different linkage types are formed in different sizes *in vivo,* via binding through one of the seven lysines (Lys29, Lys33, Lys63, Lys6, Lys11, Lys27 and Lys48) and N-terminal methionine (Met1) of Ub (Kirisako et al. 2006; Peng et al. 2003; Tagwerker et al. 2006). As shown in Figure 1.7, target proteins could be monoubiquitinated (Figure 1.7a) by binding of a single Ub, multiubiquitinated (Figure 1.7b) by binding of more than one ubiquitin to different amino acids or polyubiquitinated (Figure 1.7c), by the attachment of a ubiquitin chain. Monoubiquitination or multiubiquitination of substrates are involved in the entrance of certain targets into vesicles in secretory/endocytic pathway (Hicke 2001), while polyubiquitination, besides broader roles it may probably have, is involved mostly in Ub-proteasome degradation pathway (Harper and Schulman 2006; Pickart and Fushman 2004).

Given the significant functions Ub has, ubiquitination is a tightly controlled process. Several enzymes are involved in ubiquitination of a target protein: E1 (ubiquitin-activating), E2 (ubiquitin-conjugating) and E3 (ubiquitin-ligase) enzymes are responsible for introducing Ub to substrate proteins (Figure 7d). E1 enzyme activates and charges the Ub and binds to its catalytic cysteine via a thioester binding. This binding causes a structural change in E1 and supports its binding to E2 enzyme to pass the Ub to it. E3 ligase is needed for E2 enzyme to transfer activated Ub to substrate protein. The E2 and E3 enzymes are responsible to determine the linkage type of Ub chains (Huang et al. 2007a; Liu and Walters 2010). Human genome is predicted to code for 2 E1, 40 E2 and more than 600 E3 enzymes (Deshaies and Joazeiro 2009).

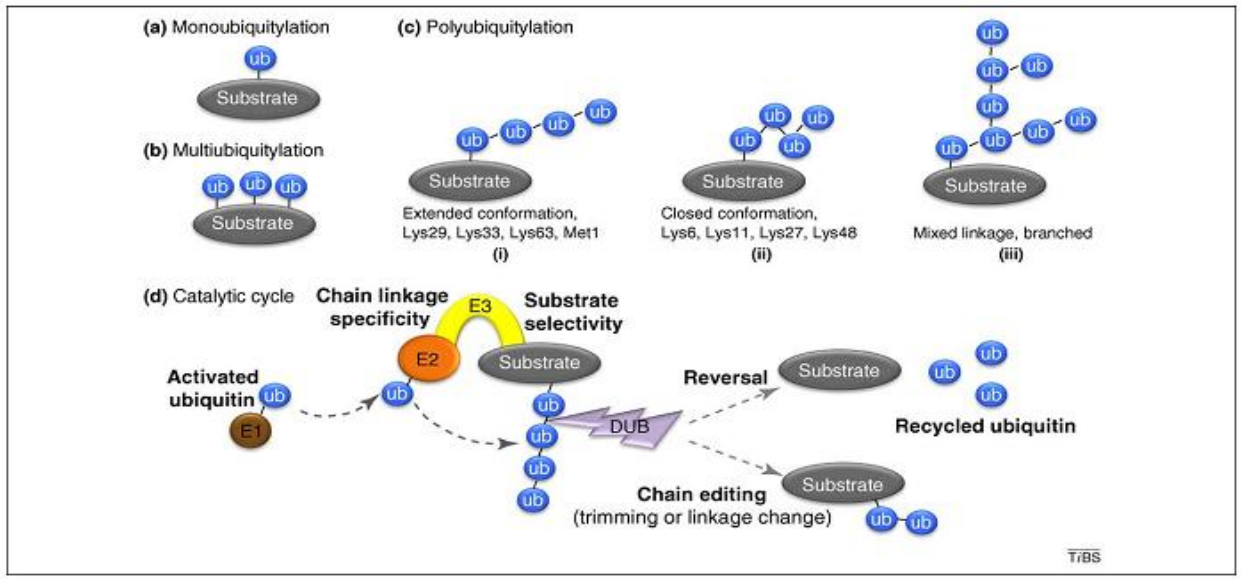

Figure 1. 7 Protein ubiquitination. Substrate protein (grey) is: (a) monoubiquitinated by attaching of a single Ub (blue), (b) multiubiquitinated from different sites or (c) polyubiquitinated with chains of different conformations: Three conformational shapes (i) extended, (ii) closed and (iii) mixed linkaged-branched (multiple Ubs in forked shape, attaching to a common moiety) could be formed depending on which Lys was used to form ubiquitin chains. (d) E1 Ub-activating enzyme (brown) activates the Ub and directed it to attach to the substrate protein by coordinate function of E2 Ub-conjugating (orange) and E3 Ub-ligase (yellow) enzymes. DUBs (purple) are reversing the ubiquitination event by removing the Ubs from chain to recycle the Ub or to edit the length or linkage type of the chain (Liu and Walters 2010).

Among the vast roles ubiquitination play in the cells, the best known function is proteolysis of target proteins. Polyubiquitination by Lys48 is a signal for ubiquitin-proteasome degradation via 26S proteasome and known as the main pathway, regulating the degradation of misfolded and short-lived proteins (Schwartz and Ciechanover 1999). Eukaryotic proteins to be degraded by this pathway have to be necessarily attached to Ub and get poly-ubiquitinated (Finley and Chau 1991; Hershko 1991). The 26S proteasome consists of 20S core catalytic complex and two 19S regulatory caps on both sides. The 20S structure consists of four rings (heptameric) with structural (α) and catalytical (β) subunits. The β1, β2 and β5 subunits are responsible for the caspase-like, trypsin-like and chymotrypsin-like functions respectively in mammals. Each 19S regulatory complex is composed of 19 subunits, a 10-protein base, binding directly to α ring of 20S subunit and a 9-protein lid to which Ub chains bind (Cheng 2009; Marques et al. 2009).

Defects in delivery of ubiquitinated substrates to proteasome or other destinations inside the cell could disrupt the normal cell function. Besides Ub ligases, well studied in this field, deubiquitinating enzymes (DUBs) play role in reversing the ubiquitylation process by hydrolyzing the isopeptide bond between Ub and substrate protein (Hussain et al. 2009; Nijman et al. 2005b).

Approximately, 100 DUBs are predicted to be encoded from the human genome (Nijman et al. 2005b). Based on sequence and structure similarity, DUBs are divided into 5 groups (Nijman et al. 2005b): ubiquitin specific proteases (USPs, Ubp), ovarian cancer (OTU), ubiquitin C-terminal hydrolase (UCH), jab1/MPN domain associated metalloproteases (JAMM) and Machado-Joseph disease (MJD). Except JAMMs (metallopeptidases), other DUBs are cysteine proteases, relying on a thiol group of a cysteine, located at the active site. The catalytic domains of DUBs are shown in Figure 1.8. The DUBs specifically cleave ubiquitin-linked molecules at the Gly76 of ubiquitin (Amerik and Hochstrasser 2004).

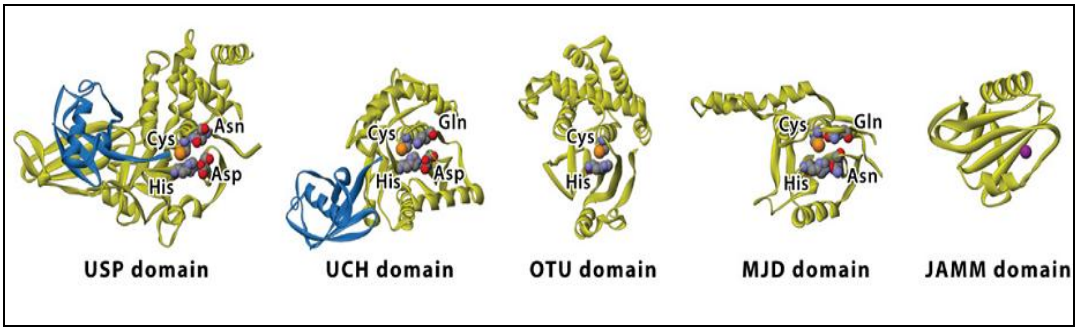

Figure 1. 8 The structure of catalytic domains of 5 DUBs family members. Catalytic points are shown as Van der Waals spheres: (gray: carbon, blue: nitrogen, red: oxygen, orange: sulfur and purple: zinc). The OTU domain doesn't contain the conserved Asp in its catalytic center and the Asn/Glu/Gln (used to stabilize the oxyanion hole in these proteases). Figure has been taken from (Nijman et al. 2005b).

DUBs could act as both tumor suppressors and oncogenes, playing role in different cancer related pathways such as: receptor tyrosine kinase (RTK) signaling, signal transduction, gene transcription, DNA repair, protein degradation, cell proliferation, and mitosis (Hussain et al. 2009).

For example, Usp8 (a homolog of human USP8) plays a role in RTK signaling. Binding of ligand to the RTKs leads to autophosphorylation of cytosolic domains of the receptor and downstream phosphorylation cascades of mediators (transferring signals to the nucleus), recruiting Cbl Ub ligases to ubiquitylate activated receptor (Thien and Langdon 2001). The receptors are further internalized and reach to multi-vesicular-body (MVB) from where the receptors are recycled to the membrane or passed to the lysosome to be degraded (Mosesson et al. 2008). However, Huang et al showed that ubiquitination was necessary for transportation of receptor to MVB and not required for receptor internalization (Huang et al.

2007b). This process could be reversed by Usp8 through deubiquitinating of internalized endosomal cargos. Experiments in adult mice revealed that inactivation of Usp8 caused liver failure and death within 4-6 days. Markedly, cells with deficient Usp8 showed no or low levels of growth factor receptors, indicating the role of USP8 in the reversal of ubiquitination and protein degradation (Niendorf et al. 2007). An example of such regulation is deubiquitination of ERBB2, a member of RTKs, by Usp8 and consequently, recycling back of the ERBB2 to the cell surface, where its function and signaling pathway is associated with tumorigenesis (Meijer and van Leeuwen 2011).

USP9, another member of DUBs family, is involved in signal transduction and cancer. USP9 interacts and stabilizes β-catenin, an important regulator of APC mutations and remarkable member of Wnt signaling pathway (Gumbiner 1997; Murray et al. 2004; Taya et al. 1999).

As the regulator of transcription, USP22 deubiquitinating enzyme was shown to play role in histone deubiquitination. H2A ubiquitination lead to accumulation of this histone protein on silenced promoters, while ubiquitinated H2B (uH2B) accumulates at active promoter regions. In human, deubiquitination of uH2B is accomplished by USP22 (Daniel et al. 2004; Henry et al. 2003; Zhang et al. 2008b), activating the transcription. As an example, USP22 knockdown caused a decrease in the transcription of MYC and p53 (Hussain et al. 2009). USP3 was also reported to play role in deubiquitination of H2A and H2B *in vivo* regulate genomic stability (Nicassio et al. 2007). In addition, USP21 was another regulator of ubiquitinated H2A (uH2A) both *in vitro* and *in vivo* (Nakagawa et al. 2008), affecting transcription of related genes.

USP1 and USP28 are among DUBs, regulating DNA repair and as a result involved in human cancers. USP1, negatively regulate mono-ubiquitinated FANCD2, which

interact with BRCA1/BRCA2 complex, and DNA repair (Nijman et al. 2005a). Furthermore, USP28 was a stabilizer of MYC by deubiquitinating of ubiquitinated MYC and therefore, preventing its degradation by proteasome (Popov et al. 2007a; Popov et al. 2007b).

USP7 (Herpes Associated USP: HAUSP), USP2, USP3 and USP20 were investigated and determined as the regulators of cell proliferation (Hussain et al. 2009). HAUSP was reported to bind to Vmw110 protein, viral encoded and needed for lytic cycle of herpes simplex virus (Everett et al. 1997). USP7 was first reported to stabilize p53 by deubiquitinating it, revealing a tumor suppressor function. Further studies on USP7, revealed that USP7 destabilizes p53 in a complex mechanism involving p53 and its E3 ligase Mdm2 in which the stability of p53 was increased in the absence of USP7, revealing an oncogenic role for it (Brooks and Gu 2004; Cummins and Vogelstein 2004; Li et al. 2004; Li et al. 2002). Other findings for USP7, revealed an oncogenic role for this enzyme by deubiquitinating of Ub-PTEN (an antagonist of Akt) and preventing its nuclear localization, provided by its ubiquitination. Reduced nuclear localization of PTEN, caused by USP7 was associated with tumor aggressiveness (Song et al. 2008).

USP2 is another enzyme that has interesting roles such as regulating Mdm2 functions. USP2 depletion caused a reduction in Mdm2 levels and increase in p53 levels by deubiquitinating of Mdm2 and affecting tumor progression (Stevenson et al. 2007). USP4 is another regulator of cell proliferation and its binding directly to retinoblastoma (Rb) protein was shown (Blanchette et al. 2001; DeSalle et al. 2001). It was also shown that USP4 was able to transform NIH3T3 and made athymic mice to get more tumorigenic (Gupta et al. 1994; Gupta et al. 1993).

As can be seen from above examples DUBs play vital roles in cells and when deregulated have vital consequences. Our gene of interest, *USP32* is a highly

conserved gene and together with *TBC1D3* (derived from a segmental duplication that is new and absent in a number of mammals) evolutionarily formed the *USP6* gene which is a hominoid specific chimeric gene. Although *USP32* and *TBC1DC* genes are expressed in a variety of human tissues, *USP6* is expressed only in testis and ovary (Akhavantabasi et al. 2010; Paulding et al. 2003). Interestingly, USP6 (aka Tre-2, TRE17), is classified as an oncogene with the potential of transforming NIH3T3 cells (Onno et al. 1993; Papa and Hochstrasser 1993). Another finding on USP6 states that a translocation t (16:17) (q22:p13) in aneurysmal bone cysts, generates a fusion gene in which the promoter region of osteoblast cadherin 11 gene (*CDH11*) (16q22) is located behind of *USP6* coding sequence (17p13), revealing a novel oncogenic mechanism for fusion protein as CDH11 has a normally very active promoter (Oliveira et al. 2004).

USP32 (3' end) shows a 97% sequence similarity to USP6, with its function not well characterized yet. The shared sequences between USP32 and USP6 harbor conserved cysteine and histidine domains (present in all Ubiquitin Specific Proteases), critical for the enzymatic function of these proteins. Due to the high similarity of *USP32* to *USP6*, the known oncogene, similar or overlapping functions for proteins, coded from these genes may be suggested.

1.1.5 Subcellular Localization of USP32

USP32 gene/protein has not been characterized. We, in our laboratory, aim to characterize this as of yet unknown gene. In this thesis, we explore the subcellular localization of this protein to help us better understand its function, while other functional and structural studies were also performed in our laboratory.

Proteins may be considered to be localized, according to their functions (Dreger 2003). Understanding the localization of a protein reveals information about its

function and possible pathways they are involved in as well as interacting proteins. Finding the subcellular localization could be an initial step toward characterization of novel genes.

There are different techniques to reveal the subcellular localization of proteins. For example, in proteomic scale, localization could be performed by fractionation of different cell organelles followed by mass spectroscopy analysis. In addition, other techniques such as: immune fluorescence technique, using antibodies against protein of interest or tagged sequences (example: human influenza hemagglutinin (HA)-tag, MYC-tag, Flag-tag) as well as generating fluorescent fusion proteins (that is fusing the protein of interest to a fluorescent proteins such as Green Fluorescent Protein (GFP), Yellow Fluorescent Protein (YFP) and Red Fluorescent Protein (RFP)) could be used in localization studies.

In this study, we generated EGFP fusion USP32 proteins to perform localization studies. Initially we started our localization studies with Fluorescence Protease Protection (FPP) assay, a method developed by Lorenz et al as mentioned in part 1.5.1, followed by investigations with confocal microscopy.

1.1.6 Fluorescence Protease Protection (FPP) Assay

Fluorescence protease protection is used to investigate the topology of the protein inside the cells (Lorenz et al. 2006). In this technique, the coding sequence (CDS) of the protein of interest is cloned upstream and/or downstream of a fluorescent protein-expressing gene (e.g. Green Fluorescent Protein (GFP), Yellow Fluorescent Protein (YFP) or Red Fluorescent Protein (RFP), in order to express fusion protein in the cells. Consequently, permeabilization of plasma membrane (which is rich in cholesterol) with digitonin, followed by protease treatment, reveals the location of

the protein by following the fluorescence signal being released from the cells (Figure 1.9).

This assay determines if a protein is cytoplasmic or membrane bound and in the case if it is attached to a membrane inside the cell, which terminus of the protein is faced the cytoplasm and lumen.

This study used this technique to investigate the subcellular localization of USP32-GFP fusion protein as well as partial fragments of USP32 fused to EGFP.

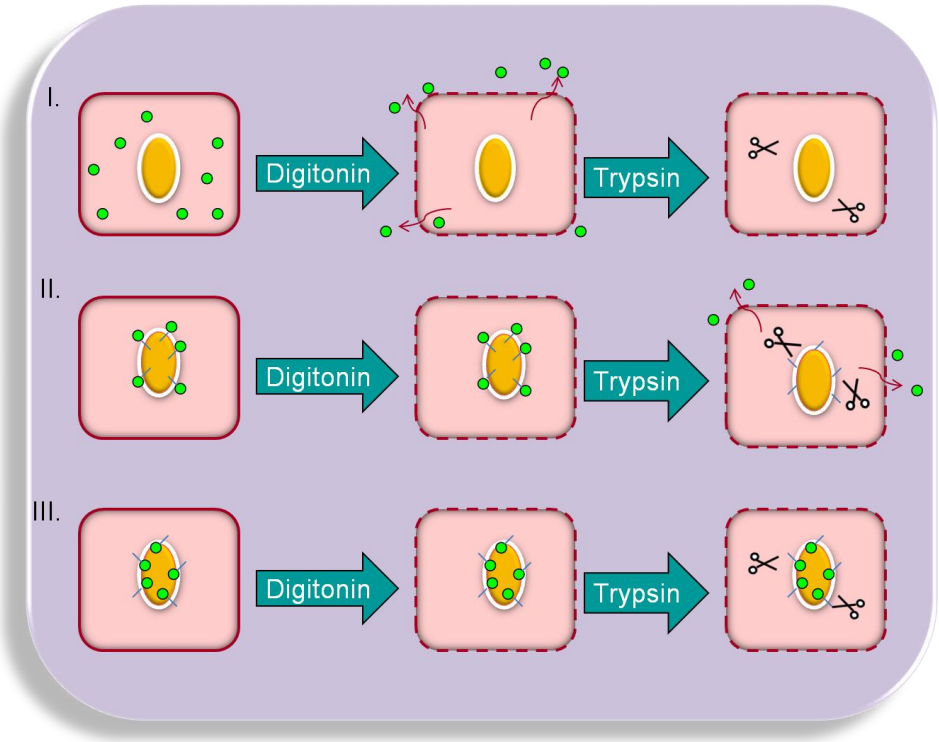

Figure 1. 9 The schematic of Fluorescence Protease Protection (FPP) assay in the cell expressing proteins of interest, fused to GFP protein**. I.** Cytoplasmic localization of the fusion protein, in which a gradual loss of green fluorescence signal is detected from the cell after permeabilization (digitonin treatment). No fusion protein remains inside the cell for protease (Trypsin) cleavage. **II.** Membrane bound topology of the fusion protein, in which the terminus of fusion protein containing GFP faces the cytoplasm. No loss of green fluorescence signal is detected from the cell after permeabilization (digitonin treatment). The GFP terminus of the fusion protein is exposed to protease (Trypsin) cleavage. **III.** Membrane bound topology of the fusion protein, in which the terminus of fusion protein containing GFP faces the lumen of an organelle membrane. The loss of green fluorescence signal is detected from the cell neither after permeabilization (digitonin treatment) nor after protease (trypsin) treatment. The technique was developed by Lorenz et al., 2006.

1.2 microRNA-125b as a Potential Tumor Suppressor

1.2.1 microRNAs: Biogenesis and Function

microRNAs (miRs or miRNAs) are non-coding single stranded RNAs, processed from endogenous hairpin transcripts to 16-29 nt long mature structures (Ambros et al. 2003; Kim 2005; Lee et al. 2004). These small molecules target mRNAs and are responsible for post transcriptional regulation of gene expression by deadenylation of target mRNAs, mRNA cleavage or translational repression (Bartel 2004; Beilharz et al. 2009; Eulalio et al. 2009; Kim 2005). The microRNA genes are dispersed throughout the genome, located in intergenic regions, in a antisense direction to known genes (Lagos-Quintana et al. 2003; Lau et al. 2001; Mourelatos et al. 2002) or located in intronic regions of their host genes (Lee et al. 2004). Recent evidence suggests that the number of microRNA genes in human has exceeded up to 1,000 (Perera and Ray 2007). It is estimated that microRNAs target ~20-30 % of human mRNAs and it is also predicted for a particular miRNA to potentially target ~200 different mRNAs (Krek et al. 2005; Perera and Ray 2007; Rajewsky 2006).

microRNAs are generally transcribed as long pri-microRNA (primary microRNA) transcripts, by RNA polymerase II (pol II) and consequently, they contain 5' cap and 3'poly (A) tail structures (Lee et al. 2004). However, there are some microRNAs located within Alu repeats, whose transcriptions are speculated to be under the regulation of RNA polymerase III (pol III) (Borchert et al. 2006).

pri-microRNA sequences generally undergo processing by a microprocessor complex, composed of Drosha (an RNase III enzyme) and DGCR8/ Pasha (a double-stranded RNA- binding protein) to generate stem loop structures called pre-microRNAs (precursor microRNAs) (Gregory et al. 2004; Han et al. 2004; Han et

al. 2006; Lee et al. 2003), which are approximately 60-70 nucleotides in size. The pre-microRNA structures are exported from the nucleus to the cytoplasm by a member of the Ran-dependent nuclear transport receptor family called exportin 5 (Exp5) (Bohnsack et al. 2004; Lund et al. 2004; Yi et al. 2003). Pre-microRNAs, processed by Drosha and transferred to the cytoplasm, are used as substrates for a further processing event, performed by Dicer, a cytoplasmic RNase III. Dicer cleaves the pre-microRNAs to form an approximately 22 nucleotide long duplex mature microRNA structure (Bernstein et al. 2001; Grishok et al. 2001; Hutvagner et al. 2001). One strand of this short-lived duplex, with less stable 5' end plays the role of mature microRNA regulator (known as 'guide' strand and indicated by -5p in miRbase database), while the other strand with stable 5'end at complementary duplex is degraded (known as 'passenger' strand and indicated by miR* and recently -3p in miRbase database) (Khvorova et al. 2003; Krol and Krzyzosiak 2004; Matranga et al. 2005; Schwarz et al. 2003). The guide strand is loaded into the RISC (RNA induced silencing complex, containing proteins from argonaute family (Ago2)), generating a functional complex to target mRNA transcripts by direct base pairing, resulted in mRNA degradation or translation repression (Du and Zamore 2005; Filipowicz et al. 2008; Guo et al. 2010). The general mechanism of microRNA processing is shown in Figure 1.10.

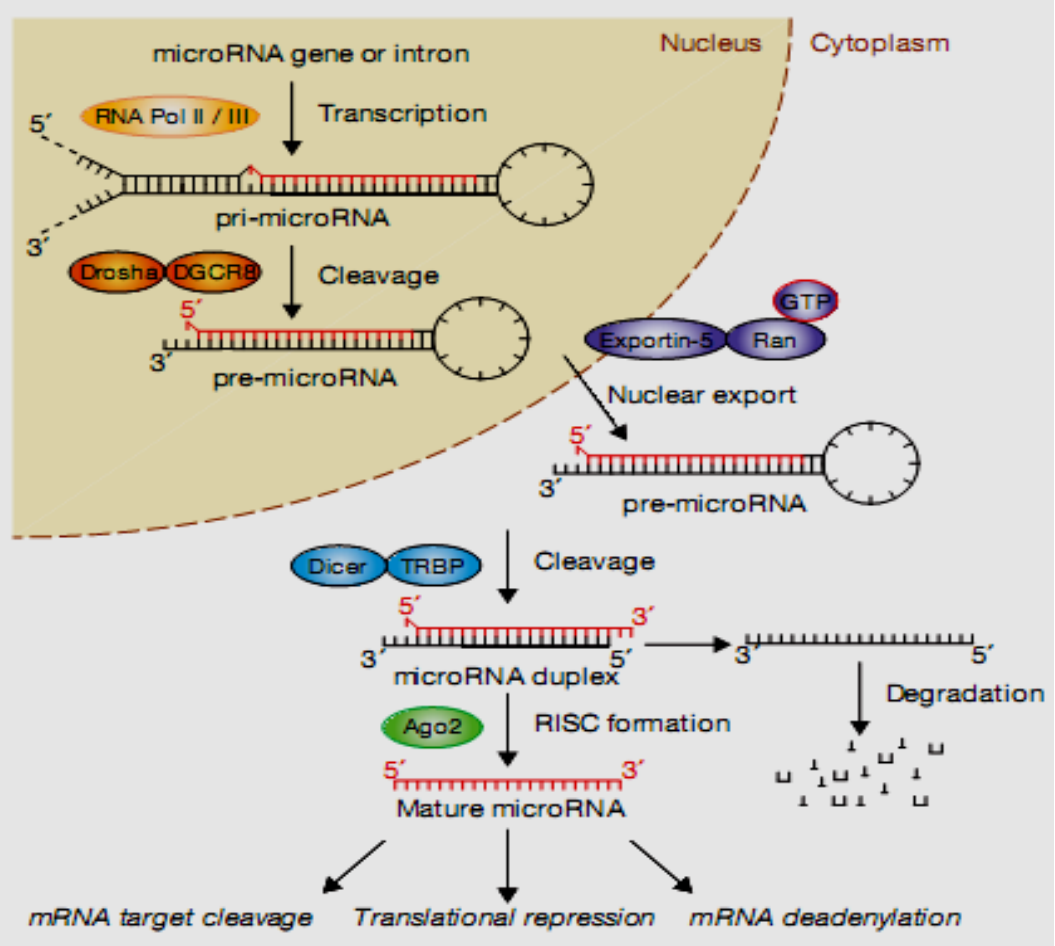

Figure 1. 10 The general microRNA processing pathway. Inside the nucleus, the pri-microRNA is polymerized by pol II or III, and cleaved by the Drosha–DGCR8 microprocessor complex, resulting with a stem loop structure (pre-microRNA). Exportin-5–Ran-GTP, export the pre-microRNA to the cytoplasm, where it is further cleaved and processed to a mature microRNA by Dicer in complex with RNA-binding protein TRBP. The functional strand (guide: indicated in red color) of the mature microRNA is further located on RISC complex and bind to target mRNAs to perform cleavage, repression of translation or deadenylation of its targets. The passenger strand (indicated in black) is degraded. Figure is taken from (Winter et al. 2009).

A wide range of studies in the microRNA field revealed that these small non-coding RNAs have critical roles in several biological events such as development, cell cycle and proliferation, differentiation and apoptosis.

1.2.2 microRNAs in Cancer

Various studies revealed abnormal DNA copy numbers and expression abnormalities for microRNAs in different human cancers (Calin and Croce 2006; Deng et al. 2008; Erson and Petty 2009; Esquela-Kerscher and Slack 2006). Interestingly, bead based follow cytometry and microarray studies on microRNA expression suggested that microRNAs may be widely down regulated in tumors compared to normal tissues (Lu et al. 2005; Zhang et al. 2008a). Other studies revealed a tumor specific mixed down regulation and up regulation patterns of microRNA expression (Calin et al. 2005; Volinia et al. 2006; Yanaihara et al. 2006).

The alteration of microRNAs expression could occur in different cancers through several mechanisms such as: copy number alterations due to amplification/deletion/ translocation of genomic regions, activation or repression of transcription, epigenetic modifications, defect in microRNA processing machinery, or point mutations. These alterations of microRNA expression could change the expression of their target genes and consequently affect normal cell processes including: apoptosis, differentiation, cell proliferation, DNA repair (Deng et al. 2008; Ha 2011).

The first evidence showing the link between particular microRNAs and cancer was reported through the *miR-15a* and *miR-16-1* down regulation chronic lymphocytic leukemia (CLL) (Iorio et al. 2010). A region of 13q14, normally harboring these microRNAs was deleted in more than 50% in the CLL patients, resulting in deletion

or down regulation of these microRNAs in ~68% of the CLL patients (Calin et al. 2002). Further studies showed the suppression of BCL2 expression under the regulation of these 2 microRNAs, suggesting a tumor suppressor role for them in CLL (Cimmino et al. 2005). Additional studies revealed the deletion of these microRNAs in pituitary adenomas (Bottoni et al. 2005), and in breast and ovarian cancers (Zhang et al. 2006).

The microRNA deregulation as a result of copy number abnormality was also detected as amplification for C13orf25, located at 13q31-32 in lymphoma patients. Interestingly, this region contains polycistronic miR-17~92 cluster with a known oncogenic role for resulted mature microRNAs in lymphoma and other human cancers (Hayashita et al. 2005; He et al. 2005; Tagawa and Seto 2005).

Calin et al performed a comparative bioinformatics study on the loci of 186 microRNA genes, revealed from public databases and reported to have genetic alterations, and revealed these microRNAs were frequently located at common breakpoints, minimal regions of loss of heterozygosity (LOH), minimal regions of amplification or fragile sites (Calin et al. 2004). These findings were in agreement with experimentally obtained results from an array based comparative genomic hybridization (aCGH) study, performed in 227 human tumors (Zhang et al. 2006). In addition, further study in ovarian tumors suggested an approximately 15% down regulation of microRNAs in response to genomic copy number loss (Zhang et al. 2008a). All together, these results support the fact that alteration of DNA copy number is common in cancer, partly giving rise to deregulation of microRNA expression.

As another mechanism for microRNA deregulation in cancer was the transcriptional alteration, shown for miR-17-92 family. This microRNA cluster is under the regulation of c-MYC, a highly amplified and overexpressed transcription factor in

human cancers. Overexpression of oncogenic miR-17~92 clusters was consequently reported in many cancers (Chang et al. 2008; O'Donnell et al. 2005). miR-34 is another example of down regulated tumor suppressor microRNA in cancer which is under the regulation of tumor suppressor p53 transcription factor (Corney et al. 2007; He et al. 2007).

Epigenetic factors can also regulate the microRNA expression. For example, miR-127, a microRNA under the control of epigenetic factors, is generally expressed in normal but absent in cancer cells. miR-127 was shown to be among microRNAs, whose expression was restored by chromatin-modifying drugs: 5-aza-2'-deoxycytidine and 4-phenylbutyric acid. Interestingly, this microRNA was predicted to target proto-oncogene *BCL6*, with decreased protein expression after treatment with mentioned drugs (Saito et al. 2006).

microRNAs can contribute to cancer as oncogenes or tumor suppressors, depending on the wide range of their targets (Deng et al. 2008; Lujambio and Lowe 2012), as illustrated in Figures 1.11 A, B and C.

A.

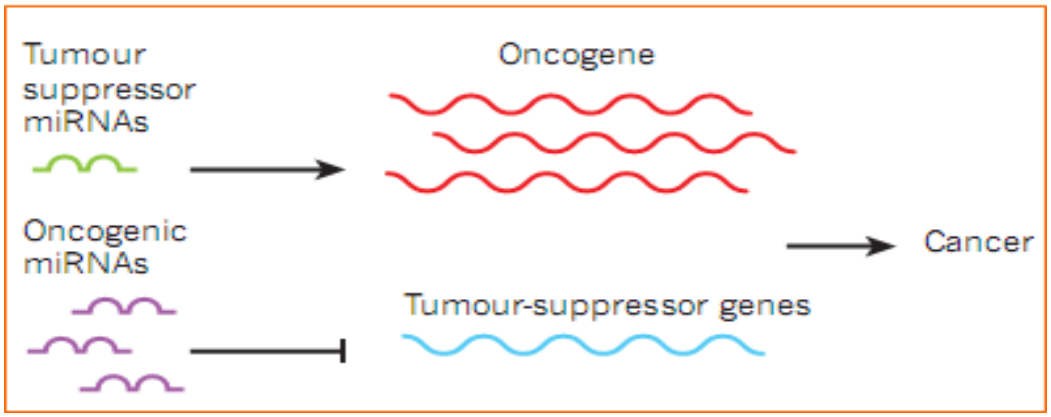

Figure 1. 11 Illustration for the contribution of microRNAs to cancer.

B.

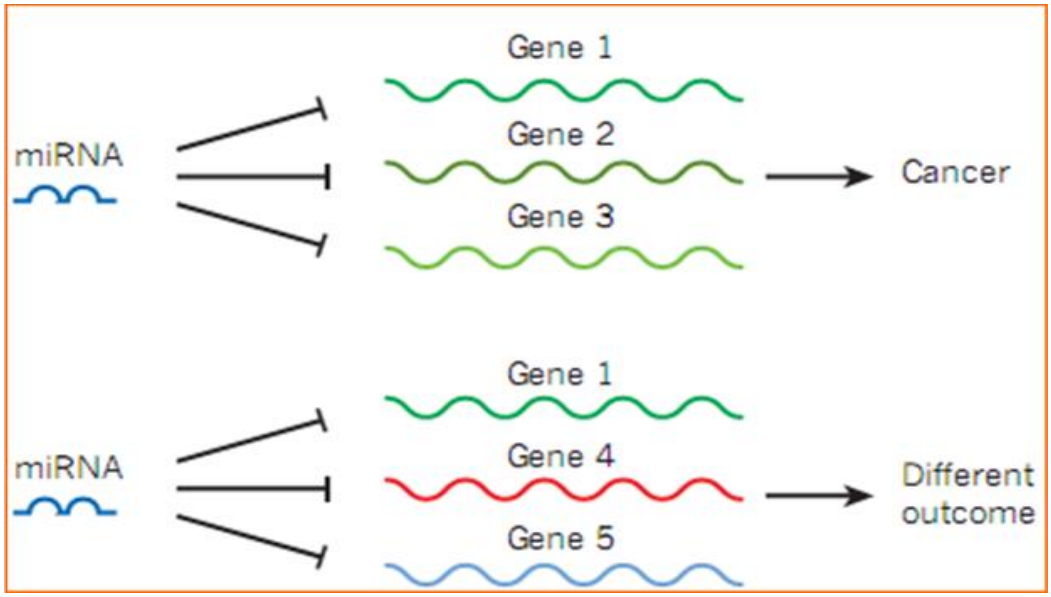

C.

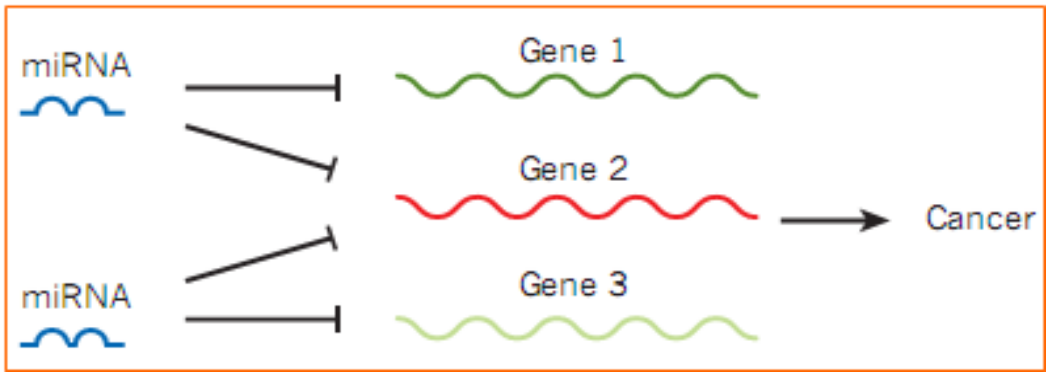

Figure 1. 11 (Continued) Illustration for the contribution of microRNAs to cancer. **A.** microRNAs can act as tumor suppressors, as their down regulation in cancer causes the activation of oncogenes. In addition they can function as oncogenes, by inhibiting the tumor suppressor genes. **B.** microRNA genes can contribute to cancer or lead to other outcomes, depending on which target genes are regulated by microRNAs in different cancer and healthy cells. **C.** microRNAs can contribute to tumor progression by acting separately or together to regulate one or several pathways. Figures are taken from (Lujambio and Lowe 2012).

microRNAs can interfere with different aspects of cancer cells such as cell proliferation, apoptosis, angiogenesis, migration, invasion and metastasis. For example microRNAs can be regulated by and regulate target key proteins whose function affect cancer progression (Figures 1.12A and B). The involvement of a number of key microRNAs in different cancers: their mechanism of regulation, targets and clinical applications are summarized in Table 1.2.

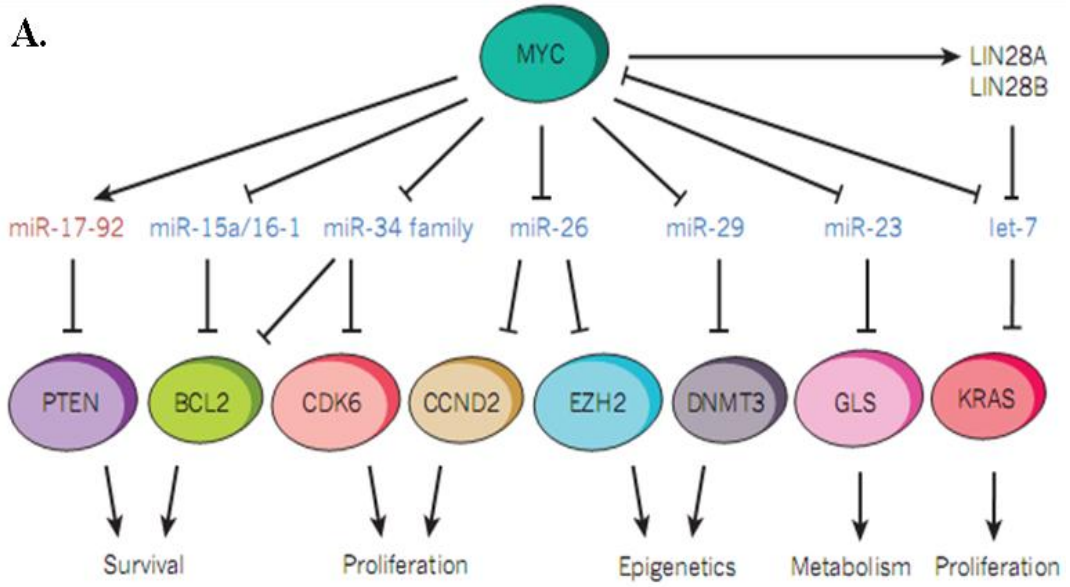

Figure 1. 12 microRNA regulation of cancer pathways. **A.** The oncogene transcription factor MYC can regulate different pathways through direct or indirect activating the oncogenic microRNAs (miR-17-92 cluster, whose name is shown in red) or suppressing tumor suppressor microRNAs (names are written in blue). These microRNAs are involved in different pathways by regulating their downstream targets. A regulatory loop was found in which MYC suppresses *let-7* and itself is suppressed by this microRNA. In cancer, *let-7* is down regulated by several possible regulators as well as MYC itself, leading to constitutive activation of MYC oncogene.

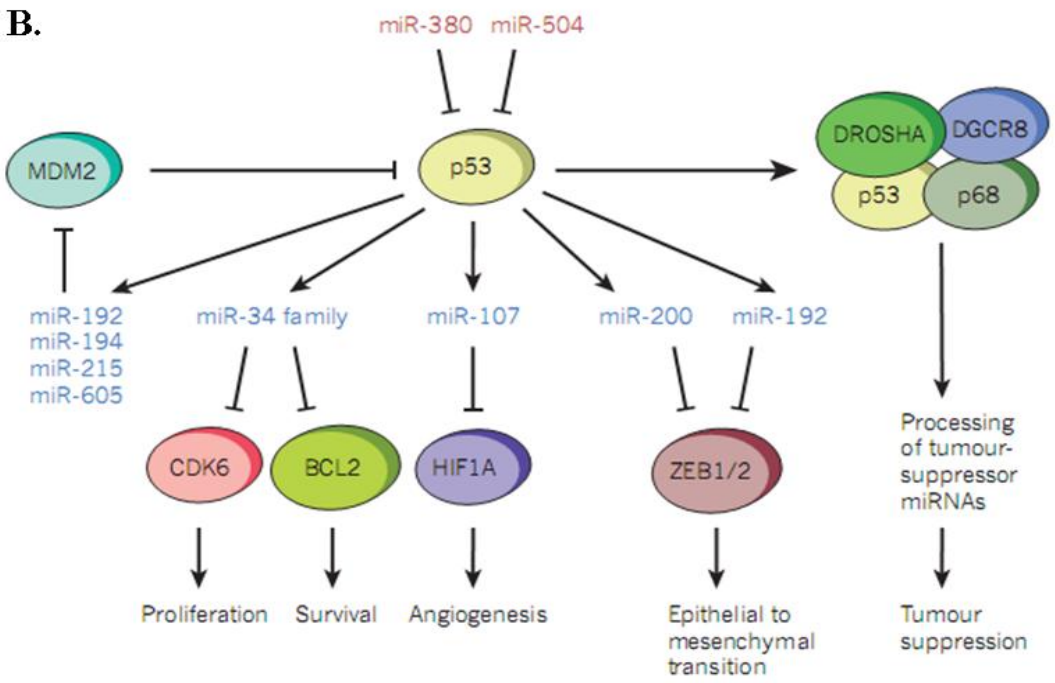

Figure 1. 12 (Continued) microRNA regulation of cancer pathways. **B.** The tumor suppressor transcription factor p53 protects several antitumor pathways, through activating tumor suppressor microRNAs (in blue), followed by their target regulations. A regulatory loop was also detected in this pathway in which activated microRNA genes through p53 pathway block MDM2, resulted with increasing p53 stability. Oncogenic microRNAs (with their names, indicated in red) also can negatively regulate p53. Furthermore, processing of several tumor suppressor microRNAs is regulated by p53. Figure taken from (Lujambio and Lowe 2012).

Table 1. 2 The involvement of key microRNAs in cancer. Table is taken from (Lujambio and Lowe 2012)**.**

microRNA	**Function**	**Genomic location**	**Mechanism**	**Targets**	**Cancer Type**	**Mouse model**	**Clinical application**
miR-17-92 cluster	Oncogene	13q22	Amplification and transcriptional activation	*BIM*, *PTEN*, *CDKN1A* & *PRKAA1*	Lymphoma, lung, breast, stomach, colon & pancreatic cancer	Cooperative with MYC to produce lymphoma, overexpression causes lymphoproliferative disease	Inhibition & detection
miR-155	Oncogene	21q21	Transcriptional activation	*SHIP1* &*CEBPB*	Chronic lymphocytic leukemia, lymphoma, lung, breast & colon cancer	Overexpression induces pre-B-cell lymphoma and leukemia	Inhibition & detection
miR-21	Oncogene	17q23	Transcriptional activation	*PTEN*, *PDCD4* &*TPM1*	Chronic lymphocytic leukemia, acute myeloid leukemia, lung, breast, stomach, prostate, colon & pancreatic cancer	Overexpression induces lymphoma	Inhibition & detection

Table 1. 2 (Continued) The involvement of key microRNAs in cancer.

microRNA	Function	Genomic location	Mechanism	Targets	Cancer Type	Mouse model	Clinical application
miR-15a/ 16-1	Tumour suppressor	13q31	Deletion, mutation, Transcriptional repression	*BCL2 & MCL1*	Chronic lymphocytic leukemia, prostate cancer & pituitary adenomas	Deletion caused Chronic lymphocytic leukemia.	Expression with mimics and viral vectors
Let-7 family	Tumour suppressor	11 copies: multiple location	Transcriptional repression	*KRAS, MYC & HMGA2*	Lung, , stomach, colon, ovarian & breast cancer	Overexpression suppresses lung cancer	Expression with mimics and viral vectors
miR-34 family	Tumour suppressor	1p36 & 11q23	Epigenetic silencing, deletion and transcriptional repression	*CDK4,MYC & MET*	Lung, colon, kidney, bladder & breast cancer melanoma & neuroblastoma	No published studies	Expression with mimics and viral vectors
miR-29 family	Oncogene Tumour suppressor	17q32 & 1q30	Transcription activation Deletion & transcriptional repression	*ZFP36* *DNMTs*	Breast cancer & indolent chronic lymphocytic leukemia Acute myeloid leukemia, aggressive chronic lymphocytic leukemia & lung cancer	Overexpression induces chronic lymphocytic leukemia.	No published studies

As shown in Table 1.2, cancer related microRNAs function as oncogenes or tumor suppressors. Also it is possible for a microRNA to act as both oncogene and tumor suppressor, according to the tissue in which cancer progresses and depending on the targets (this is the case of miR-29 family). For this reason, microRNAs could be considered as oncogenes in some cancers but tumor suppressors in other cancer types, depending on the gene expression profile and the availability of targets.

1.2.3 microRNA-125 Family and Cancer

According to the sequence similarity, microRNAs genes are classified into families. Based on the information on miRBase database, in human, microRNA-125 family is composed of 3 members: has-miR-125a, has-miR-125b-1 and has-miR-125b-2, expressed from 3 distinct genes located on 19q13.33, 11q24.1 and 21q21.1 respectively. These 3 microRNA genes have exclusive stem-loop structures (pre-microRNA). miR-125b-1 and miR-125b-2 have the same mature sequences, differing from the mature miR-125a by 3 nucleotides around their 3' sequences, while all members share a same seed sequence. Figure 1.13 shows the structure of stem-loops for miR-125 family members together with the mature sequences.

Based on the information from Cancer Genome Project database (http://www.sanger.ac.uk/genetics/CGP/), miR-125b1 locus, located on 11.q24.1 was reported as an LOH (Loss of Heterozygosity) region in 18 out of 40 breast tumors. Studies in young breast cancer patients also revealed frequent allelic losses on 11q24.1–q25 chromosomal band which was reported to be associated with poor patient survival (Gentile et al. 1999). This information suggests the existence of potential tumor suppressors in this region.

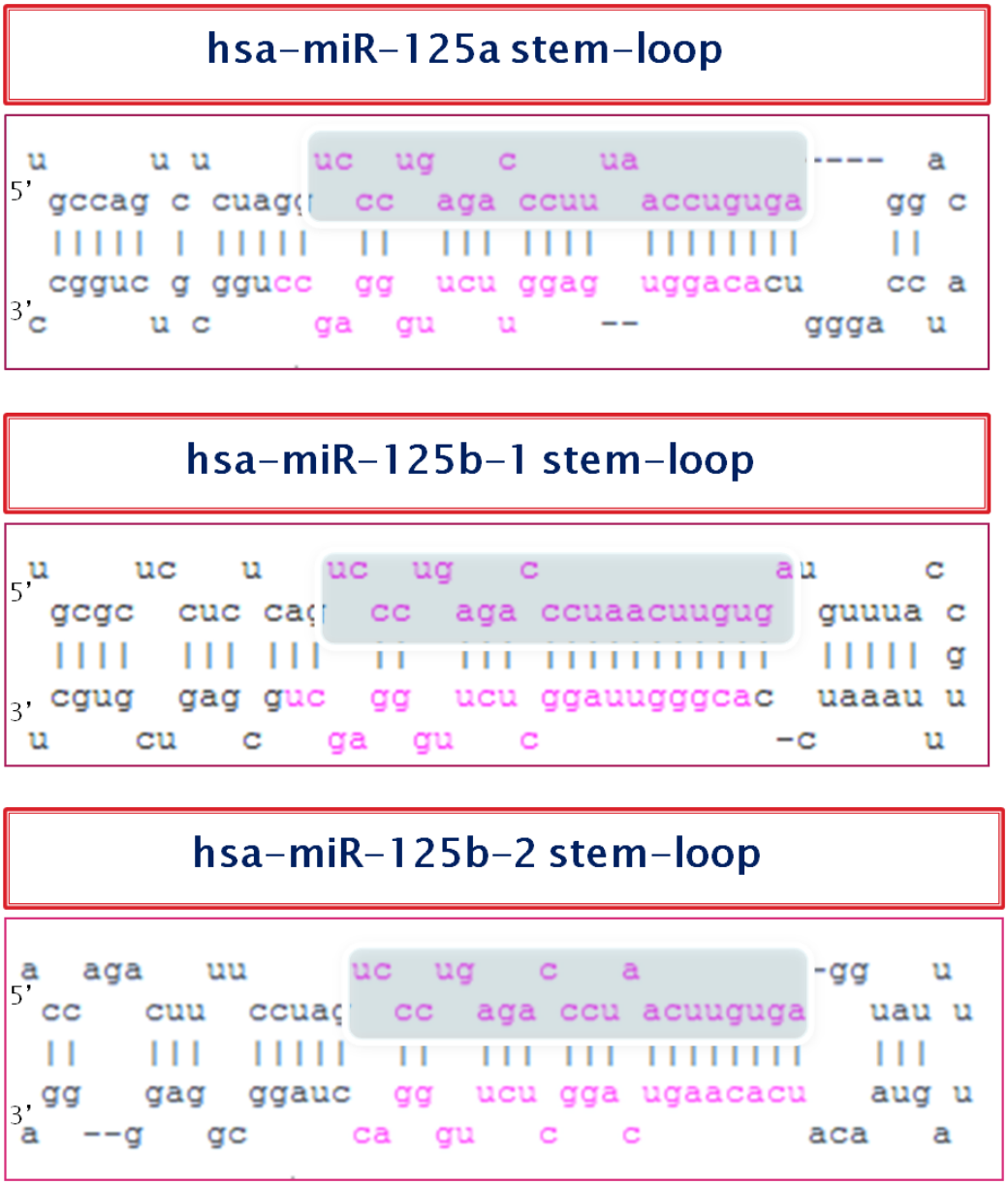

Figure 1. 13 The stem-loop structure of the members of miR-125 family. The sequences for guide strand of mature microRNAs, shown in grey rectangles. The figure is taken from miRBase database.

miR-125 is one of the microRNAs, found to be highly deregulated in different types of cancers. Results from a high throughput microRNA microarray analysis revealed that miR-125b1 was among down regulated microRNAs in ovarian cancer tissues

(Iorio et al. 2007). Down regulation of miR-125b was further detected in patients with squamous cell carcinoma of tongue (Wong et al. 2008) as well as oral squamous cell carcinoma (Henson et al. 2009). Microarray studies also revealed miR-125b among down regulated microRNAs in prostate cancer (Ozen et al. 2008). Another study, performed to reveal the expression of miR-125a, showed down regulation of this microRNA in non-small cell lung cancer tissues, with correlation to metastasis (Jiang L 2010).

In breast, microRNA microarray and northern blot studies on 76 primary breast tissues, compared to 10 normal breast tissues revealed a significant down regulation of miR-125b, but not miR-125a in breast tissues (Iorio et al. 2005). In another study, performed in biopsy samples from breast cancer patients, miR-125b was detected as down regulated microRNA in 13 of ERBB2 expressing, compared to 7 ERBB2 negative samples, revealing a negative correlation between miR-125 and ERBB2 (Mattie MD 2006).

miR-125 was shown to be a regulator of cell proliferation. The role of miR-125b on inhibition of cell proliferation was shown in mouse mesenchymal stem cells (ST2 and D3 cells) (Lee et al. 2005; Mizuno et al. 2008). Overexpression of miR-125b was also affecting the proliferation of U251 glioma stem cells (in which miR-125b is down regulated) (Shi et al. 2010).

A functional study was performed in different breast cancer cell lines by ectopically expressing miR-125 or miR-125 inhibition. Results from this study revealed that miR-125a and miR-125b affect MCF7 cells' proliferation. Ectopic expression of miR-125a was also shown to decrease the migration of MCF7 cells in this study (Guo et al. 2009).

Two of the targets of miR-125a and miR-125b were discovered by Scott et al, to be *ERBB2* and *ERBB3* oncogene family from receptor tyrosine kinases (Scott et al.

2007). By transfecting miR-125a and miR-125b and performing functional assays they showed significant decreases in cell proliferation, migration, invasion and anchorage independent growth in SKBR3 (ERBB2-dependent cells), while no significant change was detected in MCF10A (normal immortalized human mammary epithelial cells) cells when these miRNAs were transfected.

Vitamin D Receptor (*VDR*) and human vitamin D3 hydroxylase (*CYP24*) were found to be other targets of miR-125b, playing role in calcitriol (hormonally active form of vitamin D, 1α,25-dihydroxyvitamin D3 with anti proliferative effect) metabolism. One of the functions of VDR is uptake of the calcitriol into the cells, while CYP24 inactivates calcitriol. In addition, VDR, which is a transcription factor, regulate the expression of *CYP24*, revealing a regulatory loop in this pathway. When miR-125b was overexpressed in MCF7 cells, calcitriol lost its anti-proliferative effect, possibly because of its effect on the regulation of *VDR* (Mohri et al. 2009).

miR-125b was also shown to target BCL3 (an activator of NF-κB) in ovarian cancer possibly contributing to cell cycle arrest. A decrease in cell proliferation was observed in these cells as a result of miR-125b regulation of BCL3 (ectopic expression of miR-125b decreased the BCL3 protein levels) (Guan et al. 2011). E2F3 (an inhibitor of pRB and activator of Cyclin A2) was also shown as another target of miR-125b, detected in bladder cancer, possibly regulating cell cycle progression through G1/S transition (Huang et al. 2011). *MUCIN 1*, a signaling protein which activates NF-κB was shown to be a target of miR-125b in BT-549 breast cancer cell lines (Rajabi et al. 2010).

HUR oncogene (coding for a stress induced RNA binding protein), is a regulator of cell proliferation, migration and apoptosis and was shown to be targeted by miR-125a in BCCLs (Guo et al. 2009). Recent studies also revealed the regulation of v-

ets erythroblastosis virus E26 oncogene homolog 1 (ETS1), a regulator of cell proliferation, by miR-125b (Zhang et al. 2011).

Interestingly, controversial findings do exist which suggest an oncogenic role for miR-125b rather than the proposed tumor suppressive role. For example, two other targets of miR-125b were detected which are known to be required for the induction of apoptosis: pro-apoptotic Bcl-2 antagonist killer 1 (*BAK1*) and Bcl2 modifying factor (*BMF*). BAK1 was shown to be targeted by miR-125b in prostate cancer as well as breast cancer (Shi et al. 2007). In breast cancer, miR-125b was shown to be increased in taxol (mitotic inhibitor agent) resistance cells, targeting *BAK1* and making cells resistant to apoptosis (Zhou et al. 2010). miR-125b-1 and miR-125b-2 were shown to regulate BMF in U251 human glioma cell lines. miR-125b induced decrease in the BMF protein levels caused inhibition of apoptosis in these cells (Xia et al. 2009). p53 is also among tumor suppressor targets of miR-125a and miR-125b (Le et al. 2009; Zhang et al. 2009). These tumor suppressor targets of miR-125b suggest an oncogenic role in these pathways for miR-125b. This function possibly could be changed among cancers, in a target and cancer dependent manner.

Clearly, a better understanding of miR-125b is needed to delineate its role and function in cancer cells, emphasizing the fact that miRNAs may both act as tumor suppressors and oncogenes based on the context and the tissues they are expressed in.

1.3 Aim of the study

Cancer is a complex disease and deregulation of many pathways and their associated genes could contribute to tumor progression. For this reason, functional characterization of cancer related genes could help better understand the mechanism of their functions.

In this study we aimed to investigate two independent cancer related genes to better understand their functions and to study their potential involvements in neoplastic cells. Our specific aims were:

A) to characterize the role of *USP32*, as a potential oncogene in breast cancer, which codes for a hypothetical protein. For this aim, we investigated the subcellular localization of USP32 protein, via generating USP32-GFP fusion protein for full length and overlapping fragments of USP32 and performed localization and co-localization studies in HeLa cells.

B) to investigate the function and targets of *miR-125b,* as a tumor suppressor in breast cancer. For this purpose, we chose to use low miR-125b expressing breast cancer cell lines in which miR-125b expression was restored. An already existing miR-125b transfected MCF7cell line was used. A second model system was also generated in T47D cells by stably transecting miR-125b. Throughout the study, we used these model cells to explore the effects of restored miR-125b expression in breast cancer cells.

CHAPTER 2

MATERIALS AND METHODS

2.1 Localization of USP32

2.1.1 Cell Culture and Growing Conditions

HeLa cells were obtained from ŞAP institute (Ankara, Turkey) and were grown in MEM with Earle's salts and 10% FBS, and 1% Penicillin/Streptomycin. Cells were incubated at 37^{o}C with 95% humidified air and 5% CO_2.

2.1.2 Polymerase Chain Reactions (PCRs) and Agarose Gel Electrophoresis

2.1.2.1 Colony PCR

Colony PCRs were performed, using Taq DNA polymerase (Fermentas) in 10 µl reactions. dNTP, primers and enzyme were used at final concentrations of 0.2 mM, 0.5 µM and 0.12 unit respectively.

2.1.2.2 Agarose Gel Electrophoresis

Agarose gels were prepared, using Agarose (AppliCham) and Tris-Borate-EDTA (TBE) buffer. Ethidium bromide (EtBr) was used at a final concentration of 0.5 μg/ml prior to gel solidification. 10X loading dye was used to the final concentration of 1X. The appropriate DNA marker was used to determine the size of the DNA (shown in Appendix D) in each experiment. Electrophoresis was carried out at 75-100 volts. Depending on the size of DNA products which were run on the gel, 0.8%-3% agarose gels were prepared and used in the experiments. DNA products were run on the agarose gel containing 0.5 μg/ml EtBr.

2.1.2.3 DNA Extraction from Agarose Gels

After confirming the size of the samples, the parts of the gel containing DNA were cut and DNA was extracted, using gel extraction kit (Roche), according to manufacturers' guidelines. The DNA was eluted in dH_2O at the end of the extraction.

2.1.3 Bioinformatics Tools for Predicting the Subcellular Localization of USP32

The following programs were used to predict the subcellular localization of USP32 protein; Subnuclear: http://array.bioengr.uic.edu/subnuclear.htm, ESLpred: http://www. imtech.res.in/raghava/eslpred/, Hum-mPLoc: www.csbio.sjtu.edu.cn /bioinf/hum-m ulti-2/, knowPredsite: http://bio-cluster.iis.sinica.edu.tw/kbloc/, SubLoc: http:// www.bioinfo.tsinghua.edu.cn/ SubLoc/, HSLpred : http:// www. imtech.res.in/ raghava/hslpred/, UniProtKB-SubCell: http://www.uniprot.org/news/ 2007/ 10/23/ release, IMB.The University of Queensland: www.imb.uq.edu.au/.

2.1.4 Cloning and Ligation Reactions

2.1.5 Cloning of *USP32* Gene into pEGFPN1 and pEGFPC1 vectors

The full length and partial fragments (I, II and III) of *USP32* and the position of primers for PCR amplifications are shown in Figure 1. The full and partial fragments of *USP32* CDS were PCR amplified, using primers indicated in Figure 2.1 and High Fidelity DNA polymerase (Roche).

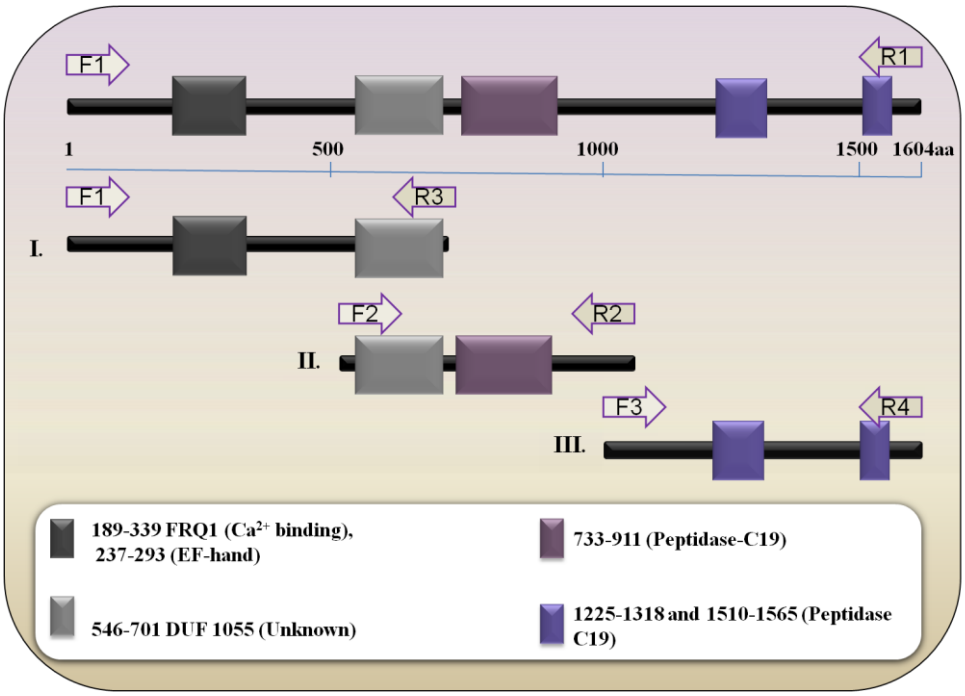

Figure 2. 1 The position of primers for PCR amplification of full length (1604 aa) and partial fragments of USP32 (I: USP32-I. II: USP32-II and III: USP32-III). The sequences of primers are shown in Appendix A.

2.1.5.1 Cloning of USP32-full Length and USP32-I into pEGFPN1

USP32 full length and USP32-I, previously were cloned into PCR® 8/GW/TOPO®TA vector (Invitrogen, as shown in Appendix B). The USP32- PCR® 8/GW/TOPO®TA constructs and pEGFPN1 vector (Clontech, Appendix B) were double digested with Apa1 and Xho1 enzymes. The digestion products were run on and extracted from agarose gel. pEGFPN1 was further treated with Alkaline phosphatase (Roche) and purified, using Phenol:Chloroform:Isoamyl Alcohol. High concentrated T4 DNA ligase (Roche) was used for all ligation reactions.

2.1.5.2 Blunt End Cloning of USP32-II and USP32-III into pEGFPC1

For blunt end ligations, USP32-II and *USP32*-III fragments, previously cloned into PGL3 Vector and pEGFPC1 vector (Clontech, Appendix B), were double digested with Not1 and Sal1 restriction enzymes and incubated for 12-16 h at 37ºC. Double digested constructs and pEGFPC1 vector were further purified, using Phenol:Chloroform:Isoamyl Alcohol method. In order to generate blunt ends, samples were treated with S1 nuclease (Fermentas), prior to gel electrophoresis and gel extraction. Ligation was performed as described above.

2.1.6 Preparation of Competent *E. coli* Cells

A single bacterial colony (*E. coli*), grown on LB-Agar medium (Appendix C) was inoculated into 10 ml of LB medium (Appendix C) in a 50 ml falcon and incubated at 37°C for 12-16 h. 600 µl from overnight growth culture was put in 100 ml LB medium and grown for further 2-3 hours, until OD600 reached to 0.6. After the culture medium reached to the expected bacterial growth density, it was separated into 4 sterile pre-chilled centrifuge tubes. The tubes were placed on ice for 10 minutes and further centrifuged at 4000 rpm for 10 minutes. The supernatant was

discarded from the tubes and the pellet in each tube was resuspended in 5 ml $CaCl_2$ (10 mM, ice cold), on ice and centrifuged for 10 minutes at 3000 rpm at 4°C. The supernatant was discarded and the pellet was dissolved in 1 ml $CaCl_2$ (75 mM, ice cold) and 200 µl of ice-cold glycerol was added. The competent bacterial cells were divided into aliquots and rapidly frozen in liquid nitrogen. The aliquots were kept at -80°C for long term storage.

2.1.7 Transformation of Competent *E.coli* Cells

The chemically competent *E. coli* cells (stored in 10 mM $CaCl_2$ and 20% glycerol, at -80°C) were incubated on ice for 15 min. After cells were thawed, 100 µl competent bacteria were placed in each 1.5 ml eppendorf tube. 5 µl of each ligation reaction and 10-100 ng of control plasmids were added to the reaction tubes and incubated on ice for 30-45 min. The cells were further incubated at 42°C for 45 second and immediately placed on ice. After 5 min, 450 µl S.O.C (Appendix C)/ LB (Luria-Bertani Medium, media were added to each vial. The vials were incubated at 37°C and shaked at 200 rpm for 1 h. 100-400 µl of the transformed cells were cultured in selective LB-Agar plates containing proper selection antibiotics.

2.1.8 Storage of Bacterial Cultures

The bacterial cells were mixed with sterile 60% glycerol in 3:1 ratio (0.75 ml of bacterial culture and 0.25 ml of 60% glycerol) in 1.5 mL tubes. The mixture was gently vortexed and was frozen in liquid nitrogen and then transferred immediately to -80°C for long term storage. For the next use, the frozen surface of the culture was scraped: using a sterile loop and the frozen culture on the loop was inoculated into a new LB medium containing antibiotic. The remaining part of the frozen culture was restored immediately at -80°C, before it was thawed.

2.1.9 Transfection of Mammalian Cells with USP32 Constructs

For localization studies of USP32 cells, 1-3x10^5 HeLa cells were seeded in 6-well tissue culture plates. After 24 h, the complete medium was sucked off from the cells and replaced with fresh complete medium without antibiotic (penicillin-streptomycin). Either Fugene 6 or Fugene HD (Roche) were used for transfecting the cells according to manufacturer's instructions. USP32-full, USP32-I, USP32-II and USP32-III were transfected into cells, using 6:2, 8:2, 9:2 and 11:2 ratios for Fugene (µl): DNA (µg).

2.2 Characterization of miR-125b

2.2.1 Cell Culture and Growing Conditions

MCF10A cell line was obtained from ATCC (LGC Standards GmbH, Germany) and grown in DMEM-Ham's F-12 medium, containing 5% horse serum, 100 mg/ml Epidermal Growth Factor (EGF, Sigma), 1 mg/ml cholera toxin (Sigma), 1 mg/ml hydrocortisone (Sigma) and 10 mg/ml insulin (Sigma). MCF7, MDA-MB-231 and T47D cell lines were a kind gift from Dr. U.H. Tazebay (Bilkent University, Ankara). MCF7 cells were grown in MEM with Earle's salts and 10% FBS. MDA-MB-231 and T47D cells were grown in DMEM, with 10% FBS and 0.1% non-essential amino acids. HDQ-P1, EFM-19 and JIMT-1 cell lines were obtained from DSMZ (Braunschweig, Germany). MDA-MB-361, MDA-MB-453, MDA-MB-468, SKBR3, ZR-75-1 cells were a kind gift from Dr. I.Yulug (Bilkent University, Ankara). EFM-19 and ZR-75-1 cells were grown in RPMI 1640 with 10% FBS, HDQ-P1, JIMT1, MDA-MB-231, MDA-MB-361, MDA-MB-453 and MDA-MB-468 cells were grown in DMEM with 10% FBS and SKBR3 cells were grown in McCoy's medium with 10% FBS. All media contained 1% Penicillin/Streptomycin.

All cell lines were grown as monolayers and were incubated at 37^{o}C with 95% humidified air and 5% CO_2.

All cell lines were grown under the following conditions: frozen vials of each cell type were quickly thawed in a 37°C water bath. After thawing, the cells were plated into a T-25 flask containing pre-warmed (37°C) appropriate growth medium and incubated at 37^{o}C with 95% humidity and 5% CO_2. The cells were washed (after 24 hr) with Hanks' salts solution or Phosphate Buffered Saline (PBS) to get rid of the DMSO (Applichem), used for cell storage at -80°C. After the cells reached to full confluency, they were washed with Hanks buffer, treated with 1 ml trypsin (BioChrom) and cultured in T-75 flasks containing fresh media. Every 2-3 days, the old medium were sucked off from the flasks and replaced with the new medium.

2.2.2 Three-Dimensional (3D) Cell culture and Growing Conditions

3D 'on-top' culturing (Lee et al. 2007), each well of pre-chilled 96-well plate was coated with 15 µl of Engelbreth-Holm-Swarm (EHS, BD Biosciences) extracellular matrix (ECM) extract. 5,000 cells were plated in 96-well tissue culture plates in 30 µl of growth medium and were incubated at 37ºC for 30 minutes. Then, 3 µl of EHS and 30 µl of ice-cold growth medium was mixed and added to each well. The cells were grown in the culture for 24 h and images were taken, using Olympus CKX41 inverted microscope.

2.2.3 RNA Isolation, DNase treatment and cDNA synthesis

Total RNA was isolated from the cell lines, using Trizol RNA isolation reagent (Invitrogen), when they were ~70% confluent. The cultured cells in the T-75 flasks were treated with 8 ml Trizol and incubated at room temperature to allow the nucleoprotein complexes to be completely dissociated. After 5 minutes, the cells

were transferred to a 15 ml sterile centrifuge tube and 0.2 ml of chloroform per 1ml of Trizol (total of 1.6 ml chloroform/ T75 flask) was added. The tubes were shaked vigorously for 15 seconds and incubated at room temperature. After 2-3 minutes, samples were centrifuged at 4700g for 20 minutes at 8ºC. The aqueous phase, nearly equal to 60% of the original Trizol volume, which contained the total RNA, was transferred to a fresh sterile tube and 4 ml isopropyl alcohol (0.5 ml per 1ml of Trizol) was added in order to precipitate the RNA. After 10 minutes incubation at room temperature, samples were centrifuged at 4700g for 20 minutes at 8ºC. The RNA pellet was washed with 70% ethanol (8 ml) and further centrifuged at 4700g for 7 minutes at 8ºC. Finally, the air-dried RNA pellets were dissolved with RNase free water (50-100 µl).

Total RNA from the cells was also isolated using High Pure RNA isolation kit (Roche), according to manufacturer's instruction. Quantity and purity of RNA was determined using Nanodrop. After using either of the RNA isolation methods, DNase treatment was performed. For DNase treatment, 10-50 µg isolated total RNA samples were treated with 10 units of recombinant DNase I (Roche,) and incubated at 37ºC for 1 hour. Phenol:Chloroform:Isoamyl Alcohol (25:24:1, v/v) extraction was performed in order to purify the samples. In brief, same volume of acidic Phenol:Chloroform:Isoamyl Alcohol was added to samples and centrifugation at 13,000g for 20 min at 4ºC was carried out after vortexing and incubating the samples on ice for 10 min. The upper phase, containing RNA, was collected in 1.5 ml eppendorf tubes and incubated over night at -20ºC after addition of 3 volume 100% ethanol and 1/10 volume NaAc (3 M). The tubes were centrifuged at 13,000g for 20 min at 4ºC and the pellet was washed with 70% ethanol. The pellets were air-dried and re suspended in 25-50 µl RNase free water after centrifugation at 14,000 rpm for 20 min at 4ºC. Lack of DNA contamination was further tested by PCR.

cDNA was synthesized from isolated RNA samples, using Revert Aid First Strand cDNA Synthesis Kit (Fermentas), according to manufacturer's guidelines. In brief, total 1 µg total RNA and 0.5 µg oligo (dT) or Random Hexamer (RH) primers (provided by the kit) and 10 µ1 DEPC-treated water were mixed gently and spun down for 3-5 seconds in a micro centrifuge. Then the tube was incubated at 70°C for 3 minutes and chilled on ice. The tube was briefly centrifuged and again placed on ice. 4 µ1 of 5X reaction buffer, 1 µ1 of Ribo lock Ribo nuclease inhibitor (20 U/µ1) and 2 µ1 of 10 mM dNTP mix were added and the tube was briefly mixed and centrifuged. The reaction was incubated for 5 minutes at 37°C followed by the addition of 1 µ1 of RevertAid M-MuLV Reverse Transcriptase (200U/µ1) to the mixture. The reaction was incubated at 42°C for 60 minutes and stopped by incubating the mixture at 70°C for 10 minutes. The tube was chilled on ice and the cDNA was stored at -20°C.

For mature miRNA quantification experiments, cDNA was synthesized from RNA samples, isolated via Trizol, as mentioned above. Briefly, RNA was isolated from 1 well of 6-well plate. A total of 15 µL cDNA was synthesized from each sample (using Taqman miRNA reverse transcriptase kit, catalog number: 4366596) from 100 ng total RNA, using miR-125a, miR-125b and U6 specific stem loop RT (Reverse Transcribe) primers (TaqMan ® MicroRNA Assays, Assay ID 000448 and ID 000449 for miR-125a and miR-125b, respectively and TaqMan ® MicroRNA Assays, Assay ID: 001093 for *RNU6B* as reference gene).

2.2.4 Polymerase Chain Reactions (PCRs)

2.2.4.1 RT-PCRs

RT-PCRs were performed, using Taq DNA polymerase (Fermentas and AppliChem), according to manufacturers' instructions. The thermal conditions for

PCRs are given in Figure legends for each experiment. The total volume for PCR reactions were 30 µL.

2.2.4.2 Quantitative RT-PCRs for Mature miRNA Detection

To detect the mature levels of miR-125, Taqman assay kit (Applied Biosystems) was used according to manufacturer's instructions for PCR amplifications. In brief, 1.33 µl of synthesized cDNA, as mentioned above was used in each PCR reaction (in 20 µl) containing 2X Taqman PCR mastermix (TaqMan ® Universal PCR Master Mix, No AmpErase ® UNG, 200 Rxn, Cat #: 4324018) and 20X miRNA assay mix (specific for miR-125a, miR-125b and RNU6B). PCR reactions were performed in 10 µl. The qRT-PCRs were run on Corbett Rotor-Gene 6000 (Qiagen, Corbett, Germany). PCR conditions were: initial denaturation at 95^{o}C for 15 min, followed by 40 cycles at 95^{o}C for 15 s and 60^{o}C for 60 s. *RNAU6B* was used as a reference gene. To calculate expression level of mature miRNAs, ΔΔCt method was used (Livak and Schmittgen 2001). Each experiment was run in 3 biological replicates.

2.2.5 Phalloidin and DAPI Staining

$3x10^5$ stably transfected MCF7 cells were seeded and grown on 25x25 mm cover slips in 6-well tissue culture plates. After 24 h, cells were washed in PBS and fixed in 3.7% formaldehyde solution in PBS for 5 minutes. Fixation was stopped by adding 0.1 M glycine in PBS for 5 minutes. Cells were permeabilized for 1 min in 0.1% Triton X-100 (Sigma). For filamentous actin staining, fixed and permeabilized cells were incubated with 40 µM phalloidin (Fluorescin Isothiocyanate, Sigma, Cat #) staining solution in PBS for 40 minutes at room temperature. Nuclei were stained with 30 nM DAPI solution (Invitrogen), at room

temperature for 5 minutes. After washing the cover slips several times in PBS, images were captured, using Zeiss LSM 510 with 40X oil objective (Central Lab, METU). Image quantification (area occupied by protrusions per cell outline in pixels) was done by S.CO LifeScience (Germany).

2.2.6 Transfection of Mammalian Cells

To generate stable cell lines that express miR-125b, either miR-125b1-pSUPER construct or empty pSUPER vector was transfected into T47D cells by Fugene HD (3:2, Fugene:DNA ratio), according to manufacturer's instructions. Stable cell lines were selected, using 500 µg/ml of G418 (Roche). Polyclonal cells were expanded, continuously using G418 at final concentration of 250 µg/ml, after all mock transfected control cells were killed.

For *ARID3B* silencing, ARID3B-short hairpin RNA (shRNA) and non specific control (with no homology to human genome) oligos (IDT), were cloned (previously in our lab) into pSR-GFP/Neo (pSUPER) vector, were transiently transfected to MCF7 cells, using Fugene-HD transfection reagent (3:2, Fugene:DNA ratio), according to manufacturers' guidelines.

For transfection of anti-miR-125 and control oligos (22-24 bases), 2'-*O*- methyl oligos were used to inhibit miR-125a (5'-UCACAGGUUAAAGGGU CUCAGGGA-3', IDT) and miR-125b (5'-UCACAAGUUAGGGUCUCAGGGA-3', IDT). As a negative control, nonspecific 2'- *O*- methyl oligonucleotide (5'-AAGCGAAGCAGUGCGUCAAGUA-3', IDT) was used. Fugene-HD (Roche) was used (6:2 Fugene: oligo ratio) for transfections. Oligo final concentrations were 1.5 µg/ml. The final concentration of these oligos for luciferase assay was 100nM. Transfection was confirmed by Taqman qRT-PCR to detect mature miR-125 after anti-miR oligo transfection.

2.2.7 Functional Assays

2.2.7.1 Cell Proliferation Assay (MTT)

Cell proliferation assay, based on MTT (Methylthiazole Tetrazolium) via metabolically active cells was performed for miR-125 expressing breast cancer cells. $1x10^4$ MCF7 and T47D cells, stably transfected with miR-125b or control vector were seeded into each well of 96 well tissue culture plates in a final volume of 100 µl complete growing media. The MTT labeling reagent (5 mg/ml MTT in PBS) was added to the cells between 1- 9 days. The cells were incubated with MTT labeling reagent for 4 h. The absorbance was detected at OD570 nm after overnight solubilization with a 1% solution of SDS.

For transient *ARID3B* silencing, $1.5x10^4$ MCF7 cells were seeded per each well of 96 well plate and transfected 24 h after seeding. MTT assay was performed as mentioned above. Absorbance at OD570 was measured 72 h after transfection.

2.2.7.2 Migration Assay

For investigating the migration property of MCF7-125 and MCF7-EV cells, approximately $1x10^6$ cells were pre-starved in MEM-Earle's medium with 1% FBS in a T-25 tissue culture flask. After 24 h of serum starvation, cells were rinsed with Hanks salt solution and trypsinized. Growing medium containing FBS was used for neutralizing the trypsin and cells were harvested after centrifugation at 1,000g for 5 min. Cells were washed with Hanks salt solution to wash the FBS and 200,000 cells in 0.1 ml MEM-Earle's medium with 1% FBS were plated on the upper wells of transwell migration chambers (Corning). Medium containing 10% FBS was added to lower wells. Cells were allowed to migrate through an 8 µm pore membrane for 24 h. Cells on the upper surface of the membrane were removed by scrubbing with

sterile cotton swabs. 100% methanol was used to fix cells on the lower surface of the membrane for 10 minutes. Fixed cells were stained with Giemsa for 2 minutes and membranes were washed twice (or more) with distilled water. Cells on the lower side of the membrane were documented and counted under a Leica light microscope (10X objective). 3 random fields were counted per membrane and 6 membranes in 3 independent experiments were used.

To perform migration assay for MCF7 cells treated with anti-125b and control oligos, MCF7-125 cells were transfected with 1.5 μg/mL anti-125b and nonspecific control oligos (in medium containing 1% FBS), using Fugene HD (6:2 Fugene:oligo ratio). After 24 h, 200,000 cells in 0.1 ml MEM-Earle's medium with 1% FBS were plated on the upper wells of transwell migration chambers. Medium with 10% FBS was added to the lower wells. Cells were allowed to migrate for 24 h. 6 membranes were used in 3 independent experiments. The cells on the lower side of the membrane were stained and counted as mentioned above.

For investigating the migration properties of MCF7 and SKBR3 cells in the presence of AG825, SKBR3 and MCF7 cells, cultured in T25 tissue culture flasks, were pre-starved in McCoy's 5A modified and MEM-Earle's media with 1% FBS, respectively (approximately at 60-70% confluency). After 24 h, 200,000 cells in 0.1 ml medium containing 1% FBS and AG825 at final concentration of 50 μM (Tocris Bioscience) or DMSO were plated on the upper wells of transwell migration chambers. Medium containing 10% FBS was added to lower wells. Cells were allowed to migrate through an 8 μm pore membrane for 24 h. a total of 6 membranes in 2 independent experiments were used. The cells on the lower side of the membrane were stained and counted as mentioned above.

To test the migration rate of *ARID3B* silenced cells, MCF7 cells were harvested 8 h after transfection. 30,000 cells were plated on the transwell migration chamber in MEM-Earle's medium with 10% FBS and cells were allowed to migrate for 72 h

through an 8 µm pore membrane. Membranes were stained and cells on the lower side of the membrane were counted. Four membranes were used for each sample.

2.2.8 Protein Isolation

The whole cell extracts were prepared from cells, once they reached to approximately 70-80% confluency. Cells were washed with ice-cold PBS and incubated with RIPA buffer (0.5 ml/T75 tissue culture flask), containing 150 mM NaCl (Sigma), 50 mM Tris (Sigma) 1% Triton X-100 (Sigma), 0.5% Sodium deoxcholate (Sigma), 0.1% SDS (Sigma), Protease inhibitor cocktail (Roche) and PhosSTOP (Roche) for 15 minutes at 4^{o}C on a shaker. The cells were further scraped off the flasks by a cold plastic cell scrapper and were gently transferred to a 1.5 ml tube and centrifuged at 14,000 rpm for 15-30 min. Supernatants were collected and stored at -80^{o}C. Protein concentrations were determined using BCA protein assay, according to the manufacturers' instruction (Pierce).

2.2.9 Western Blotting

Fifty µg protein sample was denatured in 6X Laemmli buffer (12% SDS, 30% 2-mercaptoethanol, 60% Glycerol, 0.012% bromophenol blue, 0.375 M Tris) at 100^{o}C for 5 min. The proteins were run on an 8% SDS-polyacyrlamide gel at 100-120 v for 1.5- 2.5 h (depending on the size of the proteins) and were transferred to PVDF membranes (Roche), in the presence of transfer buffer at 100 v for 1.5 h. Membranes were blocked for 1 hour at room temperature in Tris Buffer Saline Tween (TBST), (20 mM Tris, 137 mM NaCl, pH: 7.6, 0.1% Tween 20) with 5% non-fat dry milk (Biorad) for ARID3B detection, 2.5% non-fat dry milk (Biorad) for ERBB2 detection, and 10% skim milk (Fluka) for pERK1/2 detection and 2.5% non-fat dry milk (Biorad,) for ALCAM detection. The membranes were then respectively incubated for 16 h at 4^{o}C with: rabbit polyclonal anti-ARID3B

antibody (1:1500, Abcam) in 5% non-fat dry milk- 0.1% TBST, mouse monoclonal anti-ERBB2 antibody (1:250, Leica) in 2.5% non-fat dry milk- 0.1% TBST, rabbit polyclonal anti pERK 1/2 (1:250, Santa Cruz) in 10% skim milk- 0.1% TBST and mouse monoclonal anti- ALCAM antibody (1:500, Leica) in 2.5% non-fat dry milk-0.1% TBST. All membranes were washed three times with 0.1% TBST, and incubated for 1 hour with peroxidase conjugated mouse anti-rabbit antibody (1:2000, Santa Cruz) in 5% non-fat dry milk-0.1% TBST, peroxidase conjugated goat anti-mouse antibody (1:2000, Santa Cruz), in 2.5% non-fat dry milk-0.1% TBST and peroxidase conjugated mouse anti-rabbit antibody (1:2000, Santa Cruz) in 10% non-fat dry milk-0.1% TBST, respectively. After washing the membranes three times with 0.1% TBST (10 min for each wash), antigen-antibody complexes were visualized with the enhanced chemiluminecence kit (Pierce) by exposure to X-ray films (Kodak). ARID3B antibody detected a 61 kDa band along with a band of unknown identity at around 50 kDa (not shown). The blots were then stripped and hybridized with monoclonal goat anti-mouse β-actin antibody (1:1000, Santa Cruz) in 5% BSA (Roche)-0.1% TBST, and with secondary anti-mouse antibody (1:2000, Santa Cruz) in 5% BSA-0.1% TBST. Antigen-antibody complexes were visualized as described above. β-Actin antibody detected a 43 kDa band. ImageJ program (http://rsb.info.nih.gov/ij/) was used for densitometric quantification of the bands. The appropriate protein marker was used as shown in Appendix D.

2.2.10 Bioinformatics Tools for Prediction of miR-125 Targets

TargetScan (http://www.targetscan.org/), PITA (http://genie.weizmann.ac.il/pubs/mir07/mir07_data.html), Pic Tar (http://pictar.mdc-berlin.de/), FindTar3 http://bio.sz. Tsinghua .edu.cn/) and miRanda (http://www.microrna.org/ microrna /home.do) programs were used for the prediction of miR-125 targets.

2.2.11 miR-125b's Predicted Target Cloning

In order to find targets of miR-125b, we used bioinformatics tools and selected three potential targets of miR-125b: v-ets erythroblastosis virus E26 oncogene homolog 1 (*ETS1),* Homeobox B7 (*HOXB7)* and zinc finger and BTB domain containing 7A (*ZBTB7A*, aka *FBI-1*) The 3'-UTR of these genes, (containing predicted poorly conserved and conserved miR-125 binding sites) were cloned into pmiR-REPORT vector (Ambion, Appendix B) for performing luciferase assay in miR-125b transfected cells. For this purpose, specific primers, containing *SacI* (in forward primer) and *HindIII* (in reverse primer) restriction digest sites and Expand High Fidelity Polymerase (Roche,) were used for PCR amplification. The cloned constructs were confirmed by colony PCR, restriction digestion and sequencing (Iontek and MCLAB companies). The 3'-UTR sequence of *ARID3B*, predicted to be targeted by miR-125b, was previously in our lab cloned downstream of luciferase gene in pmiR-REPORT vector as described above and used in luciferase assay.

2.2.12 Dual Luciferase Reporter (DLR) Assay

To investigate the regulatory effect of miR-125b on the 3'-UTR of its predicted targets, we cloned the 3'-UTR of targets, downstream of Firefly luciferase gene in pMIR REPORT vector (Ambion, Appendix B). phRL-TK vector (Promega), shown in Appendix B, containing Renilla luciferase was used as internal control. Dual-Luciferase reporter assay kit was used (Promega,) and the assay was performed in 24-well tissue culture plates, according to manufacturer's guidelines. Briefly, 24 h after transfection, cells were lysed in 100 µl of passive lysis buffer and 10 µl from cell lysates were added to 96-well tissue culture plates and used for detecting the activity of Firefly and Renilla luciferase activities by adding LAR II and Stop& Glo reagents respectively. Modulus Microplate Multimode Reader (Turner Biosystems, USA) instrument was used.

CHAPTER 3

RESULTS

3.1 Subcellular Localization of USP32 Protein

3.1.1 Predictions for Subcellular Localization of USP32 Protein

Revealing the localization of a protein may provide information on the possible function of that protein. Therefore, there are various bioinformatics tools, based on different algorithms, used to predict the subcellular localization of uncharacterized proteins. However, experimental confirmation, as expected, would be needed to validate such bioinformatics predictions.

USP32, Ubiquitin Specific Protease 32, as a potential oncogene candidate was first investigated bioinformatically to predict localization sites in the cell. To achieve this, we used Subnuclear, ESLpred, Hum-mPLoc, knowPredsite, SubLoc, HSLpred, UniPortKB- SubCell and IMB, from the University of Queensland prediction programs (Table 3.1).

Table 3. 1 Predictions for subcellular localization of USP32 protein obtained from bioinformatics tools.

Predictor	Cyto-Plasm	Nucleus	Golgi	PML Body	Lysosome	Mitochondria	References
Subnuclear	-	-	-	+	-	-	1
ESLpred	-	+	-	-	-	-	2
Hum-mPLoc	-	-	-	-	+	-	3, 4, 5, 6 and 7
knowPredsite	-	-	+	-	-	-	8 and 9
SubLoc	+	-	-	-	-	-	10
HSLpred	+	-	-	-	-	-	11
UniProtKB-SubCell	-	-	+	-	-	-	(EBI), (PIR), (SIB)
IMB.The University of Queensland	-	-	+	-	-	-	12

1. (Lei and Dai 2005), 2. (Bhasin and Raghava 2004), 3.(Shen and Chou 2009), 4. (Chou and Shen 2008), 5. (Shen and Chou 2007), 6. (Chou 2005), 7. (Shen and Chou 2006), x8. (endnote problem add by hand), 9. (Pierleoni et al. 2007), 10. (Hua and Sun 2001), 11. (Garg et al. 2005), 12. (Yuan and Teasdale 2002), EBI:European Bioinformatics Institute, PIR: Protein Information Resource, SIB :Swiss Institute of Bioinformatics.

Different protein localization programs revealed diverse predictions for USP32 protein localization. ‘’Subnuclear’’ predicted PML body localization, ‘’SubLoc’’ and ‘’HSLpred’’ programs predicted a cytoplasmic localization, ‘’ESLpred’’ predicted nucleus localization, ‘’knowPredsite’’, ‘’UniPortKB- SubCell’ and ‘’IMB’’ (from the University of Queensland) predicted a Golgi localization and ‘’Hum-mPLoc’’ predicted lysosome localization for this protein. As different results were obtained, using these prediction programs, to find the exact localization of USP32 inside the cell, we further performed subcellular localization studies as mentioned in the following sections.

3.1.2 Cloning of *USP32* into Reporter Plasmids

In order to investigate the subcellular localization of USP32 protein inside the cell, we cloned the full length of *USP32* coding sequence into pEGFPN1 (Clontech) vector (Appendix B). In addition, to find the responsible sequence for localization of USP32 protein, the full length coding sequence of USP32 was divided into 3 partial and overlapping fragments (USP32-I, USP32-II and USP32-III), containing the sequences for different domains of USP32 protein and the sequences were cloned into pEGFPN1 and pEGFPC1 vectors (Appendix B).

The position of full length and fragments of *USP32* and the primers, used for PCR amplification of these sequences are shown in Figure 3.1.

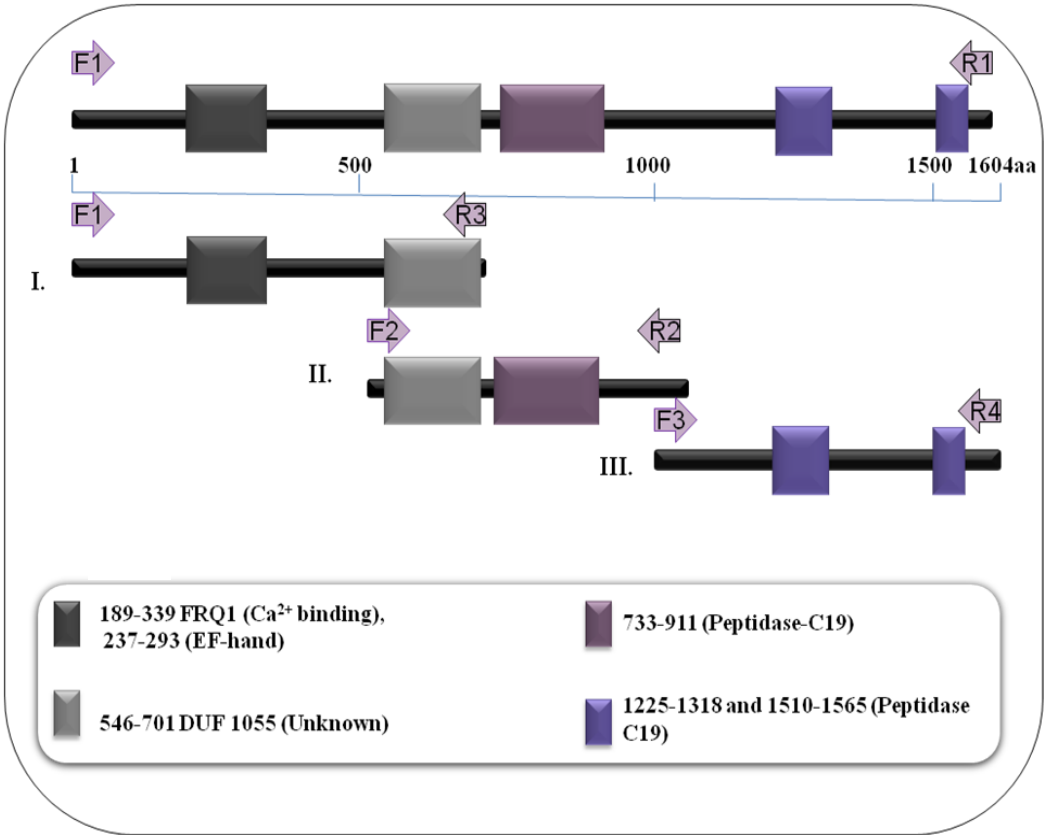

Figure 3. 1 Position of the domains of USP32 protein (Accession number: AAM97922) and primers, used for PCR amplification of full length and USP32-I (I), USP32-II (II) and USP32-III (III) fragments of *USP32*. According to NCBI (National Center for Biotechnology Information), conserved domain database, USP32 protein contains 5 domains: Ca^{2+} binding and EF-hand domains from 189-339 and 231-293 amino acids (aa), DUF 1055 domain from 546-701 aa, found in Ubiquitin Specific Proteases with an unknown function and 3 peptidase domains from 733-911, 1225-1318 and 1510-1565 amino acids. The sequences for the primers are given in Appendix A.

3.1.2.1 Sticky End Cloning of Full Length *USP32* and USP32- I Coding Sequences into pEGFPN1 Vector

To investigate the localization of full USP32 protein, the full length *USP32* coding sequence (from bases 1-4812) was PCR amplified, using specific forward and reverse primers containing *Xho1* and *Apa1* restriction sites respectively. The PCR product was cloned into TOPO-TA vector and sequenced. This construct was further digested with *Xho1* and *Apa1* restriction enzymes and ligated into pEGFPN1 vector (digested with the same restriction enzymes: *Xho1* and *Apa1*), as mentioned in Figure 3.2A, B and C.

pEGFPN1 vector (Appendix B) contains the sequence for expressing Enhanced Green Fluorescence Protein (EGFP), just downstream of its Multiple Cloning Site (MCS). Consequently, USP32-EGFP fusion protein contains USP32 at N-terminus (amino-terminus) and EGFP at C-terminus (carboxyl-terminus).

A.

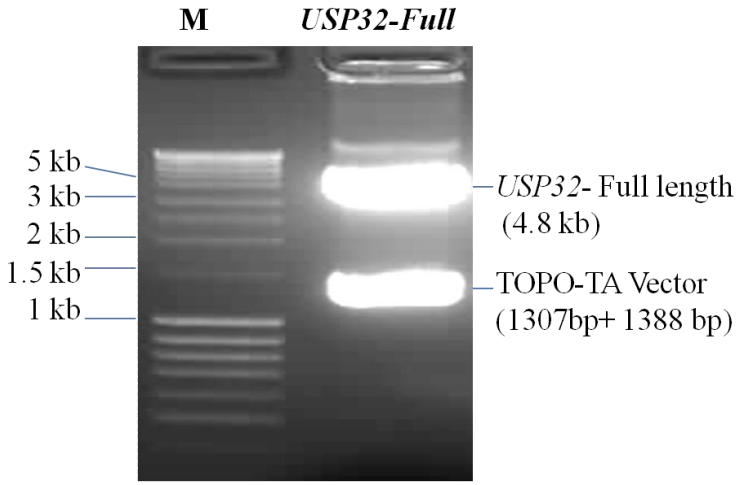

B.

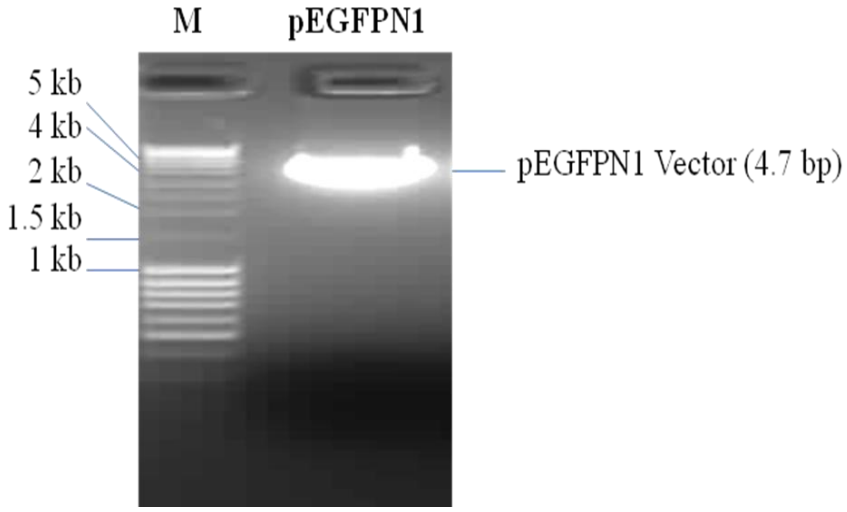

Figure 3. 2 Double digestion of USP32-Full-TOPO and pEGFPN1 vectors with Xho1 and Apa1 restriction enzymes**. A.** Double digestion of *USP32*-Full-TOPO construct with *Xho1* and *Apa1* restriction enzymes, resulted with 4 digested fragments of 104 (run fast and left the gel), 1307, 1388 bp and 4008 bp. **B.** Double digestion of pEGFPN1 vector with *Xho1* and *Apa1* restriction enzymes generated a sticky end digested vector.

The sticky end products from double digestion with *Xho1* and *Apa1* restriction enzymes (Figure 3.2), were extracted from agarose gel and ligation reactions were set up to generate USP32-GFP fusion construct. The generated construct was further confirmed by restriction digestion (Figure 3.3).

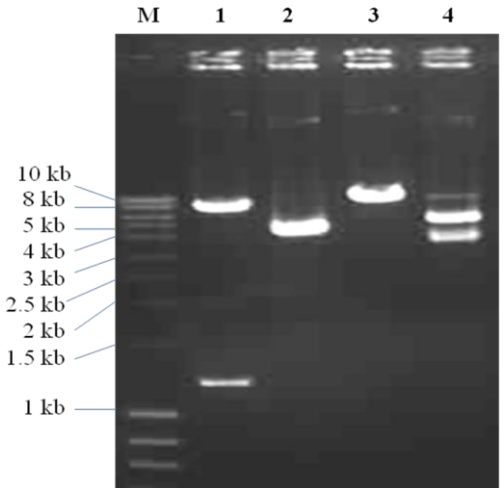

Figure 3. 3 Confirmation of cloning for USP32-Full-pEGFPN1 construct. M: MassRuler marker, lane 1: digested with *BamH1* (expected sizes: 1.218+8.297 kb), lane 2: double digested with *Xho1* and *Apa1* (expected sizes: 4.812+4.7 kb), lane 3: digested with *Xho1* (expected size: 9.5 kb) and lane 4: double digested with *Xho1-Not1* (expected sizes: 5.614+3.9 kb). M: MassRuler marker.

The sizes obtained from digestion product were correct and USP32-Full-pEGFPN1 construct was further used in the experiments.

To investigate the localization of USP32-I, the sequence (from bases 1-2199 of *USP32* coding sequence) was PCR amplified, using specific forward and reverse primers containing *Xho1* and *Apa1* restriction sites respectively. The PCR products were cloned into TOPO-TA vector, sequenced, digested, finally cloned into pEGFPN1 vector and confirmed by restriction digestion (Figure 3.4 A, B and C).

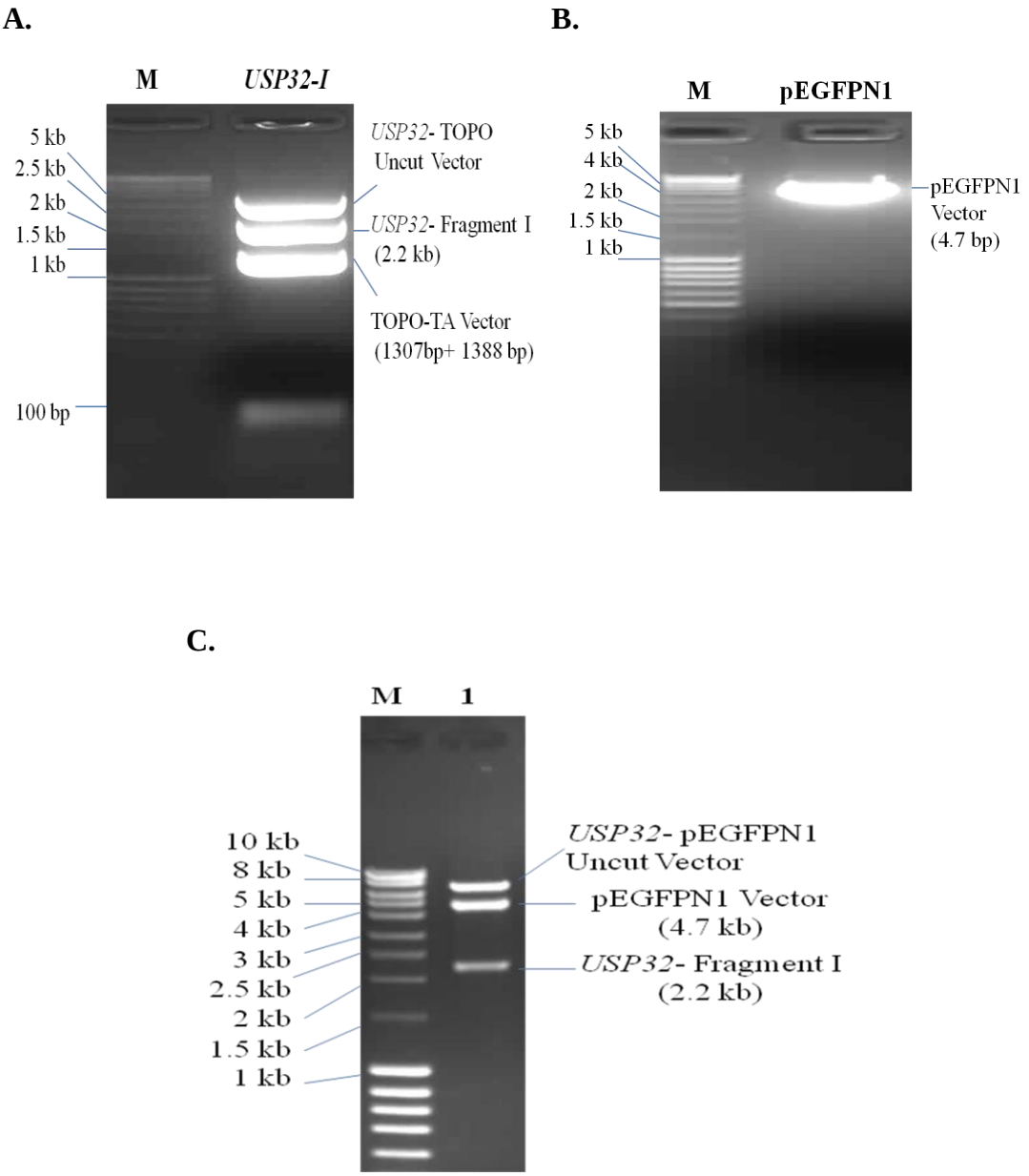

Figure 3. 4 A. Double digestion of USP32-I-TOPO construct with *Xho1* and *Apa1* restriction enzymes, resulted with 4 digested fragments of 104, 1307, 1388 bp and 2200 bp. **B.** Double digestion of pEGFPN1 vector with *Xho1* and *Apa1* restriction enzymes generated sticky ends. **C.** USP32-I-pEGFPN1 construct, double digested with *Xho1* and *Apa1* restriction enzymes: expected sizes: 2.2 kb for insert and 4.7 kb for vector. M: MassRuler marker.

The sizes after digestion confirmed that we cloned and obtained the correct construct to be further used in experiments.

3.1.2.2 Blunt End Cloning of USP32-II and USP32-III Coding Sequences into pEGFPC1 vector

In order to investigate which part of USP32 is responsible for the localization of this protein, we cloned the two other fragments of USP32: USP32-II (from bases 1500-3300 of *USP32* coding sequence) and USP32- III (from bases 3000-4812 of *USP32* coding sequence), as shown in Figure 3.1, into pEGFPC1 vector. The mentioned fragments were previously cloned into pGEX-4T-2 vector, sequenced, digested and further were cloned into pEGFPC1 vector, using blunt end cloning method. For this purpose, USP32-II-pGEX-4T-2 and USP32-III-pGEX-4T-2 constructs were digested with *Sal1* and *Not1* and pEGFPC1 vector was digested with *Sal1* restriction enzymes (Figure 3.5 A and B). All digestion products, which contained sticky end DNA at their ends, were further digested with *S1 nuclease* enzyme (to produce blunt end DNA) and used in ligation reactions.

To confirm the direction of inserts, colony PCRs and restriction digestions were performed (Figures 3.6 and 3.7).

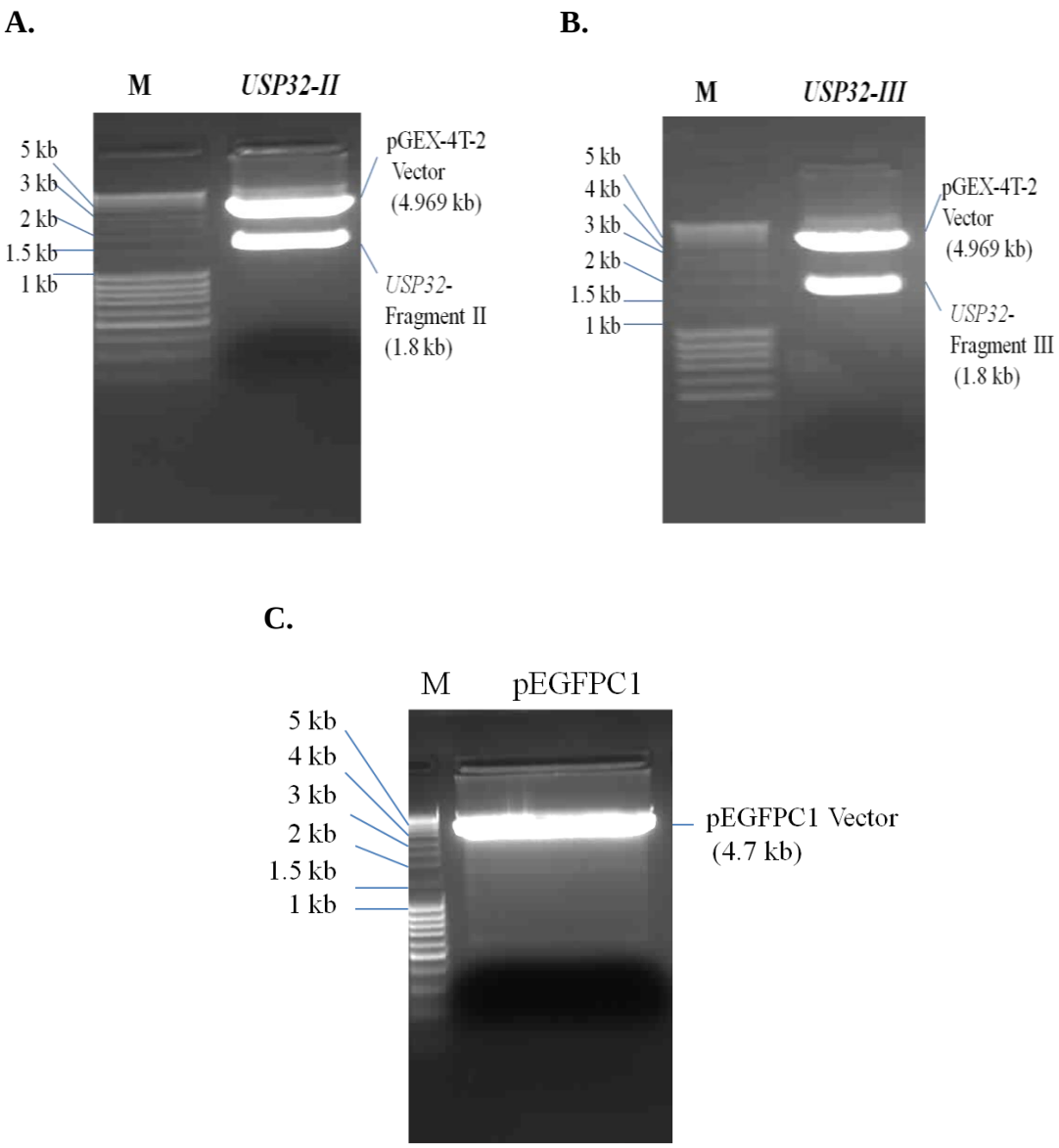

Figure 3. 5. Digestion of USP32- II- pGEX-4T-2 and USP32- III- pGEX-4T-2 constructs and pEGFPC1 vector with restriction enzymes. **A.** Double digestion of USP32- II- pGEX-4T-2 construct with *Sal1* and *Not1* restriction enzymes (expected sizes: 4.969 kb and 1.8 kb), **B.** Double digestion of USP32- III- pGEX-4T-2 construct with *Sal1* and *Not1* restriction enzymes (expected sizes: 4.969 kb and 1.8 kb). **C.** Digestion of pEGFPC1 vector with *Sal1* restriction enzyme (expected size: 4.7 kb).

A.

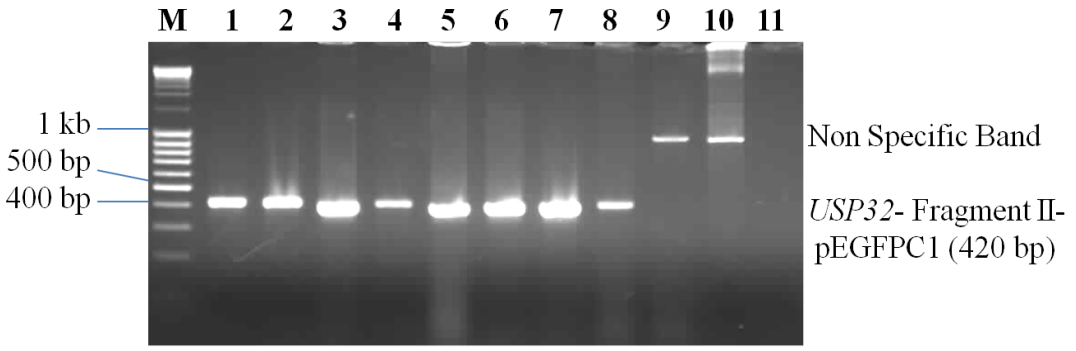

B.

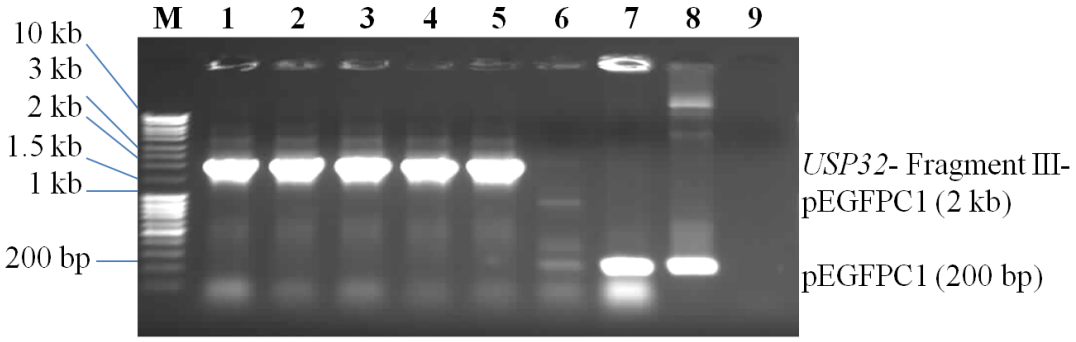

Figure 3. 6 Colony PCR for confirming the cloning of USP32-II and USP32-III fragments into pEGFPC1 vector. **A.** Cloning of USP32-II fragment into pEGFPC1 vector was confirmed, using 7F-CDS (insert specific) and SC1-R (vector specific) primer set (Appendix A). M: MassRuler, 1-8: name of colonies, 9: no insert control of cloning, 10: pEGFPC1 control and 11: PCR negative control. **B.** Cloning of *USP32*-III fragment, into pEGFPC1 vector was confirmed, using SC1F (vector specific) and SC1-R (vector specific) primer set (Appendix A). M: MassRuler, 1-6: name of colonies, 7: no insert control of cloning, 8: pEGFPC1 control and 9: PCR negative control. Sizes correspond to correct constructs: for USP32-II: 420 bp and for USP32-III: 2000 bp). PCRs were performed using initial denaturation at 95ºC for 2 min, followed by 30 cycles at 95ºC for 30 seconds (denaturation), 56ºC for 30 seconds (annealing) and 72ºC for 1 min (elongation). A final extension at 72 ºC for 10 min was used.

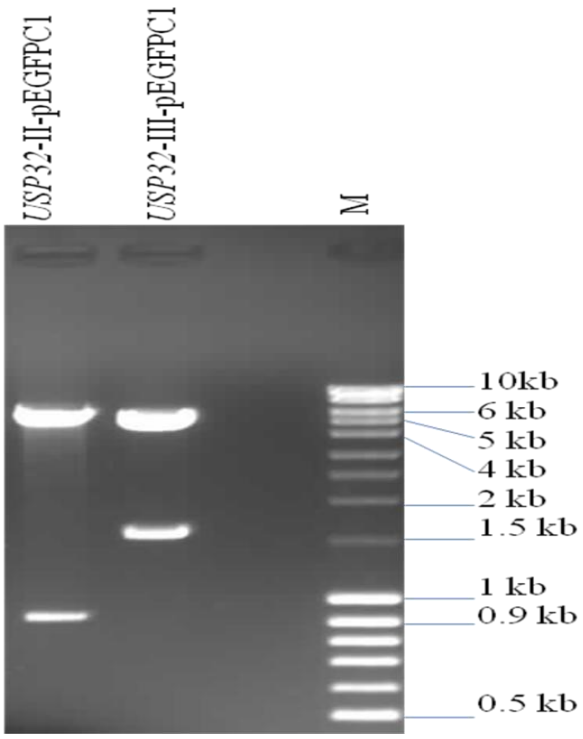

Figure 3. 7. Restriction digestion to confirm the cloning of USP32-II and USP32-III fragments into pEGFPC1 vector. Lane 1: USP32-II-pEGFPC1 construct, digested with *Hind III* restriction enzyme and expected sizes after digestion for the correct insertions are 921 bp + 5579 bp. Lane 2: USP32-III-pEGFPC1 construct, digested with *EcoRI* and expected sizes after digestion for the correct insertion are 1542 bp + 4958 bp. M: MassRuller.

As a result, we generated and confirmed the correct constructs to be further used in experiments.

3.1.3 Subcellular Localization of *USP32*- Full- EGFPN1 Fusion Protein

Finding the subcellular localization of a protein may help us understand the function of that protein. For this purpose, we performed FPP assay to reveal the topology of USP32-EGFP fusion protein inside the living cells (Lorenz et al. 2006). Permeabilization of plasma membrane (which is rich in cholesterol) with digitonin, followed by protease treatment, reveals the location of the protein by following the fluorescence signal released from the cells. This assay determines if a protein is cytoplasmic or membrane bound and in the case if it is attached to a membrane inside the cell, which terminus of the protein is facing the cytoplasm and lumen. Our purpose was to investigate the USP32 localization, using this assay. We transfected the USP32 cloned constructs (pEGFPN1-USP32-Full, pEGFPN1-USP32-I, USP32-II-pEGFPC1, USP32-III-pEGFPC1) into HeLa cells. Assay was performed 20-24 h after transfection. Before taking the images, we performed photo bleaching test for cells expressing EGFP to make sure that the loss of signal after cell permeabilization was not due to photo bleaching. The FPP assay for full CDS USP32-EGFP fusion protein is shown in Figure 3.8.

A.

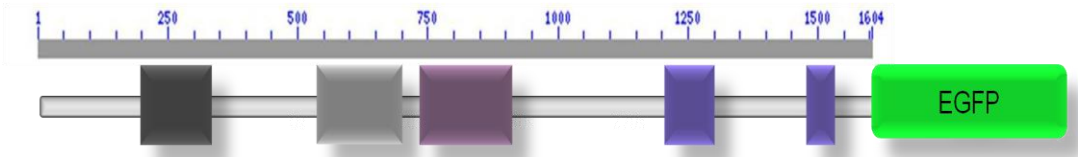

B.

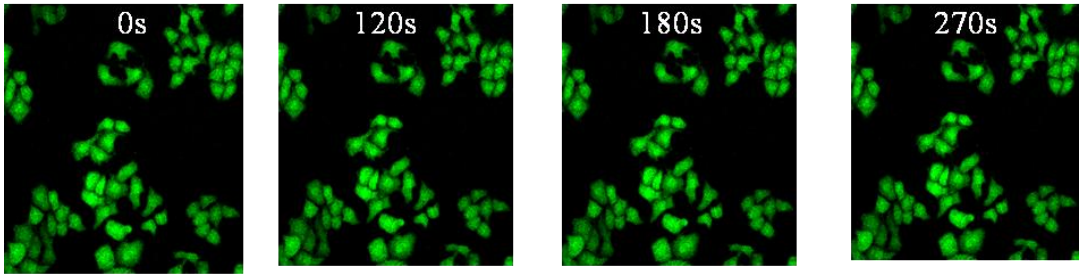

C.

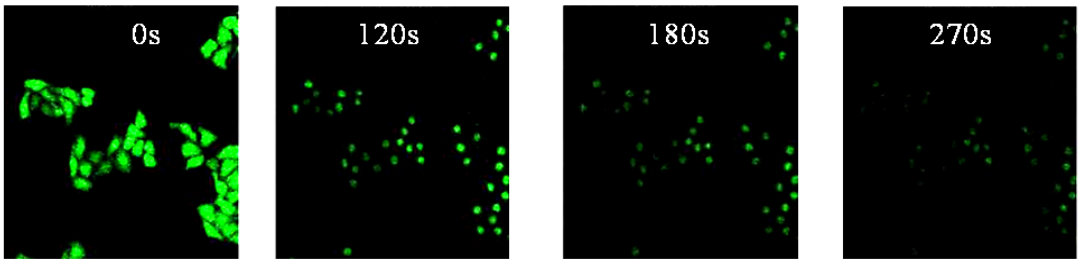

D.

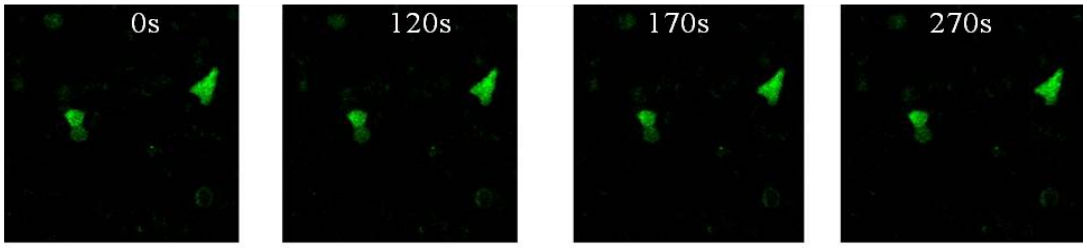

Figure 3. 8 Fluorescence protease protection assay for USP32-Full-pEGFP fusion protein in HeLa cells.

E.

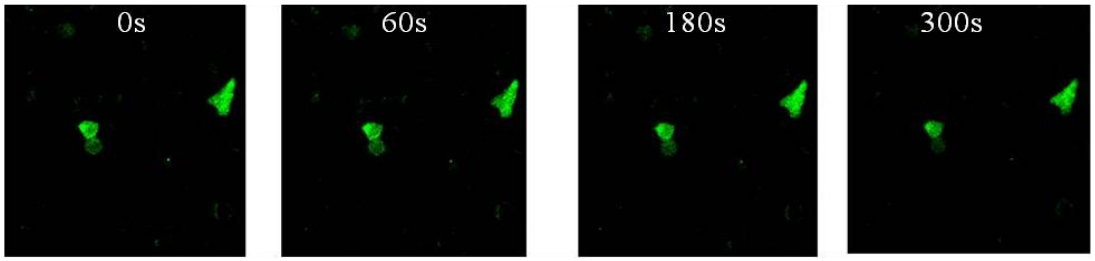

Figure 3. 8 (Continued) Fluorescence protease protection assay for USP32-Full-pEGFP fusion protein in HeLa cells. **A.** The schematic of USP32-Full-EGFP fusion protein. **B**. Photo bleaching control for pEGFPN1 vector after 0, 120, 180 and 270 s exposure to fluorescence beam of 488 nm wavelength. **C** and **D**. Permeabilization of EGFP and USP32-Full-EGFP expressing HeLa cells, respectively with 20 μM digitonin, documented at 3 different time points, after treatment. **E.** Protease treatment of USP32-Full-EGFP expressing HeLa cells, 0, 60, 180 and 300 s after treatment with 6 mM trypsin. Images (20X) were captured, using Zeiss LSM 510 microscopy (Central Lab, METU).

Results from Figure 3.8B, revealed no photo bleaching of EGFP protein, 270 s after exposure to a wavelength of 488 nm. In Figure 3.8C, Hela cells, transfected only with empty pEGFPN1 vector were treated with 20 μM digitonin for permeabilizing the cell membrane. The fluorescence signal was gradually lost after 120 s and was completely lost after 270 s treatment, indicating that EGFP protein, as is already known, is a soluble (not membrane bound) protein. In Figure 3.8D, USP32-Full-EGFP expressing HeLa cells, treated with 20 μM digitonin, indicated no fluorescence signal loss even at 270 s after permeabilization with digitonin. This result showed that USP32 protein was not a cytoplasmic or soluble protein: but rather, possibly a membrane/organelle bound protein. In Figure 3.8E, in order to find the orientation of the (membrane) bound protein, (whether the C-terminus of the fusion protein (EGFP) was faced the cytoplasm in the case if it is a membrane bound protein), the permeablized USP32-Full-EGFP expressing HeLa cells were

treated with 6 mM trypsin. Theoretically, as trypsin is a serine protease and cleaves peptide chains in an unspecific manner, it could cleave the EGFP part of the protein at C-terminus and remove the fluorescence signal, in the case the fusion USP32-EGFP protein is attached to any membrane/organelle inside the cell and the EGFP faces the cytoplasm. As no signal was lost after trypsin treatment in these cells, we concluded that EGFP was not facing the cytoplasm. In other words, it was possible that the N terminus of the fusion protein (USP32) could be facing the cytosol or that USP32 was localized to the interior of an organelle.

Further experiments for determining the exact topology of USP32-EGFP fusion protein in HeLa cells were performed (Figure 3.9). For this purpose, we investigated the exact localization of USP32 and used confocal microscopy to study HeLa cells expressing USP32-EGFP protein.

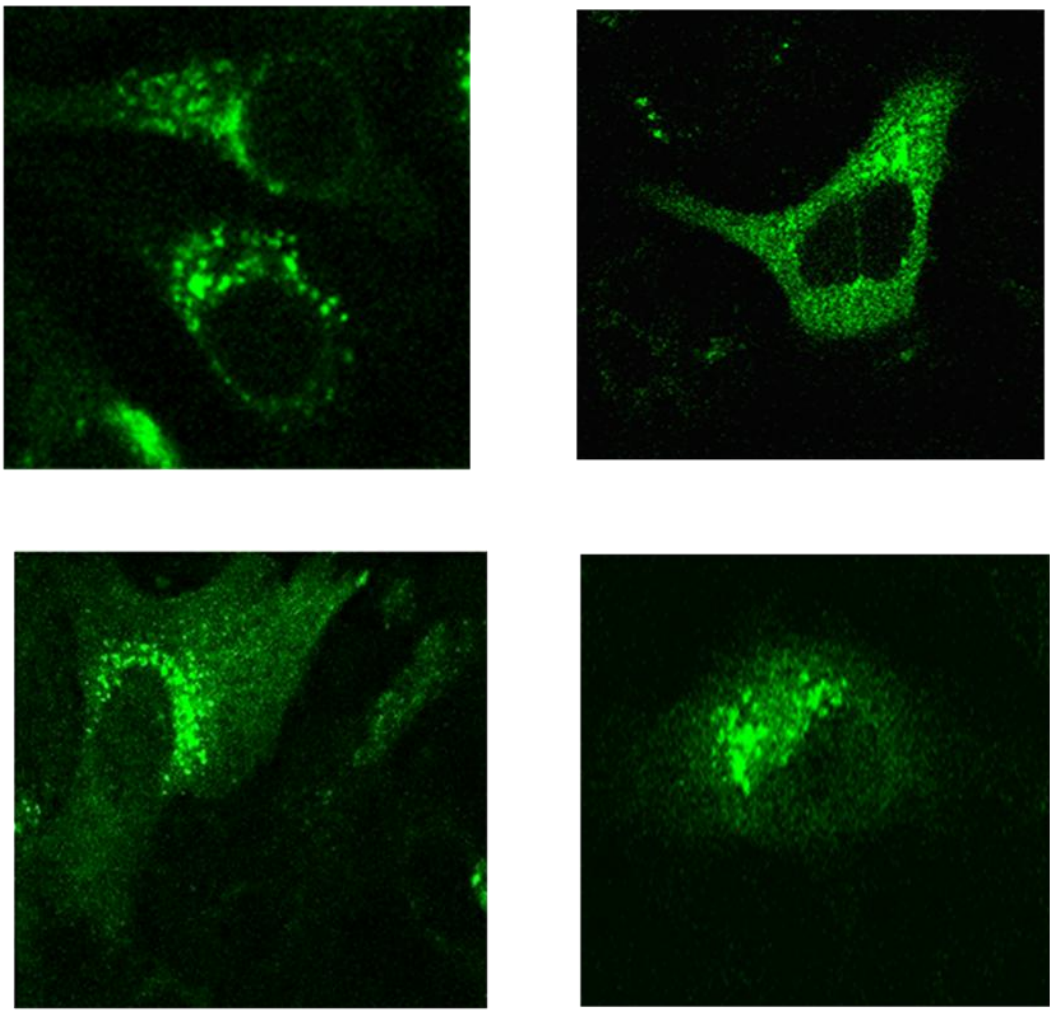

Figure 3. 9 Localization of USP32-EGFP fusion protein (USP32-Full) in HeLa cells. Images (100X) were captured via Zeiss LSM 510 confocal microscopy (Central Lab, METU).

The results on Figure 3.9 indicated a localization pattern for USP32, around the nucleus which may indicate Golgi localization. For this purpose, co-localization study to reveal the positions of USP32-EGFP fusion protein and Golgi apparatus in HeLa cells was performed by staining USP32-EGFP protein expressing cells with BODIPY-TR (BODIPY® TR C5 ceramide complexed to BSA, Molecular Probes as shown in Figure 3.10.

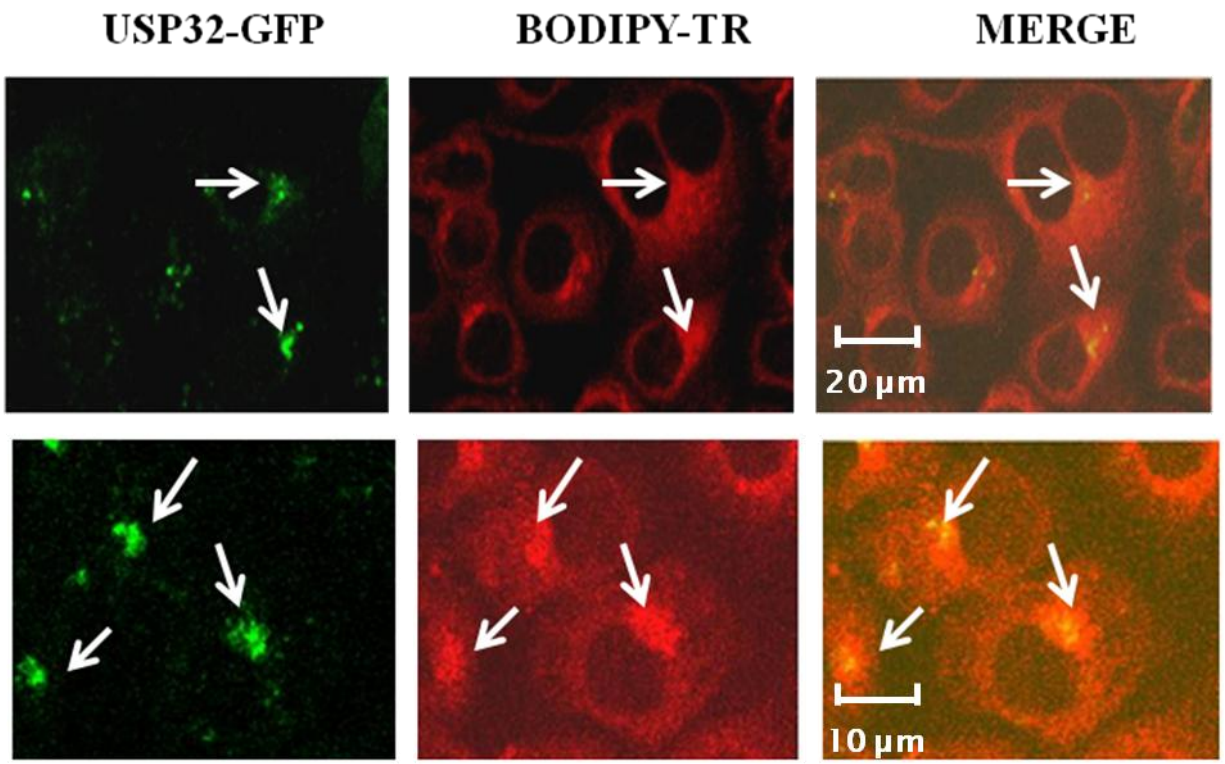

Figure 3. 10 BODIPY-TR staining of HeLa cells, expressing USP32-EGFP for detecting the location of Golgi. Images (100X) were captured via Zeiss LSM 510 confocal microscopy (Central Lab, METU).

According to merged images (obtained from USP32-EGFP expressing and BODIPY-TR stained HeLa cells), USP32-EGFP protein seemed to be localized to Golgi.

BODIPY® TR C5- ceramide stains the Golgi, revealing also a background staining of other membranes in the cell. Ceramide, together with the dye are transferred to the Endoplasmic Reticulum (ER) and further transferred to Golgi. Ceramide could be transferred further from Golgi to cell membranes. However, the Golgi apparatus is stained more prominently and we detected a partial yellow color in merged images, possibly corresponding to Golgi.

The protein localization to Golgi apparatus is not fully understood as there are not any known or conserved Golgi localization signals. For this reason, USP32 may have an as of yet unknown signal for Golgi localization. To further find the responsible region for Golgi localization of USP32 protein, the sequence of full length USP32 was divided into three fragments, and localization studies were performed for these sequences as mentioned in the following sections.

3.1.4 Subcellular Localization of USP32- I –EGFP, EGFP- USP32- II and EGFP- USP32- III fusion proteins

The PCR product of the CDS of first fragment of *USP32* (*USP32*-I), from bases 1-2199 of *USP32* coding sequence was ligated into pEGFPN1 vector to generate EGFP fusion protein. Protein contains USP32-I at N-terminus (amino-terminus) and EGFP at C-terminus (carboxyl-terminus), as shown in Figure 3.11A. The Fluorescent protection assay was performed for USP32-I-EGFP fusion protein (Figures 3.11B, C and D) and to further clarify the results, images were captured from HeLa cells, expressing USP32-I, using confocal microscopy (Figure 3.12). Assay was performed 20-24 h after transfection.

A.

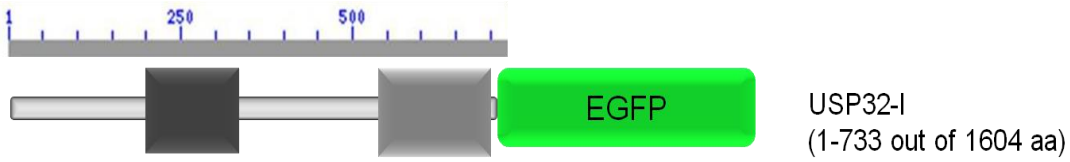

B.

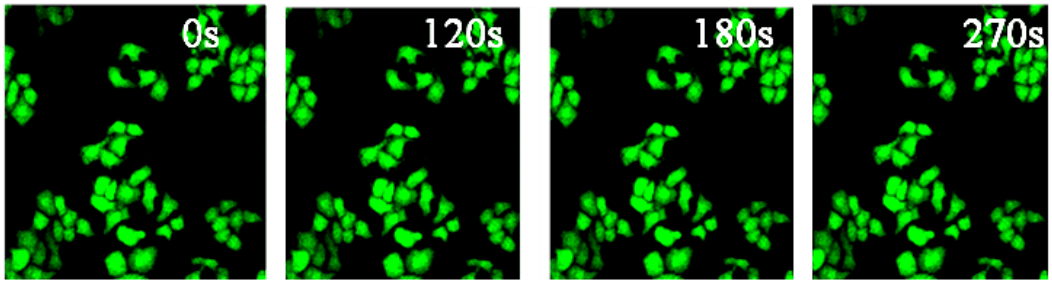

C.

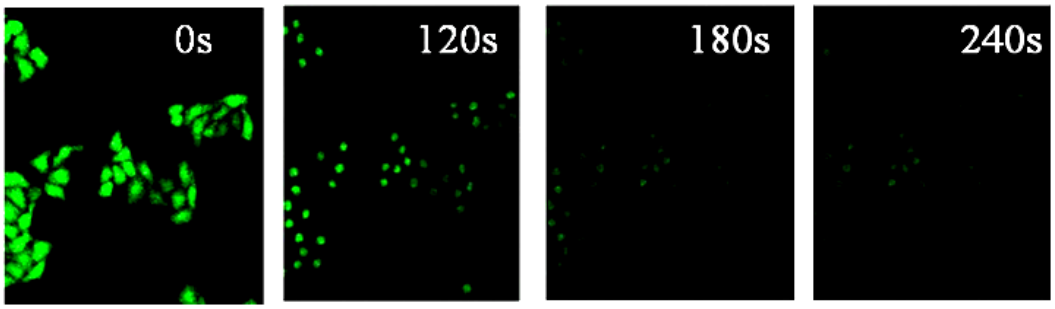

Figure 3. 11 Fluorescence protection assay for USP32-I-EGFP fusion protein.

D.

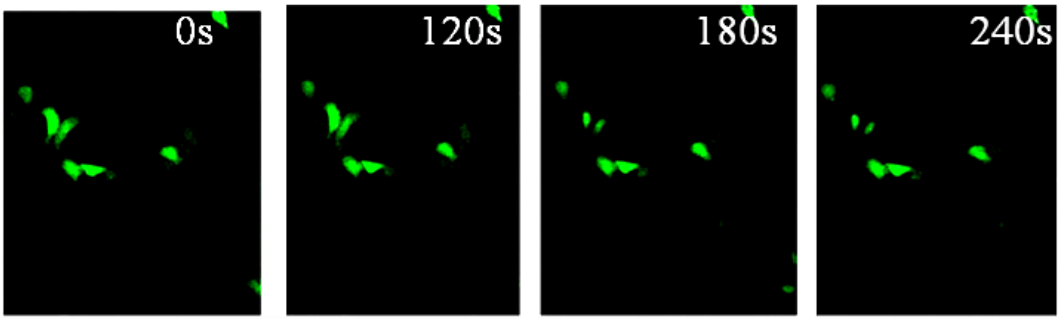

Figure 3. 11 (Continued) Fluorescence protection assay for USP32-I-EGFP fusion protein. **A**. The schematic of USP32-I-EGFP fusion protein. **B.** Photo bleaching control for pEGFPN1 vector after 0, 120, 180 and 270 s exposures to fluorescence beam of 488 nm wavelength. **C** and **D**. Permeabilization of EGFP and USP32-I-EGFP expressing HeLa cells with 20 μM digitonin, documented at 0, 120, 180 and 240 s, after treatment. Images (20X) were captured, using Zeiss LSM 510 microscopy (Central Lab, METU).

In Figure 3.11B, HeLa cells transfected only with pEGFPN1 were exposed to a wavelength of 488 nm up to 270 s, in order to ensure lack of photobleaching. No fluorescence signal was lost during this period from cells. In Figure 3.11C, HeLa cells transfected with pEGFPN1 were permeabilized with 20 μM digitonin. The cells were gradually losing fluorescent signal between 0- 120 s and the signal was almost gone at 240 s. In Figure 3.11D, USP32-I-EGFP expressing HeLa cells were permeabilized with 20 μM digitonin. No decrease in the fluorescence signal was detected from most cells, while a number of cells started to have fainter signals 240 s after permeabilization. These results suggested the possibility that some cells contained not soluble, but a membrane/organelle bound/protein, while the rest had cytoplasmic localization for this protein. To further clarify the results from Figure 3.11, images were captured from HeLa cells, expressing USP32-I, using confocal microscopy (Figure 3.12).

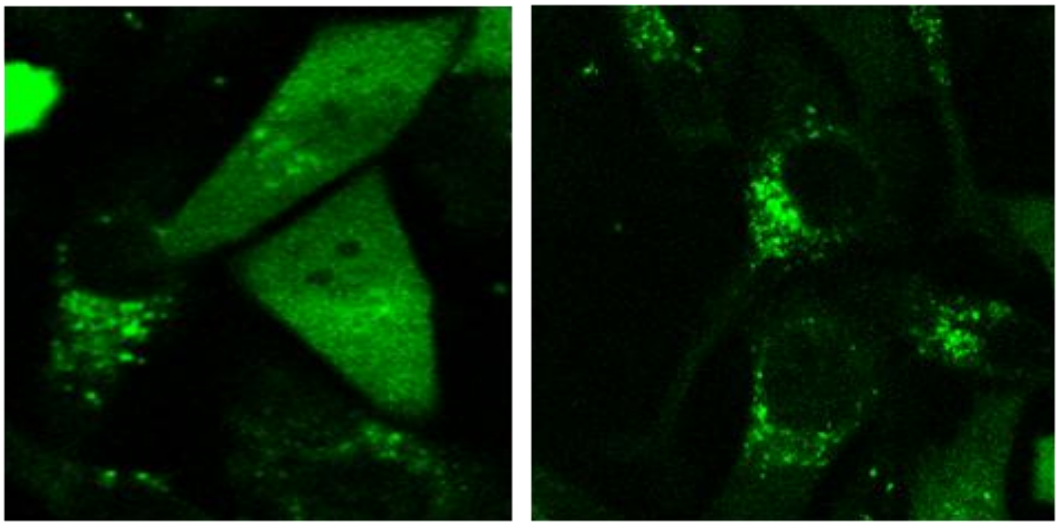

Figure 3. 12 Localization of USP32-I-EGFP fusion protein in HeLa cells, indicated by two representative images. Zeiss LSM 510 confocal microscopy (Central Lab, METU) was used for capturing the images (100X).

Fluorescence protection results (Figure 3.11), suggested the membrane /organelle bound and cytoplasmic localizations for USP32-I-EGFP fusion protein, as fluorescence signal did not fade after permeabilization of plasma membrane in most cells, but weakened in some cells. Results on Figure 3.12 also supported the observations from fluorescence protection assay. Both cytoplasmic and membrane bound/organelle localizations, may be explained by the existence of a Golgi localization signal in the sequence near the C- terminus of USP32-I, weakened by dividing the full coding sequence into fragments.

Alternatively, because cells under the investigation are in different cell cycle phases, it could also be possible that cells undergoing mitosis (with diffused Golgi apparatus), showed a cytoplasmic localization. As the last possible point, the

folding of fusion protein could also cause such observations for USP32-I-EGFP fusion protein.

In order to find the responsible sequence for Golgi localization of USP32 protein, further localization studies were performed for EGFP-USPP32-II and EGFP-USPP32-III fusion proteins and the results are shown in the next parts.

The CDS of second fragment of *USP32* (*USP32*-II), from base 1500- 330 of *USP32* coding sequence was ligated into pEGFPC1 vector and used in fluorescence protection assay (Figure 3.13), in order to generate EGFP fusion protein. EGFP-USP32-II fusion protein contains EGFP at N-terminus (amino-terminus) and USP32-II at C-terminus (carboxyl-terminus), as shown in Figure 3.13A.

A.

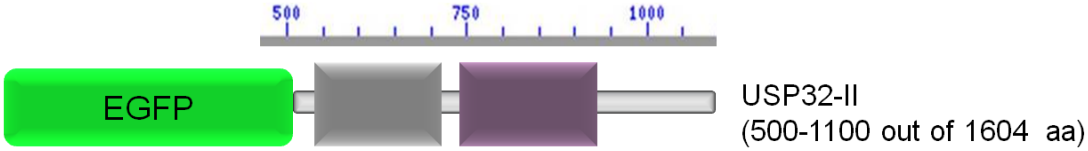

B.

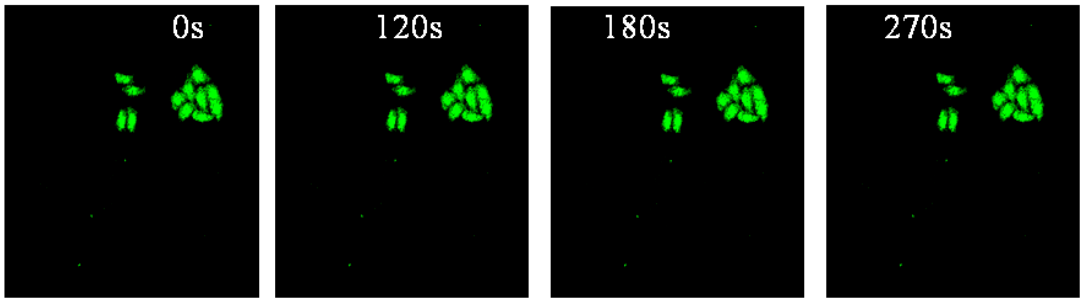

C.

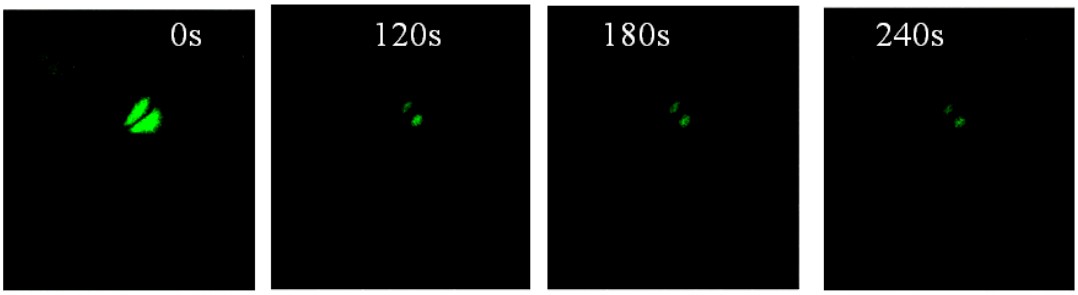

Figure 3. 13 Fluorescence protection assay for EGFP-USP32-II fusion protein. **A.** The schematic of EGFP-USP32-II fusion protein.

D.

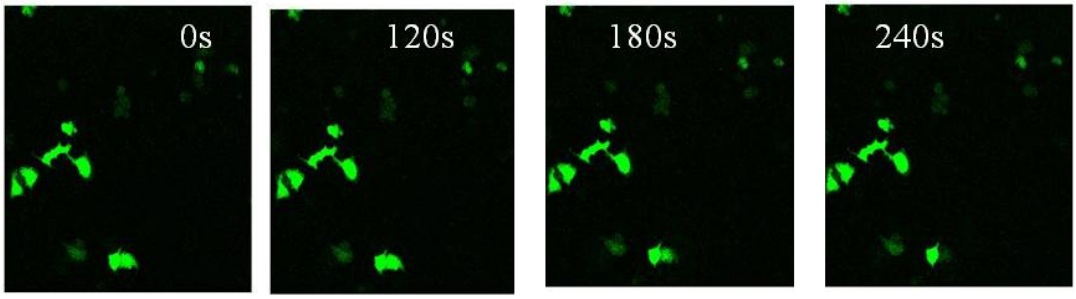

Figure 3. 13 (Continued) Fluorescence protection assay for EGFP-USP32-II fusion protein. **A.** The schematic of EGFP-USP32-II fusion protein. **B.** Photo bleaching control for pEGFPC1 vector after 0, 120, 180 and 270 s exposure to a fluorescence beam of 488 nm wavelength. **C** and **D.** permeabilization of EGFP and EGFP-USP32-II expressing HeLa cells with 20 μM digitonin, documented at 0, 120, 180 and 240 s, after treatment. Images (20X) were captured, using using Zeiss LSM 510 microscopy (Central Lab, METU).

According to the results from Figure 3.13B, the images from HeLa cells transfected with pEGFPC1 were captured after an exposure to a wavelength of 488 nm until 270 s. Results from this part ensured no existence of photobleaching in the system. In Figure 3.13C, HeLa cells transfected with pEGFPC1 were permeabilized with 20 μM digitonin. The signal was nearly lost at 240 s. In Figure 3.13D, HeLa cells transfected with EGFP-USP32-II were permeabilized with 20 μM digitonin. Most of the cells did not lose the fluorescence signal at 240 s. These results suggested the possibility that some of cells may have had a cytoplasmic soluble fusion protein, while the rest contained a membrane/organelle bound protein. This observation was similar to those observed in Figure 3.11, for EGFP- USP32-I fusion protein in previous section.

Furthermore, to confirm the results obtained from fluorescence protection assay, the localization of USP32-II-EGFP fusion proteins was determined, using confocal microscopy (Figure 3.14).

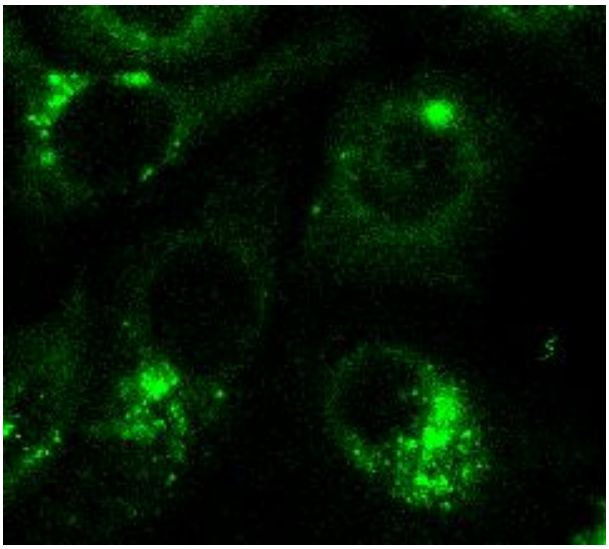

Figure 3. 14 Localization of EGFP-USP32-II fusion proteins in HeLa cells.Zeiss LSM 510 confocal microscopy (Central Lab, METU) was used for capturing the image (100X).

The results from confocal images from Figure 3.14 were consistent with the results, obtained from fluorescent protection assay, suggesting Golgi localization for EGFP-USP32-II fusion protein.

The CDS of third fragment of *USP32* (*USP32*-III) was ligated into pEGFPC1 vector and used in fluorescence protection assay (Figure 3.15), in order to generate EGFP fusion protein. EGFP- USP32-III fusion protein contains EGFP at N-terminus (amino-terminus) and USP32-III at C-terminus (carboxyl-terminus), as shown in Figure 3.15A. This construct was transfected into HeLa cells and images were captured 20-24 h after transfection.

A.

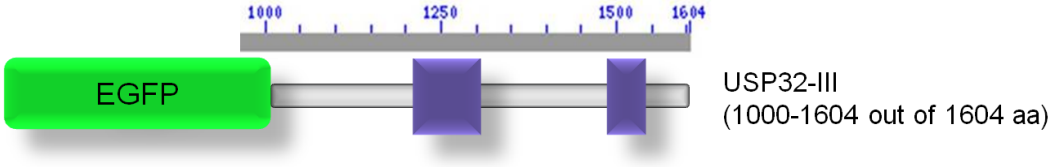

B.

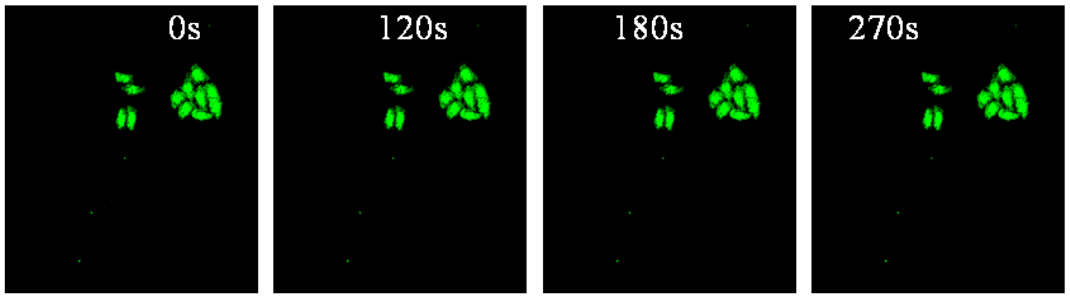

C.

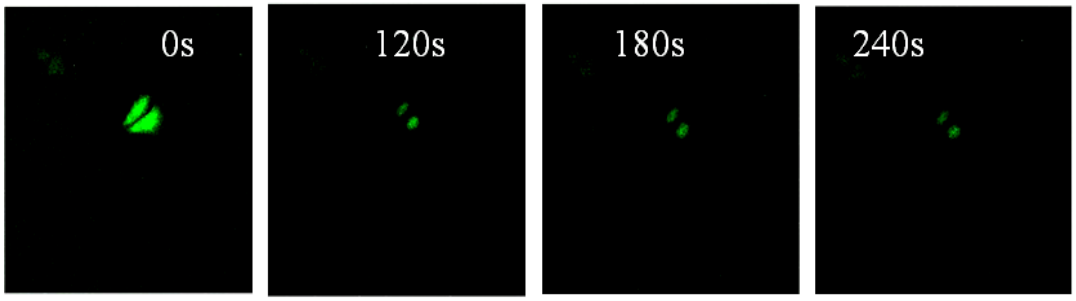

Figure 3. 15 Fluorescence protection assay for EGFP-USP32-III fusion protein.

D.

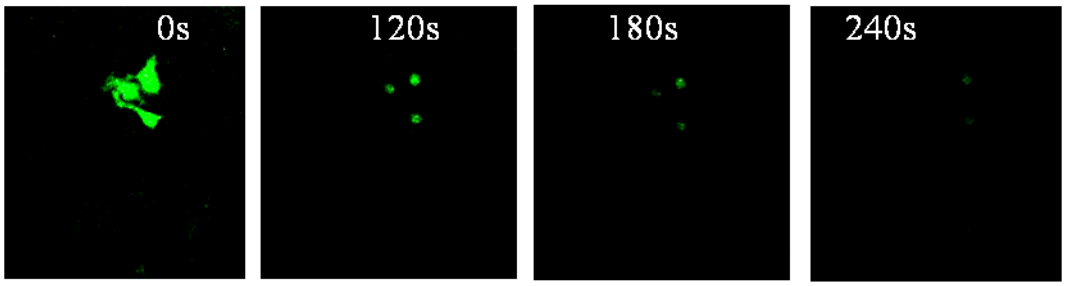

Figure 3. 15 (Continued) Fluorescence protection assay for EGFP-USP32-III fusion protein. **A**. The schematic of EGFP-USP32-III fusion protein. **B.** photo bleaching control for pEGFPC1 vector after 0, 120, 180 and 240s exposure to a fluorescence beam of 488 nm wavelength. **C** and **D:** permeabilization of EGFP and EGFP-USP32-III expressing HeLa cells with 20 μM digitonin, documented at 0, 120, 180 and 240s, after treatment. Images were captures, using fluorescent microscopy (20X).

In Figure 3.15B, HeLa cells transfected with pEGFPC1 were exposed to a wavelength of 488 nm and images were captured during 0-270 s. The results ensured lack photobleaching in the system. In Figure 3.15C, HeLa cells transfected with pEGFPC1 were permeabilized with 20 μM digitonin. The signal was nearly lost at 240 s. In Figure 3.15D, HeLa cells transfected with EGFP-*USP32*-III were permeabilized with 20 μM digitonin. The fluorescent signal was completely lost from all cells after 240 s, indicating that EGFP-*USP32*-III was a soluble protein in the cytoplasm. Further localization study, to explain this situation for localization of EGFP-USP32-III fusion protein was done and shown in Figure 3.16, revealing a soluble cytoplasmic localization for EGFP-USP32-III fusion protein.

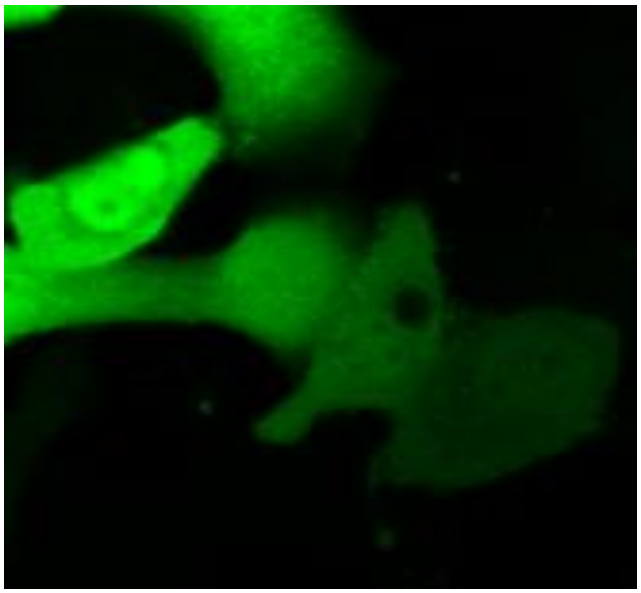

Figure 3. 16 Localization of EGFP- USP32-III fusion proteins in HeLa cells. Zeiss LSM 510 confocal microscopy (Central Lab, METU) was used for capturing the image (100X).

In conclusion, the results from fluorescence protection assay of USP32-Full, indicated that the full length USP32 protein fused to EGFP, was not a soluble protein and it suggested membrane/organelle bound localization for this protein. Confocal microscopy images from HeLa cells, transfected with USP32-Full-EGFP construct also confirmed the FPP results, suggesting a possible Golgi-like localization for USP32-Full-EGFP fusion protein. BODIPY-TR staining of USP32-Full-EGFP expressing cells suggested that USP32 was possibly localized to Golgi in HeLa cells.

USP32-I, USP32-II and USP32-III partial fragments of USP32, fused to EGFP, were also used in fluorescence protection assay. Results indicated that these fragments, fused to EGFP, could have both cytoplasmic and membrane bound/organelle localizations, as fluorescence signal did not fade after permeabilization of plasma membrane in most cells, while weakened in a number

of cells. The reason for this may be explained as the existence of a Golgi localization signal in the sequence near the end of USP32-I and start of USP32-II fragments, affected and weakened by dividing the full coding sequence into fragments. On the other hand, these observations could be because cells under the investigation were in different cell cycle phases. The results of fluorescence protection assay for USP32-III fragment of USP32 indicated that USP32-III, fused to EGFP was a soluble protein, as the cells completely lost the fluorescent signal after permeabilization, indicating the possibility of existence of no Golgi localization signal in the sequence of USP32-III. Alternatively, different folding of partial fusion proteins could also cause such observations for USP32-I, USP32-II and USP32-III fusion proteins.

3.2 Functional Characterization of miR-125b

3.2.1 Expression of miR-125a and miR-125b in Human BCCLs

Previously in our lab, we have detected decrease or loss of miR-125b-1 precursor expression in breast cancer cell lines (Akhavantabasi et al. 2012). In this study, we detected the mature levels of miR-125a and miR-125b in 10 breast cancer cell lines, compared to normal breast tissue and immortalized normal breast cell line (MCF10A), as shown in Figure 3.17 A and B.

A.

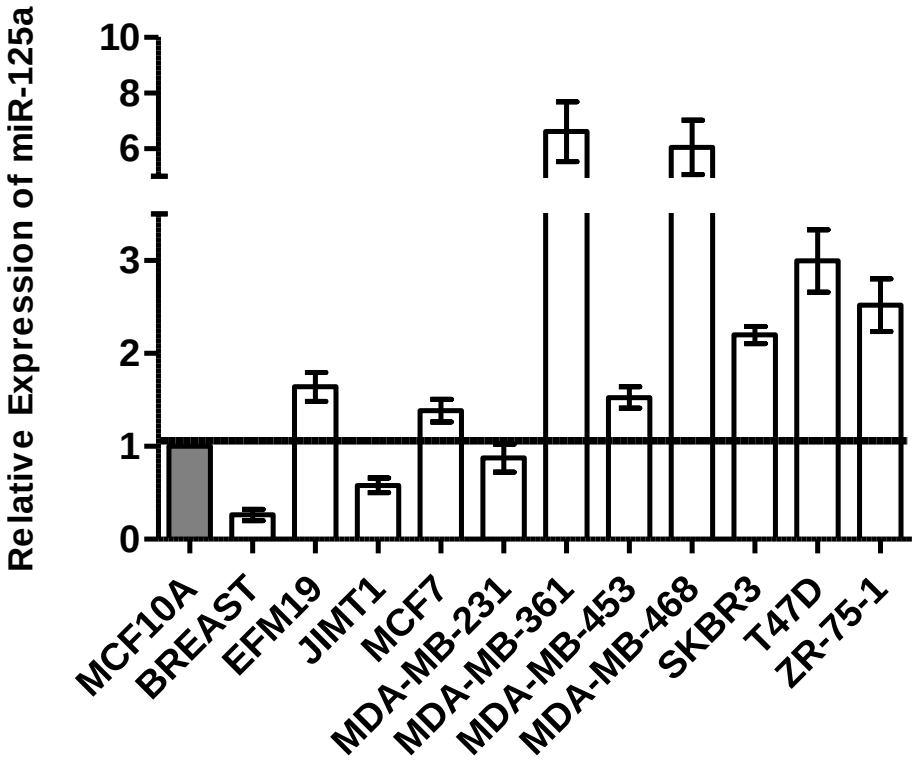

Figure 3. 17 Taqman miRNA assay to detect the mature miR-125a and miR-125b levels.

B.

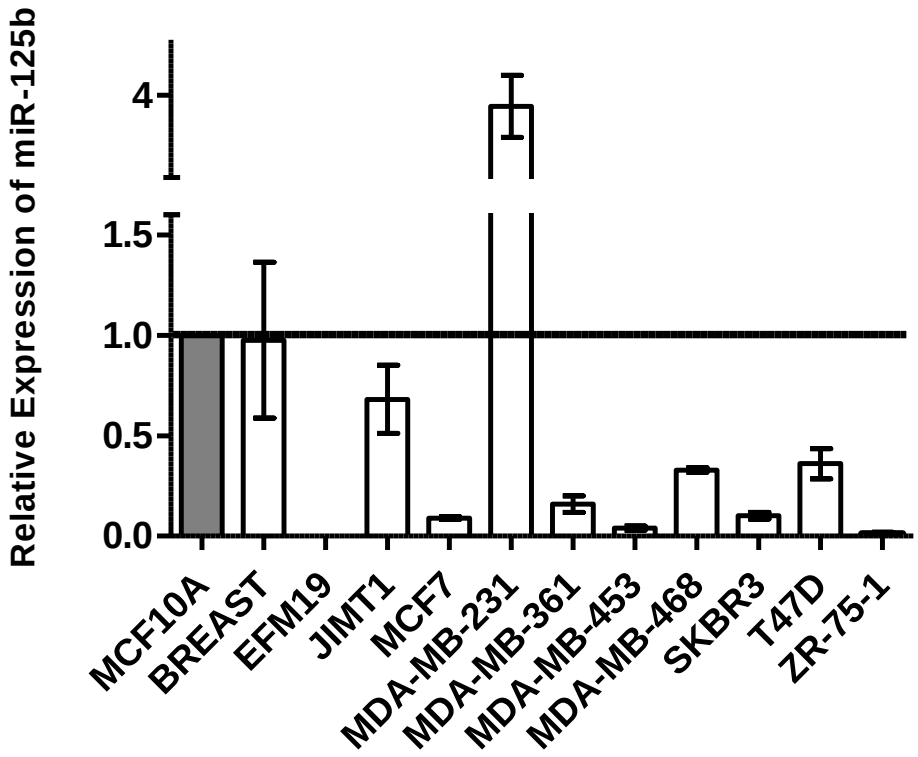

Figure 3. 17 (Continued) Taqman miRNA assay to detect the mature miR-125a and miR-125b levels. **A.** miR-125a and **B.** miR-125b levels, in normal breast tissue and MCF10A, EFM19, JIMT1, MCF7, MDA-MB-231, MDA-MB-361, MDA-MB-468, MDA-MB-453, SKBR3, T47D and ZR-75-1 cell lines. *RNAU6B* was used as reference gene. Results were normalized to the values obtained from MCF10A. Results were obtained from 2 independent experiments and 3 replicas were used for each sample.

The expression results in Figure 3.17 revealed that compared to miR-125a with an expression in nearly all breast cancer cell lines, miR-125b was dramatically down regulated in 9 of 10 cell lines, compared to normal breast and MCF10A controls, suggesting a tumor suppressor role for miR-125b in breast cancer. Further

experiments were performed in this study, to characterize miR-125b better in breast cancer.

3.2.2 Generation of Breast Cancer Model Systems to Study the Role of miR-125b-1

In order to study the possible tumor suppressor role of miR-125b, an MCF7 model system was already generated in our lab (these cells were selected as they expressed low levels of precursor miR-125a and miR-125b, according to results previously detected in our lab). To further examine the role of miR-125b in another background cell line, miR-125b precursor construct was stably transfected into T47D cells (T47D cells were chosen as we previously detected low/no expression of miR-125b-1 precursor). For this purpose, precursor sequence of miR-125b, cloned into pSUPER vector (pSUPER.retro.neo+GFP, Invitrogen, as shown in Appendix B) was transfected into T47D breast cancer cells and polyclonal stable cell line (T47D-125) was generated upon antibiotic selection. As control, T47D cell were also transfected with empty pSUPER vector (EV) and polyclonal stable cell line was selected (T47D-EV).

Three different polyclonal cell populations were tested for genomic integration (Figure 3.18) and transcript expression (Figures 3.19) of miR-125b.

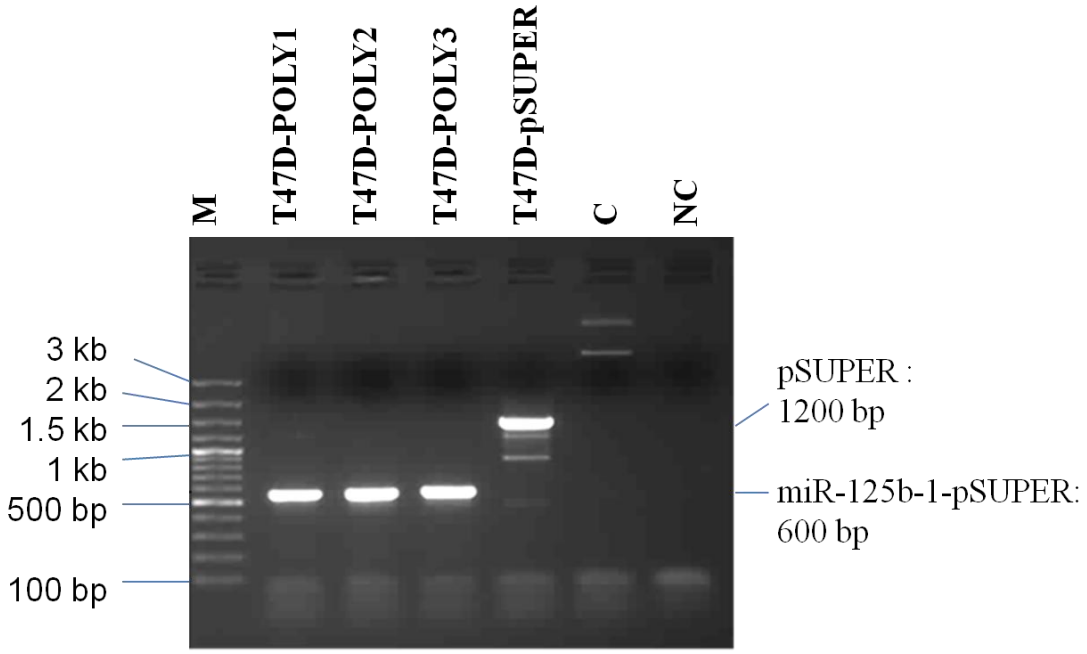

Figure 3. 18 PCR Amplification of miR-125b-1 from stably transfected T47D cells from genomic DNA, using pSUPER vector specific primers (pSUPER-F and pSUPER-R). M: GeneRuler marker, POLY: Polyclonal, C: Control for none specific template (pmiR vector) and NC: no template control for PCR. PCR was performed using initial denaturation at 95ºC for 2 min, followed by 30 cycles at 95ºC for 30 seconds (denaturation), 56ºC for 30 seconds (annealing) and 72ºC for 1 min (elongation). A final extension at 72ºC for 10 min was performed.

Results, shown in Figure 3.18 indicated the integration of miR-125- pSUPER construct and empty pSUPER vector into T47D cells. If miR-125b1 vector was inserted into the genome, a 600 bp product was detected as for empty vector, since the stuffer region wasn't excised, a 1200 bp was detected. Precursor miR-125b-1 transcript was also detected to be available in miR-125 transfected T47D cells, but not in controls as expected, detected by RT-PCR (Figure 3.19). In addition, the

existence of mature miR-125b was confirmed by qRT-PCR (Taqman assay, *RNU6B* was used as internal control) in transfected T47D cells (Figure 3.20).

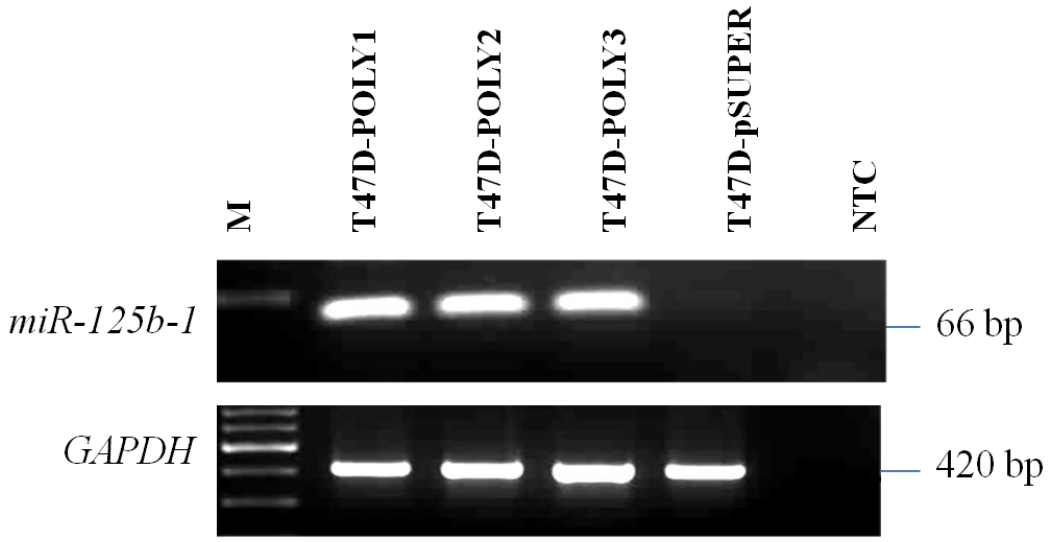

Figure 3. 19 RT-PCR for detecting the expression of precursor miR-125b-1. PCR amplification for detecting the expression of precursor miR-125b-1 from cDNA of stably transfected T47D cells. POLY: polyclonal cells, NTC: Negative Control of PCR. *GAPDH* was used to test the quality of cDNA used in PCR. PCRs were performed using initial denaturation at 95ºC for 2 min, followed by 30 cycles at 95ºC for 30 seconds, 58ºC for 30 seconds and 72ºC for 30 seconds. A final extension at 72 ºC for 10 min was performed.

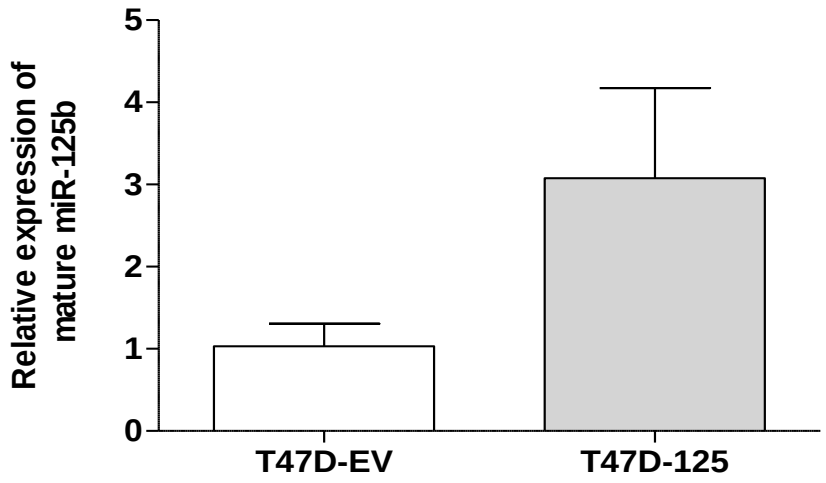

Figure 3. 20 Taqman miRNA assay for detecting the expression of mature miR-125 in T47D-125 (polyclonal 3) and T47D-EV cells. The values from miR-125 expression were normalized to the values of *RNU6B* (reference gene) expression in those cells. The results were obtained from 2 separate experiments for each sample, each in triplicates.

After confirmation of miR-125b expression in transfected T47D cells, we investigated if miR-125b expression caused any phenotypical changes. Both T47D cells and MCF7 cells also were further investigated to test the effect of miR-125b expression restoration.

From this point onwards, miR-125b expressing cells will be referred as MCF7-125b and T47D-125b, whereas the control cells will be referred as MCF7-EV and T47D-EV.

3.2.3 Functional Assays for miR-125b Expressing Cells

3.2.3.1 Cell Proliferation Assay (MTT)

As a potential tumor suppressor, we investigated if restoration of miR-125b expression in low/no miR-125b expressing cells would lower the proliferation rate. MTT assay was performed, in order to investigate the effect of miR-125b on the proliferation of both MCF7 and T47D cells (Figures 3.21 A and B).

A.

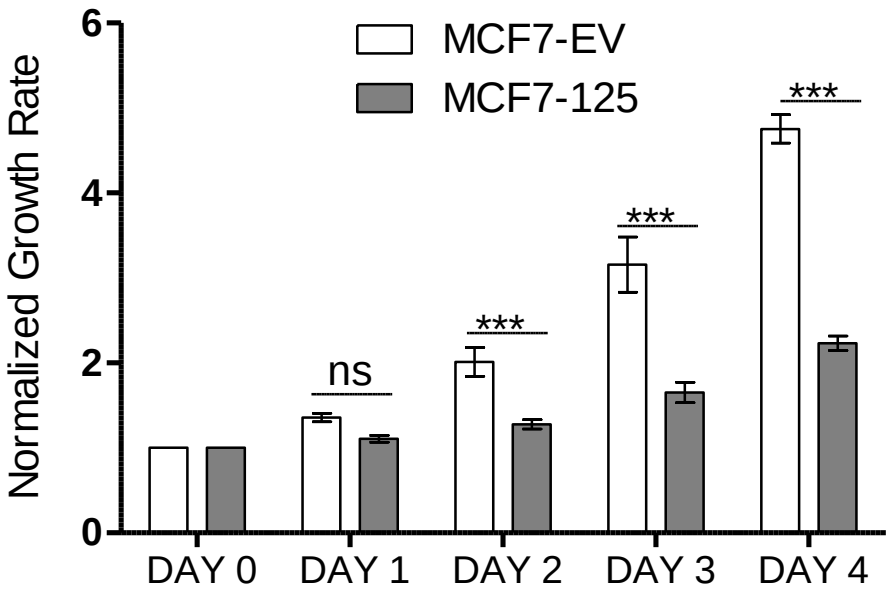

Figure 3. 21 Cell proliferation detected by MTT. **A.** 10,000 MCF7-125 and MCF7-EV cells were initially seeded into each well of 96-well cell culture plates. After 4 h incubation with MTT labeling reagent (5 mg/ml) and solubilization with a 1% solution of SDS, OD570 values were measured at days 0, 1, 2, 3 and 4. The OD570 valued were normalized to day 0 values. 8 replicas were used for each sample in two independent experiments.

B.

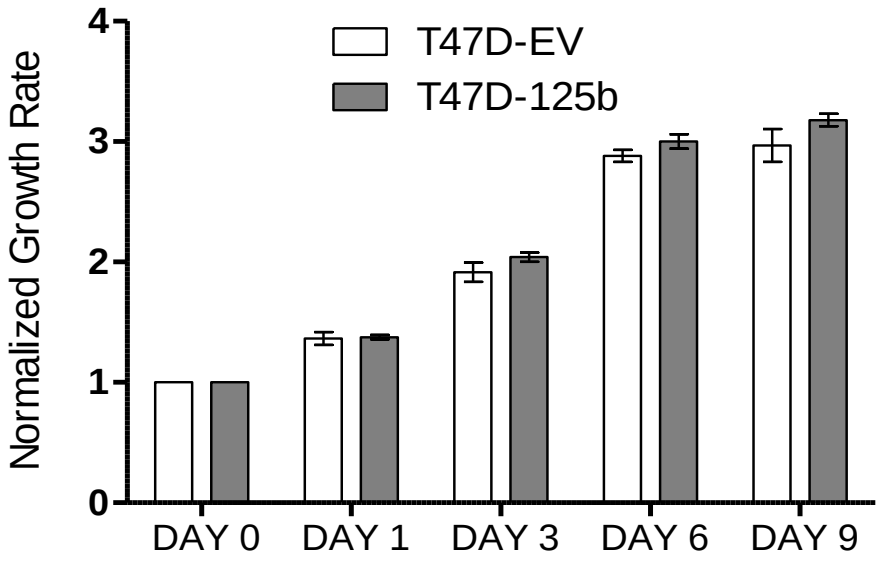

Figure 3. 21 (Continued) Cell proliferation detected by MTT. **B.** 10,000 T47D-125 and T47D-EV cells were seeded into each well of 96-well cell culture plates and OD570 values were measured at days 0, 1, 3, 6 and 9, after cells were seeded, incubated with MTT labeling reagent and 1% SDS, as mentioned above. 4 replicas were used for each sample in two independent experiments. Student t-test was used for analyzing the data. ns: no significant and ***: significant difference between normalized growth rates of MCF7-125 and MCF7-EV ($p<0.05$).

Results from Figure 3.21 indicated a 36-53% decrease in the cell proliferation of MCF7-125, compared to MCF7-EV cells from day 2 to day 4 after seeding. Interestingly, no decrease in the proliferation of T47D-125 compared to T47D-EV cells was detected in correlation with the results obtained from another study (Guo et al. 2009; Wu and Belasco 2005) in this cell line. Possible reasons for this observation were seeked. As mentioned earlier, mature miR-125b and mature miR-125a has the same seed sequences, hence the potential to target same target mRNAs. So to test whether miR-125a levels may vary and have different effects

among cell lines, miR-125a and miR-125b mature levels were detected in MCF7 and T47D BCCL (as shown already in Figure 3.17). Endogenous mature miR-125b was available in both T47D and MCF7 cell lines at low levels: however miR-125a was detected in T47D cells at higher levels, compared to MCF7 cells. miR-125a and miR-125b contain different mature sequences, while their seed sequences are similar (Figure 3.22), making it possible that they both bind and regulate same mRNA targets. In such a case, if the common target of these miRNAs was a regulator of cell proliferation, as miR-125a level was already high in T47D cells, it might not have been possible to follow the proliferative effect of miR-125b in these cells. This means that miR-125a could already have targeted a particular mRNA. Recent studies revealed the regulation of v-ets erythroblastosis virus E26 oncogene homolog 1 (*ETS1*), a regulator of cell proliferation, by miR-125b (Zhang et al. 2011). *ETS1* is predicted to be targeted by both miR-125a and miR-125b (Figure 3.23).

Figure 3. 22 The mature sequences for hsa-miR-125a, hsa-miR-125b-1 and hsa-miR-125b-2. The seed sequences are indicated in red and differences in the mature sequences are shown in blue. Sequences and accession numbers are derived from miRBase database.

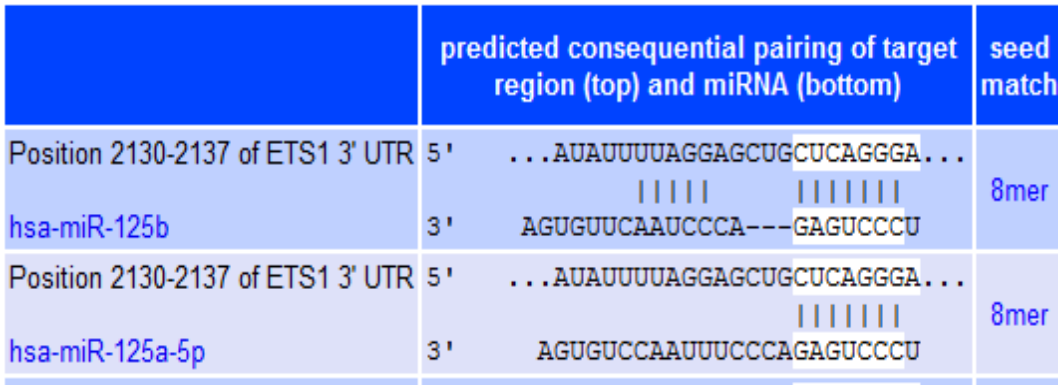

Figure 3. 23 Predicted conserved binding sites of miR-125a and miR-125b on the 3'-UTR of ETS1 mRNA by TargetScan program. miR-125a and miR-125b contain the same seed but different mature sequences.

Alternatively, no change in cell proliferation rate after miR-125b expression in T47D but not MCF7 cells may be further explained by the possibility of the existence of a different transcriptome, which may have altered the availability of miR-125b target mRNA/mRNAs, responsible for cell proliferation regulation. In this situation, T47D cells may not express the proliferation regulator target of miR-125b, expressed in MCF7. As third possibility, different Single Nucleotide Polymorphisms (SNP) at miR-125b binding sites on the 3'UTR of the target mRNAs may inhibit the binding of miR-125b in T47D cells. Moreover, in the case of indirect targets of miR-125b, different proteomes of these 2 BCCLs, where the presence or absence of different transcription activators or repressors, may alter the expression of indirect cell proliferation regulator targets.

3.2.3.2 Effect of miR-125b Expression on Cell Motility/Migration

To study if miR-125b expression affects the migration of MCF7 cells, MCF7-EV and MCF7-125b cells were plated in medium containing 1% serum on the upper well of a transwell chamber and cells were observed for their ability to migrate through 8 μm pores of a membrane to reach to the high serum containing medium (10%) in the bottom wells. 24 h after initial cell seeding, MCF7-125b cells had a ~50% decrease in their migration properties, compared to MCF7-EV cells (Figure 3.24). Furthermore, to confirm if this decrease in cell migration was due to miR-125b expression, we designed 2'-*O*-methyl anti-miR-125b (Anti-125b) and non-specific control (C-Oligo) oligos. Antisense 2'-*O*-methyl oligos are successfully used to inhibit miRNAs *in vitro* (Jiang et al. 2010; Wu and Belasco 2005). MCF7-125 cells were treated with miR-125b inhibitor oligo and migration assay was performed. Migration assay for MCF7-125 cells, treated with miR-125b inhibitor oligo indicated a significant increase in their migration, compared to mock transfected and control oligo treated cells (Figures 3.25 A). Transfection efficiency for anti-125b oligo transfection was checked by qRT-PCR (Figure 3.25 B). The alignments for mature miR-125 and antisense 2'-*O*-methyl oligos are shown in Figure 3.26.

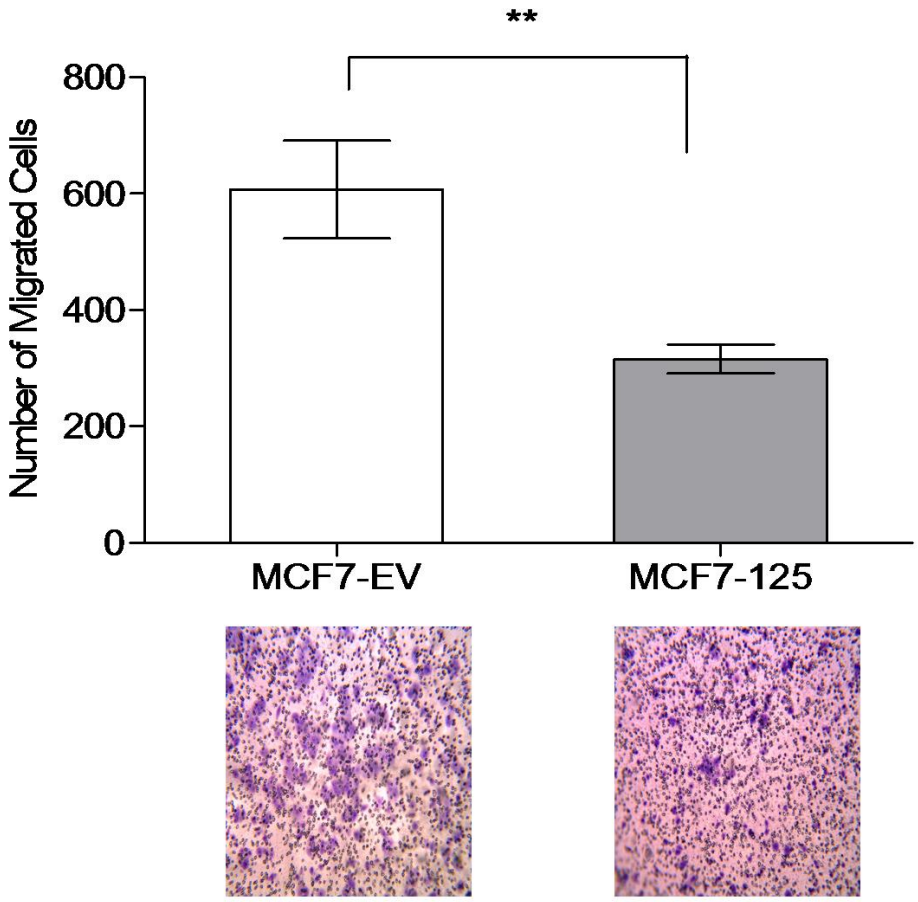

Figure 3. 24 Transwell migration assay in MCF7-EV and MCF7-125 cells. MCF7-EV and MCF7-125b cells (200,000 pre-starved (in 1% FBS)) in 0.1 mL MEM-Earle's medium with 1% FBS were plated on the upper wells of transwell migration chambers. Medium with 10% FBS was added to the lower wells. Cells were allowed to migrate for 24 h through 8 µm pores towards high serum containing medium. The cells on the lower side of the membranes were stained with Giemsa and counted, using 10X objective of a light microscope (Leica). Experiments were performed 3 independent times with at least 6 membranes. 3 random fields were counted per membrane. Student t-test was used to analyze the data. **: indicates statistical significance ($p<0.05$). Representative membrane images are given below the graph.

A. **B.**

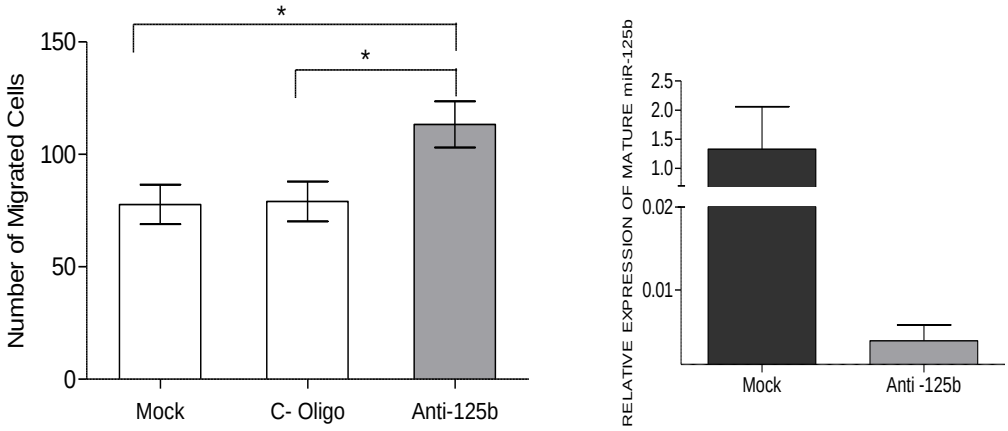

Figure 3. 25 A. Transwell migration assay in MCF7-125 cells, transfected with miR-125b and control oligos.MCF7-125 cells transfected with 1.5 µg/mL anti-125b/control oligos (C-Oligo) and mock transfected were used in migration assay. 200,000 pre-starved (in 1% FBS) cells in 0.1 mL MEM-Earle's medium with 1% FBS were seeded on the upper wells of transwell migration chambers. Cells were allowed to migrate for 24 h through 8 µm pores towards high serum containing medium (medium with 10% FBS was added to the wells on the other side of membranes). The cells on the lower side of the membranes were stained with Giemsa and counted, using 10X objective of a light microscope (Leica). All experiments were performed 3 independent times, using a total of 6 membranes. 3 random fields were counted per membrane. Student t-test was used to analyze the data. *: indicates statistical significance ($p<0.05$). **B**. Taqman miRNA assay to detect the mature miR-125b levels in anti-125b transfected MCF7-125 cells. *RNAU6B* was used as reference gene. 3 replicas were used for each sample.

Approximately 50% decrease in the level of cell migration was observed in MCF7-125 cells, compared to MCF7-EV cells, revealing the impact of miR-125b expression on MCF7 cells' migration. The recovery in the migration of MCF7-125 cells treated with Anti-125b oligo, compared to C-oligo and mock transfected cells indicated an exclusive effect of miR-125b on MCF7 cells' migration.

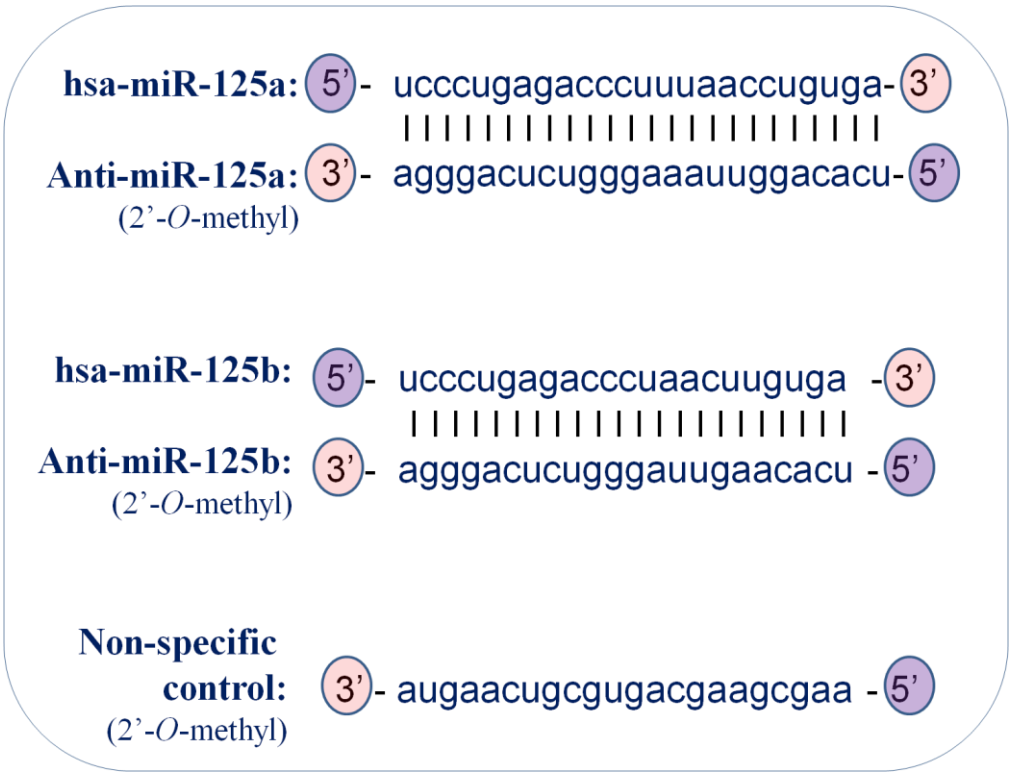

Figure 3. 26 Sequences of 2'-O-methyl anti-miR-125a and anti-miR-125b oligos and their alignments with mature hsa-miR-125a and hsa-miR-125b respectively along with the sequence for 2'-O-methyl non-specific control with no hit to human genome.

To further investigate the impact of miR-125b on MCF7 cells, we investigated the morphology of MCF7-EV and MCF7-125 cells in 3D culture.

3.2.4 Morphological Changes Due to miR-125b Expression

Extra Cellular Matrix (ECM) has a key regulatory role on the structure and function of cells and tissues. Studies revealed that mammary epithelial cells, grown on reconstituted basement membrane matrix obtained from Engelberth-Holm-Swarm murine tumor (EHS), form a polarized acini structure, expressing beta-casein and producing milk (Barcellos-Hoff et al. 1989). This indicated that ECM is necessary for cell signaling and affect its structure and function. For this purpose, we wanted to investigate the structure of MCF7-EV and MCF7-125 cells in 3 dimensional culture containing laminin-rich ECM (lrECM) (Figure 3.27). Laminin is known to be expressed from myoepithelial cells in normal breast and play important role in acini formation and milk production of breast epithelial cells (Adriance MC 2005).

For 3D 'on-top' culturing of MCF7 cells, pre-chilled plates were coated with lrECM. Cells suspended in growth medium were plated and incubated at 37ºC for 30 min. Finally EHS and ice-cold growth medium were added to the culture and images were captured after 24 h.

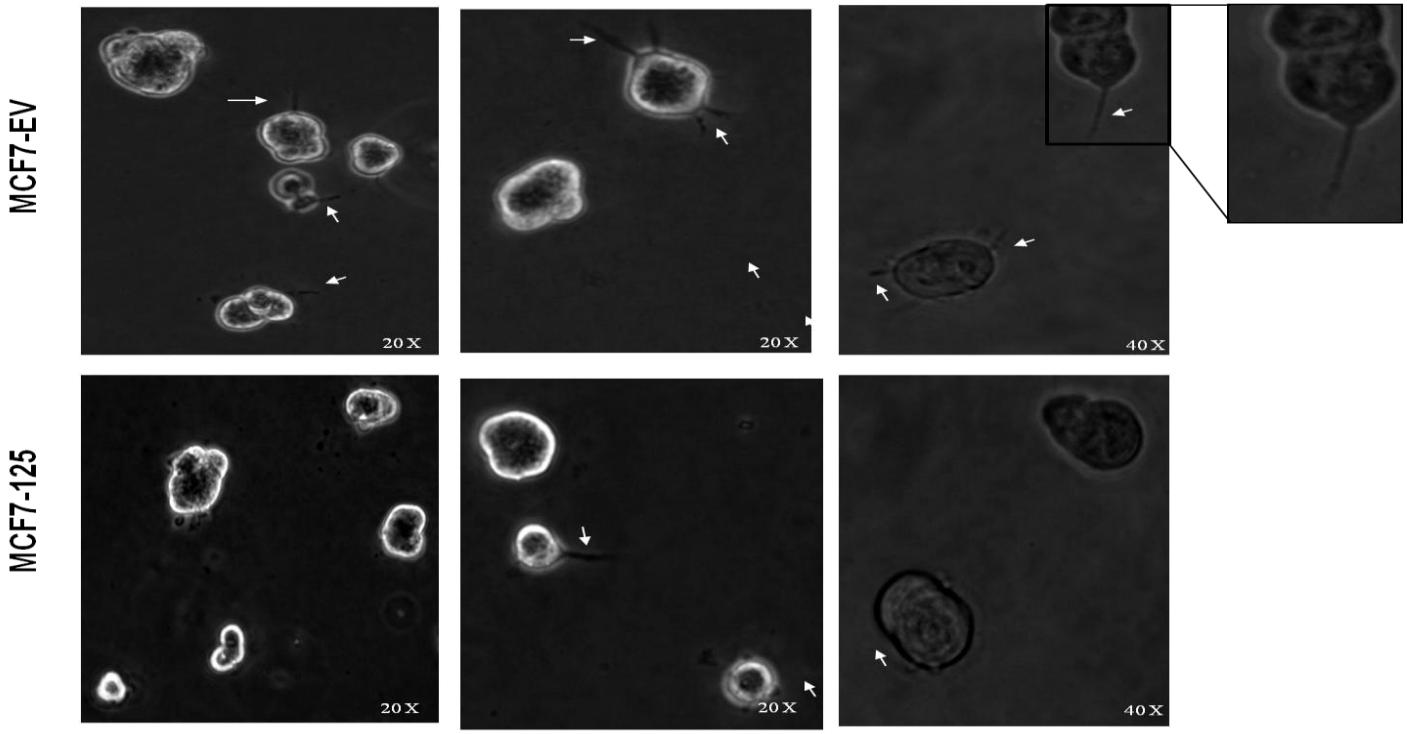

Figure 3. 27 Morphology of MCF7-EV and MCF7-125 cells, grown on 3D culture for 24 h. Images were taken, using Olympus CKX41 inverted microscope (20X and 40X). White arrows indicate the projections, extending from cell aggregates.

Results on Figure 3.27 showed that MCF7 cells form aggregates in 3D culture. Long podia-like protrusions, demonstrated by white arrows on the Figure were obvious even 24 h after culturing the cells. These projections were present in higher numbers on MCF7-EV cells, compared to MCF7-125 cells, indicating the possible regulatory role of miR-125b on the formation of these protrusions. With the possibility that these projections affect the MCF7 cells' migration, we further investigated the actin cytoskeleton (as an important regulator of cellular motility and migration) of MCF7-EV and miR-125b expressing MCF7-125 cells (Figure 3.28).

3.2.5 The Distribution of Actin Filaments in MCF7 Cells, Expressing miR-125b

The MCF7 cells transfected with miR-125 or empty pSUPER vector control were stained with phalloidin and DAPI, in order to study if miR-125 had any effect on the distribution of actin filaments and the phenotype of these cells (Figure 3.28).

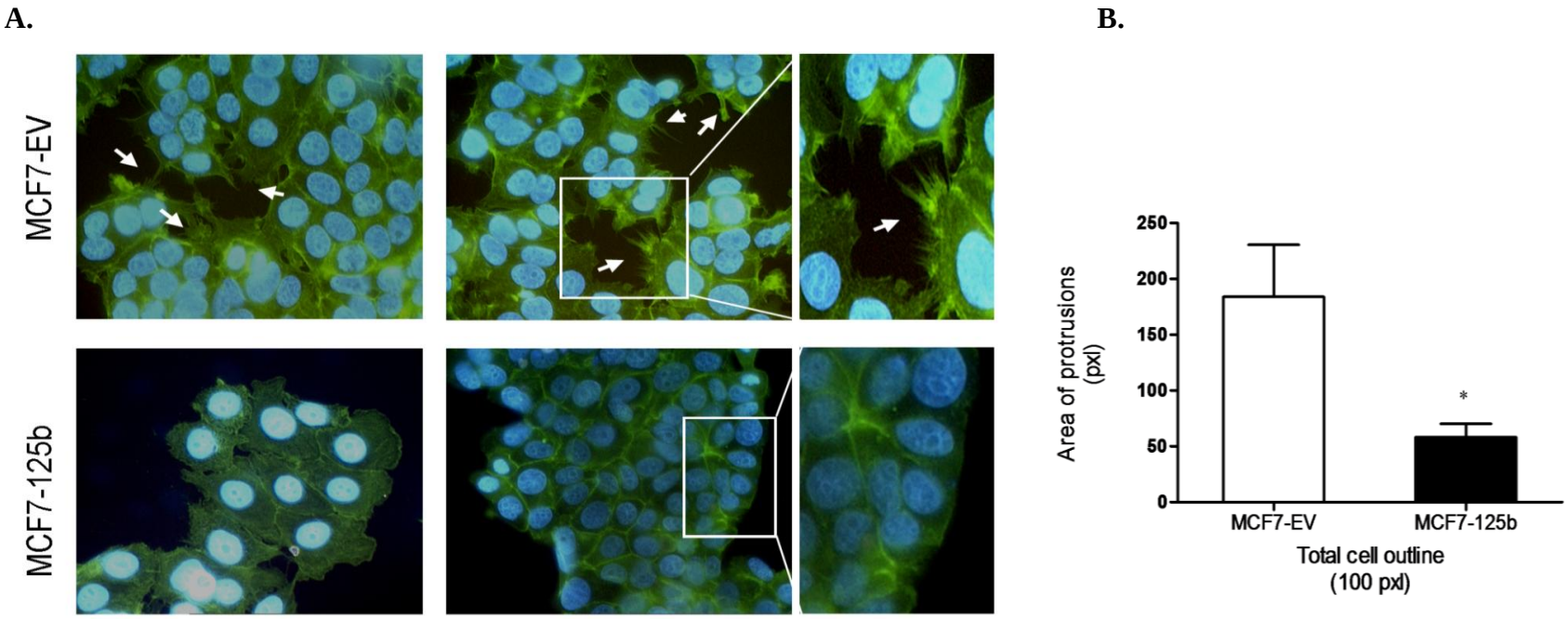

Figure 3. 28 Staining of actin filaments (green) and nucleus (blue) of MCF7 cells. **A**. MCF7 cells transfected with miR-125b1 (MCF7-125) and Empty Vector (EV) pSUPER control (MCF7-EV). The nuclei of the cells were stained with DAPI (blue). Images were taken using Zeiss LSM 510 with 40X oil objective**. B.** Quantification of cytoplasmic protrusions. Total area occupied by protrusions per cell outline (set to 100 pixels) was detected by S.CO LifeScience (Germany). Student t-test was used for analyzing the data and *: $p<0.05$).

After staining the cells with phalloidin, peripheral long cytoplasmic projections were detected in MCF7-EV, while just a diffused localization of actin filaments nearly without such projections was detected in miR-125 expressing MCF7 cells, which showed that the expression of miR-125 affected the formation of actin filaments in the protrusion structures and changed the morphology of MCF7 cells (Figure 3.28). These projections could be responsible for motility and migration of MCF7 cells and miR-125 expression reduced these projections and possibly as a result, less motility and migration was indeed observed in cells expressing miR-125, compared to control cells (Figure 3.24).

In order to investigate the actin filament status in another BCCL, expressing miR-125b, T47D-EV and T47D-125 cells were also stained with phalloidin. However, as these cells were very small and furthermore, they formed clumps, it was not possible to take clear images to follow the existence of such protrusions and actin filament formation in these cells.

Given the changes detected on the actin cytoskeleton, we focused on a target mRNA, detected in our lab earlier, *ARID3B*. The reason was that recently ARID3B was reported to affect actin filaments in limb formation of chick and mouse embryo (Casanova et al. 2011).

3.2.6 *ARID3B*: a Target of miR-125b

ARID3B is a member of the AT-rich interaction domain (ARID) family of proteins and a known retinoblastoma (RB)-binding protein (Numata et al. 1999). *ARID3B* was previously reported as an important regulator of limb bud development during embryogenesis in chick and mouse, affecting cell motility and actin cytoskeleton structure (Casanova et al. 2011). It was also shown that miR-125a was a regulator of *ARID3B* in ovarian cancer (Cowden Dahl et al. 2009). Results from luciferase assay, earlier performed in our lab revealed that *ARID3B* was a target of miR-125b.

miR-125a and miR-125b have the same seed sequences with different mature sequences. For this reason, as a confirmation of the earlier luciferase reporter assays for *ARID3B* in MCF7-EV and MCF7-125 cells, we further performed western blot analysis in these cells and detected an approximately 50% decrease in ARID3B protein level in MCF7-125 cells, expressing miR-125b, compared to MCF7-EV cells (Figure 3.29).

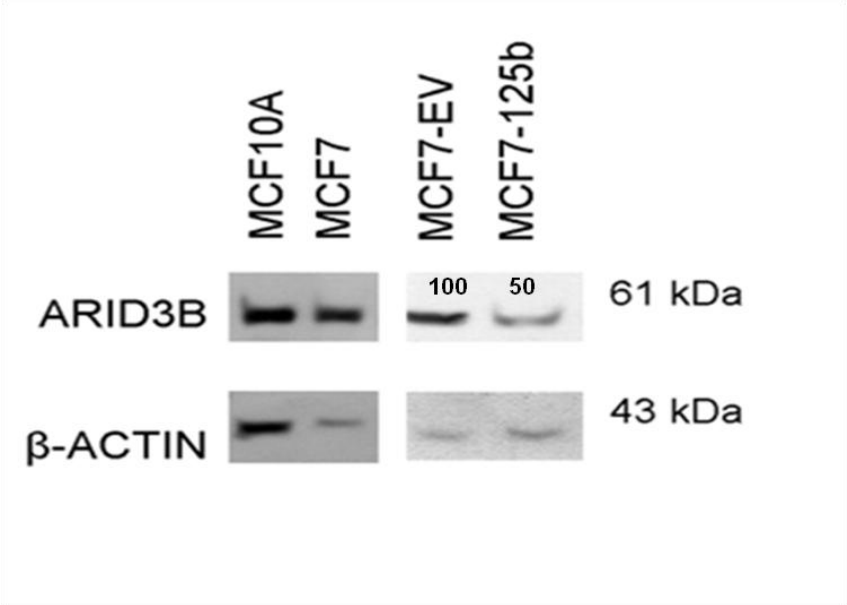

Figure 3. 29 Western blot detecting the level of ARID3B protein in MCF10A, MCF7, MCF7-EV and MCF7-125 cells. Blots were hybridized with anti-ARID3B and then with anti-β-ACTIN antibodies to test equal loading. ImageJ program was used for the quantification of the bands.

Results on Figure 3.29 revealed that ARID3B protein was expressed ~ 1.6 folds higher in MCF7 breast cancer cell line, compared to immortalized normal MCF10A cells. The level of ARID3B protein was decreased in MCF7-125 cells approximately 50%, compared to MCF7-EV cells, further confirming the targeting of *ARID3B* by miR-125b. To further investigate the role of miR-125b in the regulation of ARID3B expression, anti-125a and anti-125b oligos were used to inhibit miR-125a/b in MCF7-125 cells (Figure 3.30).

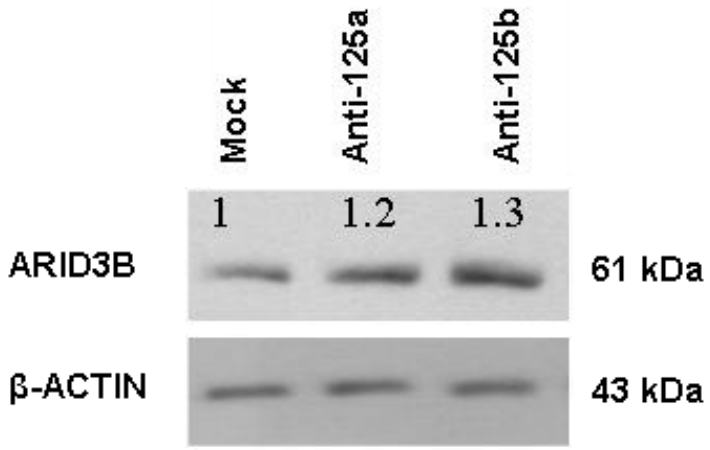

Figure 3. 30 Effect of miR-125a/b on ARID3B protein levels. Western blot for detecting the level of ARID3B protein in MCF7-125 cells, treated with anti-125a/b oligos (1.5 μg/mL). Blots were hybridized with anti-ARID3B and then with anti-β-ACTIN antibodies to test equal loading. ImageJ program was used for the quantification of the bands.

The level of ARID3B protein was restored after treatment with anti-125a/b oligos in MCF7-125 cells. miR-125a has been already shown to target ARID3B in ovarian cancer (Cowden Dahl et al. 2009) and as our results indicated, anti-125a oligo treatment, caused ~ 20% recovery of ARID3B protein level in MCF7-125 cells. In addition, MCF7-125 cells were treated with anti-125b oligos and western blot indicated ~ 30% recovery of ARID3B protein in these cells, compared to mock transfected MCF7-125 cells, confirming that miR-125b also regulates ARID3B protein levels.

In order to further confirm the connection between miR-125b and ARID3B, we also used T47D cells, with high endogenous levels of miR-125a (Figure 3.17) and

investigated the effect of anti-125b on ARID3B protein levels in these cells (Figure 3.31).

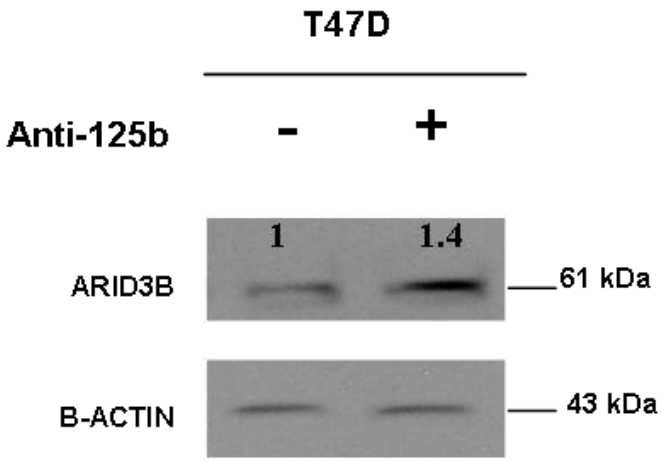

Figure 3. 31 Effect of anti-125b on the level of ARID3B protein in T47D cells. We detected an increased (1.4 fold) of ARID3B protein level in T47D cells transfected with anti-125b oligo (1.5 μg/mL), compared to mock transfected T47D cells was observed. Total protein was isolated from transfected cells, 24h after transfection. Blot was stripped and re-hybridized with β-ACTIN antibody to test equal loading. ImageJ program was used for quantification of the bands.

Results indicated that even low levels of miR-125b were also regulating the ARID3B protein in these cells with a high background expression level of miR-125a.

In order to study the effect of *ARID3B* in MCF7 cells, shRNA construct targeting *ARID3B* mRNA (previously was cloned by Serkan Tuna into pSUPER vector in our lab) and scrambled- pSUPER controls were transfected into MCF7 cells. Protein was isolated from cells, 72 hr after transfection and western blot was performed (Figure 3.32).

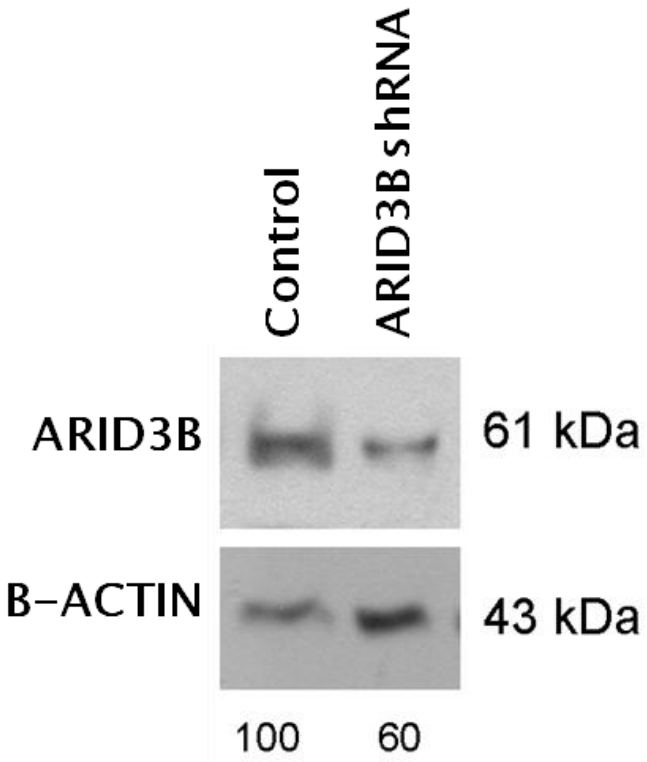

Figure 3. 32 Western blot for detecting the silencing of ARID3B in MCF7 cells. MCF7 cells were transfected with a construct containing shRNAs against *ARID3B* and control empty vector (pSUPER). Protein was isolated 72 hr after transfection and 50 µg protein was loaded to each well. Blots were hybridized with anti-ARID3B and then with anti-β-ACTIN antibodies to test equal loading.

Western blot showed a 40% decrease in the level ARID3B as a result of silencing.

To study the effect of ARID3B on cell proliferation, MCF7 cells were transfected with ARID3B shRNA and control constructs and MTT assay was performed (Figure 3.33).

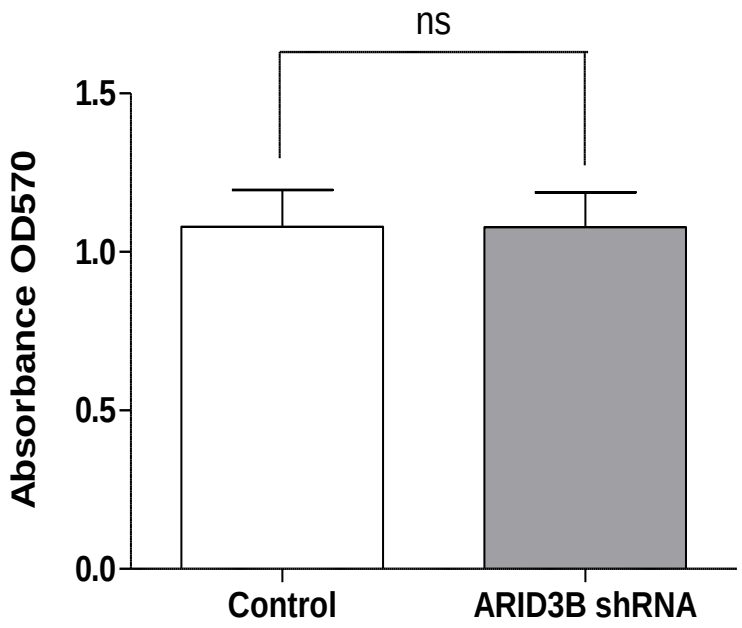

Figure 3. 33 MTT assay for MCF7 cells to detect cell proliferation rate after silencing ARID3B.MCF7 cells were transfected with a construct containing shRNAs against *ARID3B* and control empty vector (pSUPER). 15,000 cells were seeded per each well of 96 well plate and transfected 24 h after seeding, using Fugene HD (ratio for DNA: Fugene HD was 2ug:3µl). Absorbance at OD570 was measured 72 hr after transfection. Student t-test was used to analyze the data. "ns" indicates no significant difference between samples. Experiment was performed twice and at least 8 replicas were used in each experiment.

Compared to control, ARID3B shRNA caused no significant decrease in MCF7 cells' proliferation. This result indicates that ARID3B, by itself may not have an effect on cell proliferation rates, but to examine if the actin cytoskeleton related migrational changes were related to ARID3B, we investigated migration rate of ARID3B silenced cells (Figure 3.34). Results from Figure 3.34 indicated the effect of ARID3B on cell migration, revealing that that both miR-125 expression and *ARID3B* silencing caused a decrease in MCF7 cells migration (Figures 38 and 48).

To further investigate if there was a correlation between ARID3B protein and mature miR-125a and miR-125b expression levels, we performed miRNA Taqman assay (Figure 3.35 A) to detect mature miRNA levels and western blot (Figure 3.35B) to detect ARID3B levels, in 4 ERBB2 independent breast cancer cell lines (MCF10A, MCF7, MDA-MB-231 and T47D).

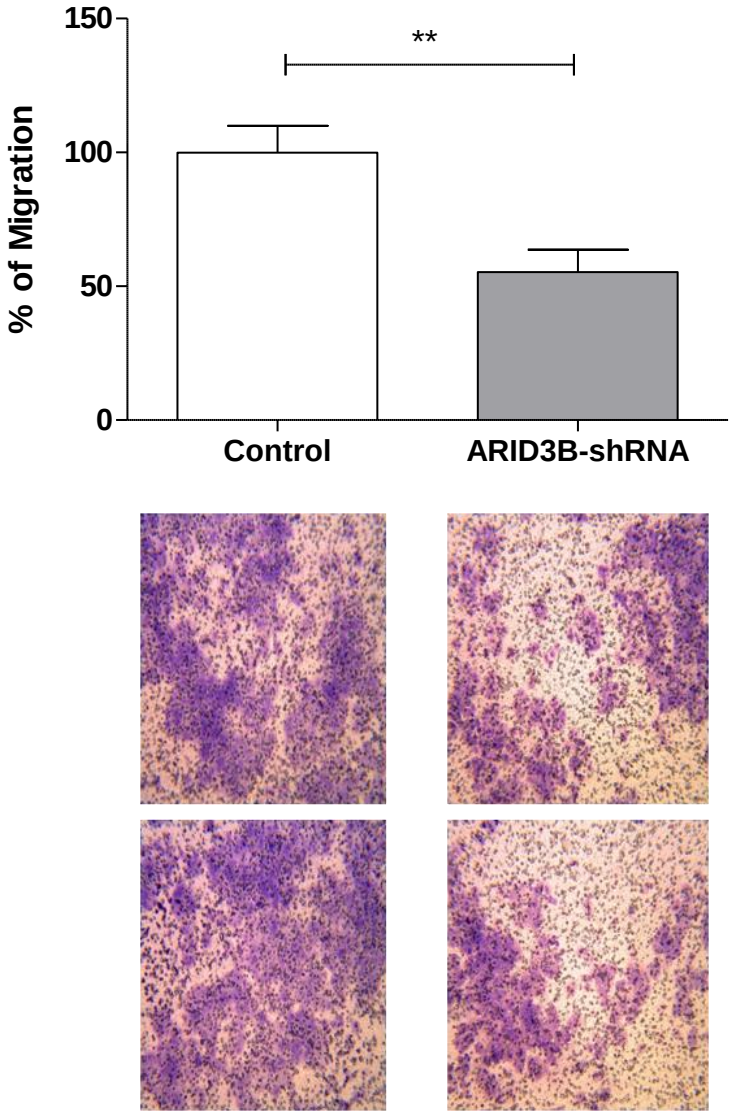

Figure 3. 34 Migration assay for MCF7 cells transfected with ARID3B shRNA.For migration assay, 8 h after MCF7 cells were transfected with a construct containing shRNAs against *ARID3B* or control empty vector (pSUPER). 30,000 of transfected cells were plated on the transwell migration chamber and cells were allowed to migrate for 72 h. 3 random fields were counted per membrane. 4 membranes were used for each sample. Student t-test was used for statistical analysis of data ($p<0.05$). Representative images are shown under the graph.

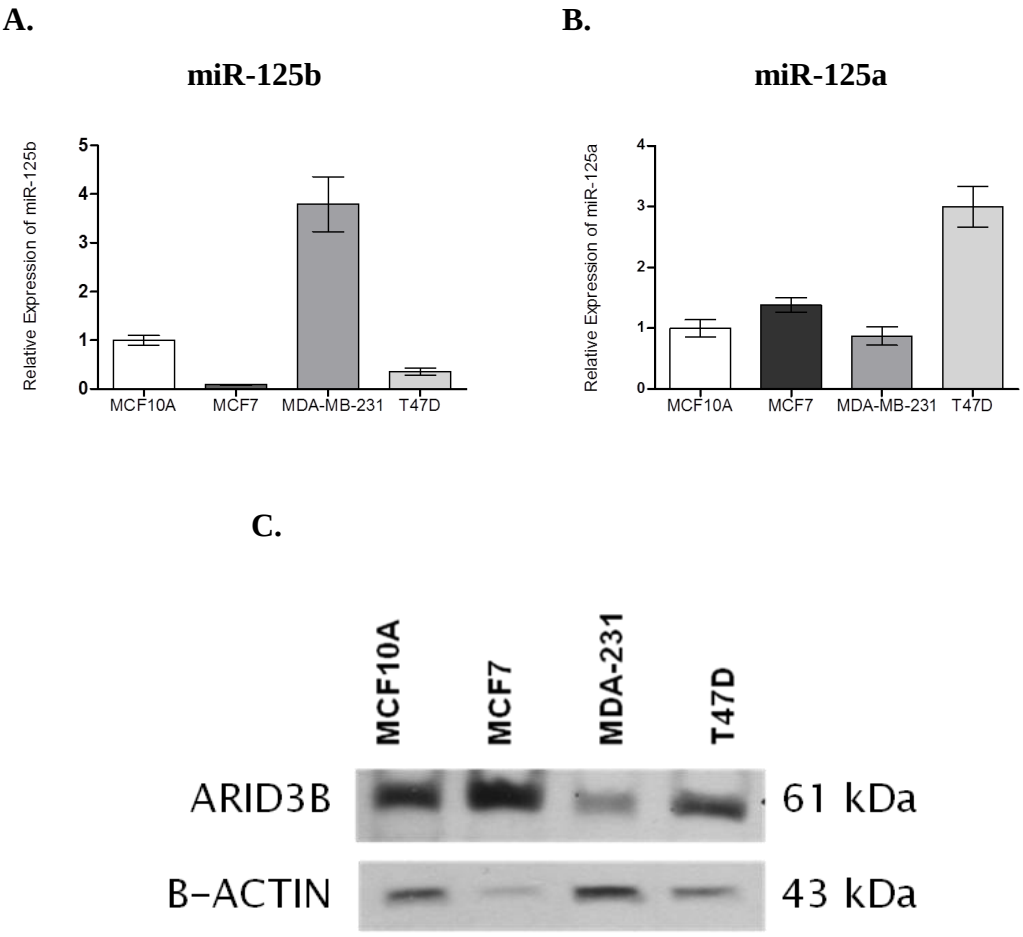

Figure 3. 35 Taqman assay and western blot for detecting the expression of miR-125 and ARID3B. **A** and **B.** Taqman miRNA assay for detecting mature miR-125b and miR-125a, respectively in MCF10A, MCF7, MDA-MB-231 and T47D breast cancer cell lines. *RNAU6B* was used as reference gene. Experiments were performed in 2 independent experiments and 3 replicas were used for each sample**.** **C.** Western blot indicating ARID3B protein levels in MCF10A, MCF7, MDA-MB-231 and T47D cells. Blot was stripped and re-hybridized with β-ACTIN antibody to test equal loading.

These results indicated an inverse correlation between mature miR-125 and ARID3B protein levels, possibly as a result of miR-125 on ARID3B expression.

The next step, we wanted to investigate some of predicted miR-125b target genes, possibly responsible for the observed characteristics of miR-125 expressing cells.

In this study, we investigated the effect of miR-125 expression on ERBB2 (an already known target of miR-125b) independent MCF7 cells. Previously, it was shown that miR-125 expression restoration in SKBR3 breast cancer cells (overexpressing ERBB2) decreased the invasion and anchorage dependent growth of these cells in an ERBB2 dependent manner (Scott et al. 2007). We further investigated the effect of ERBB2 on MCF7 cells' migration in our model cells.

3.2.7 Investigating mRNA Targets of miR-125b

Earlier, miR-125b was shown to regulate cell migration by targeting ERBB2 in ERBB2 overexpressing SKBR3 breast cancer cells. In our study, we used MCF7 cells, which are not overexpressing ERBB2 (express low level of ERBB2 protein). However, before we start finding new target genes for miR-125, responsible for cell migration, we investigated the expression of ERBB2 protein and pERK1/2 in SKBR3 (ERBB2 overexpressing cells) and MCF7 cells (ERBB2 independent cells), shown in Figure 3.36. We also investigated the involvement of ERBB2 in MCF7 cell migration (Figure 3.37).

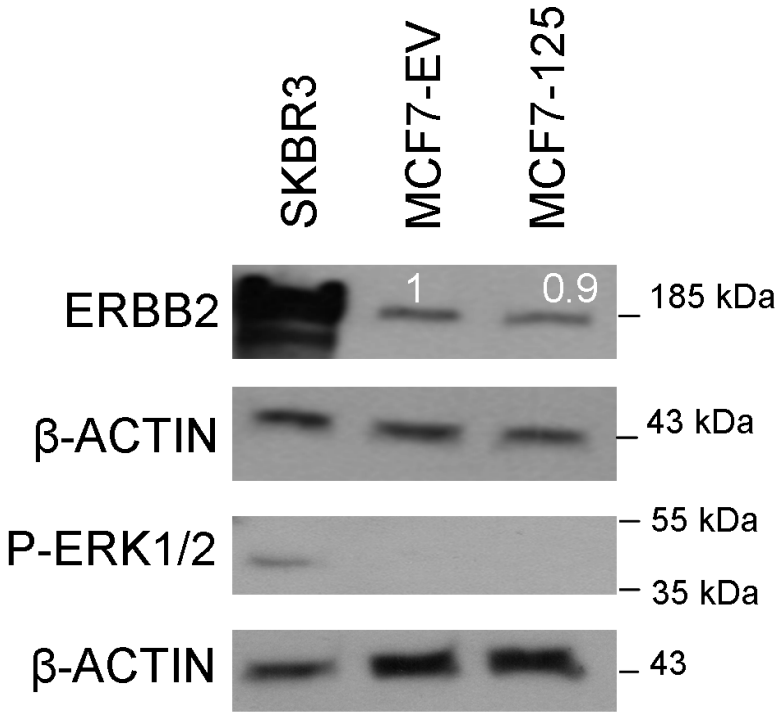

Figure 3. 36 Western blot indicating the level of ERBB2 and pERK1/2 in SKBR3 (ERBB2 overexpressing positive control cell line), MCF7-EV and MCF7-125b cells. Blots were hybridized with anti-ERBB2, anti-pERK 1/2 and then with anti-β-ACTIN antibodies to test equal loading. Image J program was used for the quantification of the bands.

The level of ERBB2 protein was detected in SKBR3, MCF7-EV and MCF7-125 via western blot. Further, to detect if ERBB2 is activated in these cells, the level of phosphorylated ERK 1/2, an ERBB2 downstream target (Spencer et al. 2000) was detected by western blot (Figure 3.36). The results indicated that the level of ERBB2 protein is low in MCF7 cells and miR-125 expression in MCF7-125b cells didn't significantly affect the level of this protein in MCF7 cells, compared to MCF7-EV cells. In addition, pERK 1/2, a known downstream target of activated ERBB2, was not detected in any of MCF7-125b and MCF7-EV cells, indicating no activation of ERBB2 signaling in MCF7 cells.

A.

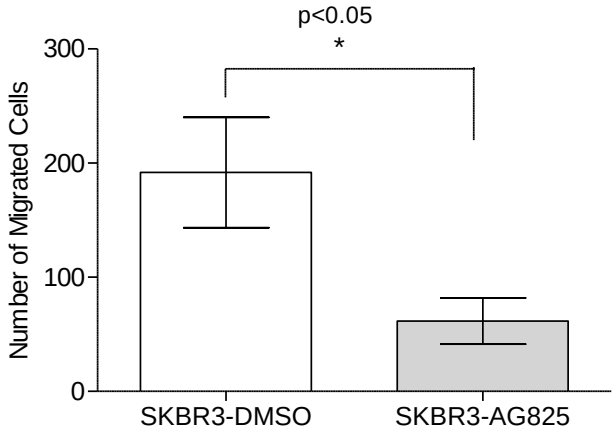

B.

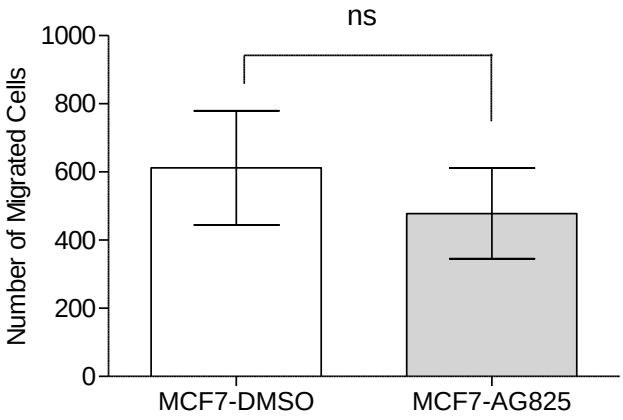

Figure 3. 37 Transwell migration assay to determine the effect of AG825 on A. MCF7 and B. SKBR3 cells' migration.200,000 pre-starved SKBR3 and MCF7 cells in 0.1 mL medium with 1% FBS and AG825 or DMSO (vehicle) were plated on the upper wells of migration chambers. Medium with 10% FBS was added to the lower wells. Cells were allowed to migrate for 24 h. 3 random fields were counted per membrane. Six membrane replicates were used for each sample. Student t-test was used to analyze the data and *: indicates statistical significance ($p<0.05$). "ns" indicates not significant.

Finally, we studied the migration properties of SKBR3 and MCF7 cells, in the presence or absence of AG825, a specific ERBB2 inhibitor (Tsai et al. 1996), as shown in Figure 3.37. The results from transwell migration assay showed no significant impact of ERBB2 inhibition by AG825 treatment on MCF7 migration, compared to positive control SKBR3 cells, revealing an ERBB2 independent effect of miR-125 on MCF7 cells' migration (Figure 3.37).

Our results indicated that migration of MCF7 was affected by miR-125b and in an ERBB2 independent manner. In addition, ARID3B, a target of miR-125 also affected the migration characteristics of MCF7 cells, suggesting that ARID3B could be considered as a downstream target of miR-125b, affecting cell migration.

Given the changes in the characteristics of MCF7-125 cells, bioinformatics tools were used to determine miR-125b targets, possibly involved in these changes. In order to find new targets of miR-125, responsible for recorded morphological changes, bioinformatics tools (TargetScan, microRNA.org, PITA and FindTar3) were used. Generally, prediction programs are based on information such as: sequence conservation, perfect base pairing of mRNA 3'-UTR to the seed sequence of microRNA, secondary structure and optimal hybridization energy for microRNA and target mRNA binding. For example, TargetScan program, predicts the microRNA- mRNA bindings, according to the incidence of conserved and poorly conserved 7-8 mer sites on mRNAs, matching the microRNA seed sequences (Lewis et al. 2005) as well as mismatch regions in the seed sequences, compensated via conserved pairings with 3'-sides of microRNA sequences (Friedman et al. 2009).

Using these prediction programs, three potential novel targets of miR-125b (v-ets erythroblastosis virus E26 oncogene homolog 1 (*ETS1),* Homeobox B7 (*HOXB7)* and zinc finger and BTB domain containing 7A (*ZBTB7A*) or *FBI-1)* were selected. These predicted targets were further investigated for the possibility of being the

targets of miR-125b by luciferase assay. *ARID3B*, another predicted target of miR-125b was earlier shown in our lab (by luciferase assay) to be the target of miR-125b.

3.2.7.1 pmiR-3'-UTR Cloning of miR-125 Potential Targets

HOXB7, a homodomain transcription factor, plays important role in Epithelial-Mesenchymal Transition (EMT). EMT is a mechanism by which primary noninvasive tumor cells obtain required characteristics for migration and invasion. In addition, *HOXB7* was shown to be overexpressed in breast cancer (Wu et al. 2006). *ZBTB7A*, another potential target of miR-125b, is a proto-oncogene and was shown to be highly expressed in breast cancer tissues (correlated with histological grade). *ZBTB7* could be a potential prognostic marker in breast cancer (Qu et al. 2010). ETS1 transcription factor is overexpressed in invasive breast cancers, correlated with poor prognosis of breast cancer patients (Zhang et al. 2011). Here we investigate the possible regulation of this gene by miR-125b via cloning their 3'UTR sequences downstream of luciferase gene into pMIR-REPORT vector and performed luciferase assay (Figures 3.38, 3.39 and 3.40). Primers, used for cloning the constructs are shown in Appendix A.

A.

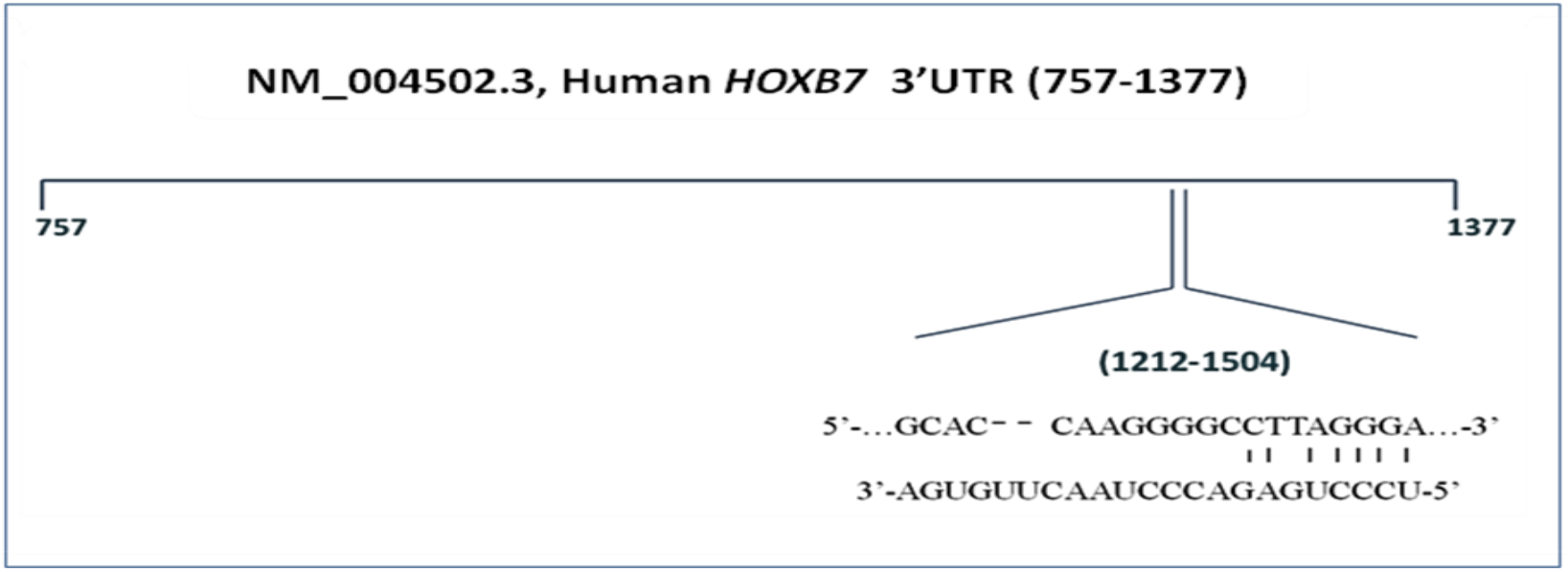

Figure 3. 38 A. Alignment of HOXB7-3'UTR and predicted binding site of miR-125b.

B.

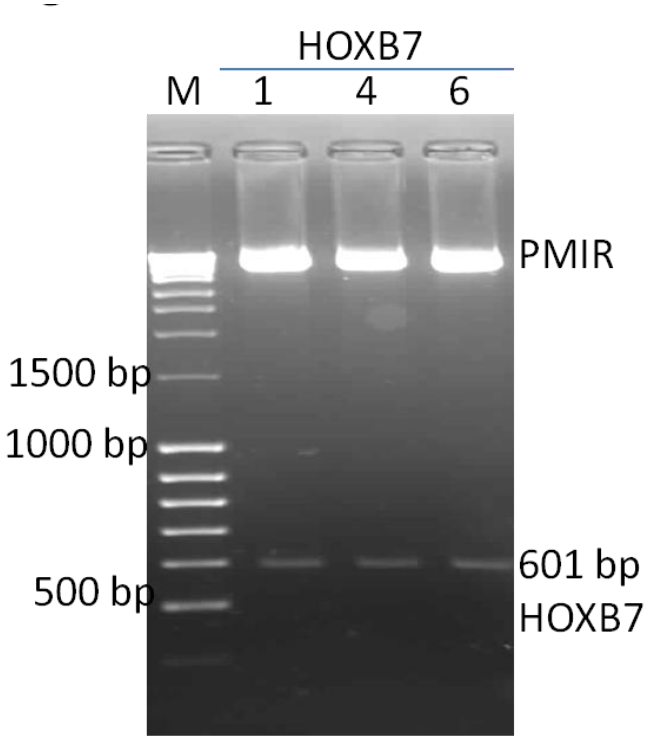

Figure 3. 38 (Continued) B. *HindIII* and *SacI* digestion for confirming the cloning of 3'-UTR of *HOXB7*. M: MassRuler marker, 1, 4 and 6: name of the constructs, obtained from different colonies.

A.

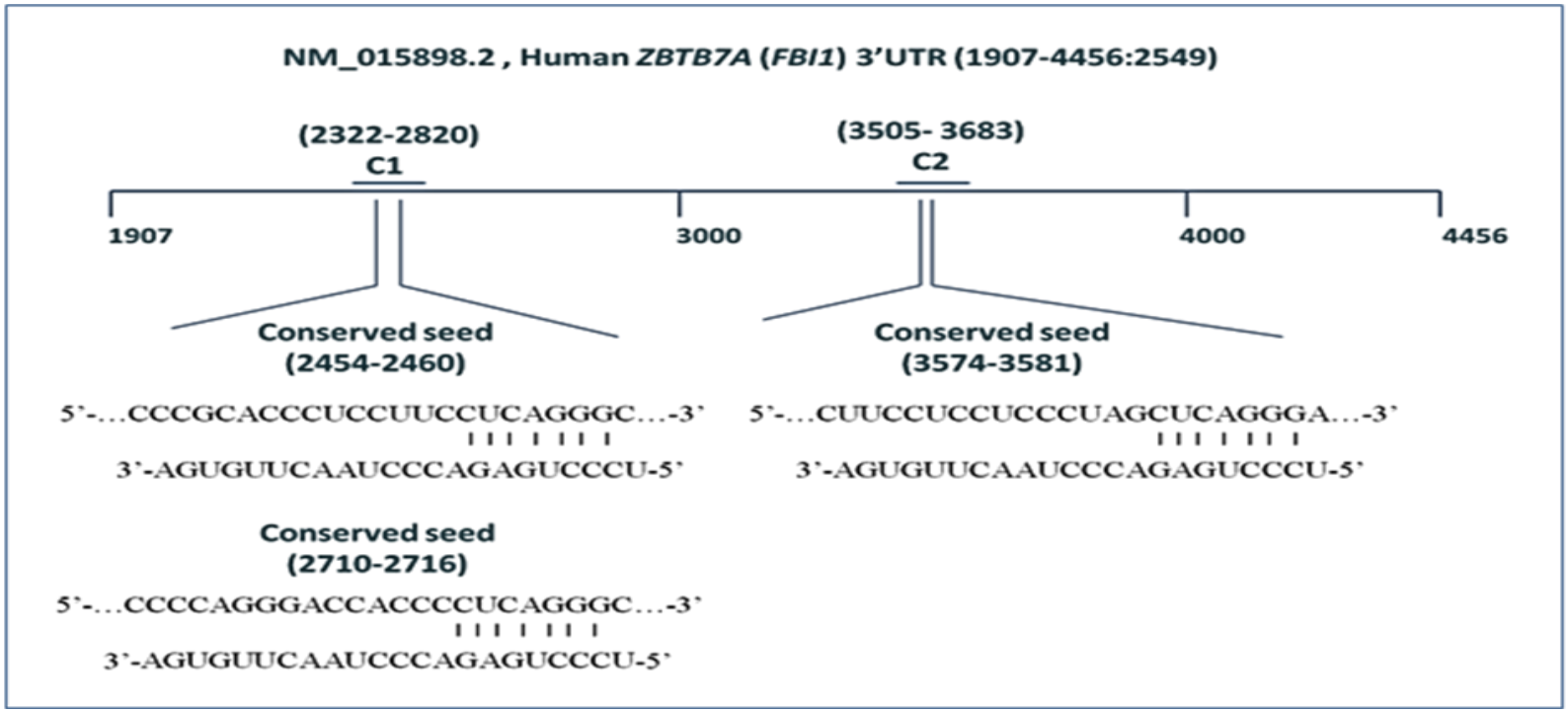

Figure 3. 39 A. Alignment of FBI1-3'UTR (C1 and C2) and predicted binding sites of miR-125b.

B.

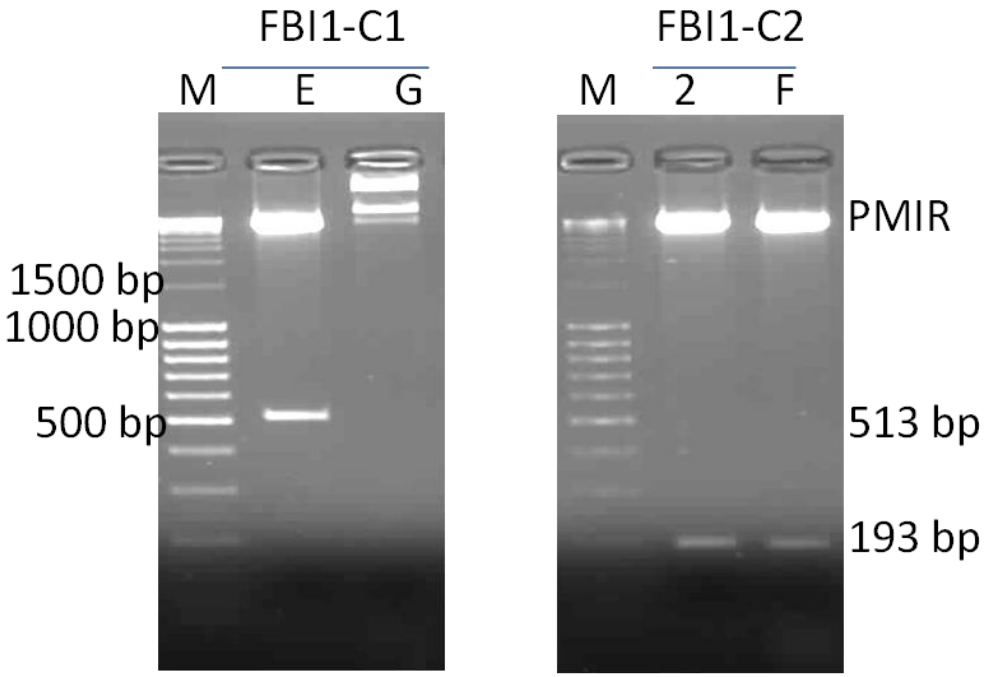

Figure 3. 39 (Continued) B. *HindIII* and *SacI* digestion for confirming the cloning of 3'-UTR of FBI1-C1 and FBI1-C2. M: MassRuler marker. E, G, 2 and F: name of the constructs, obtained from different colonies.

A.

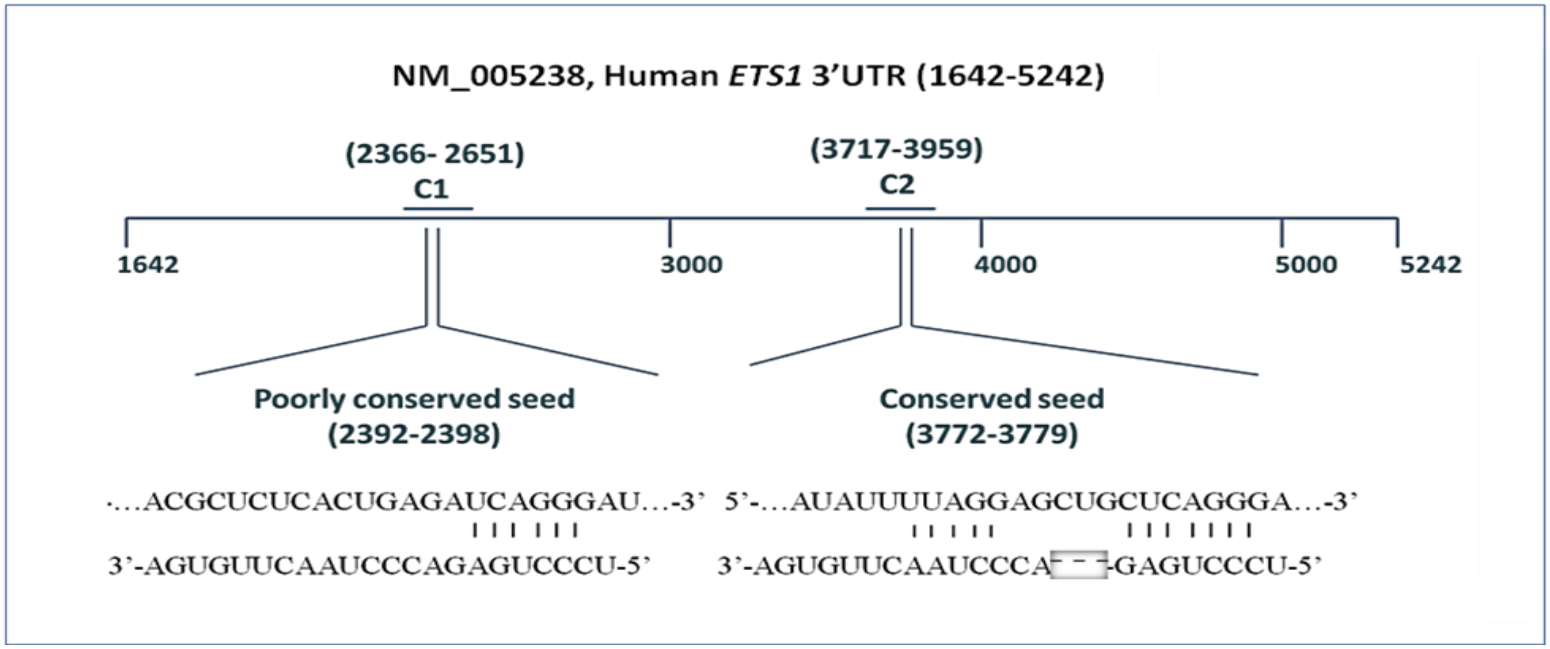

Figure 3. 40 A. Alignment of ETS1-3'UTR (C1 and C2) and predicted binding sites of miR-125b.

B.

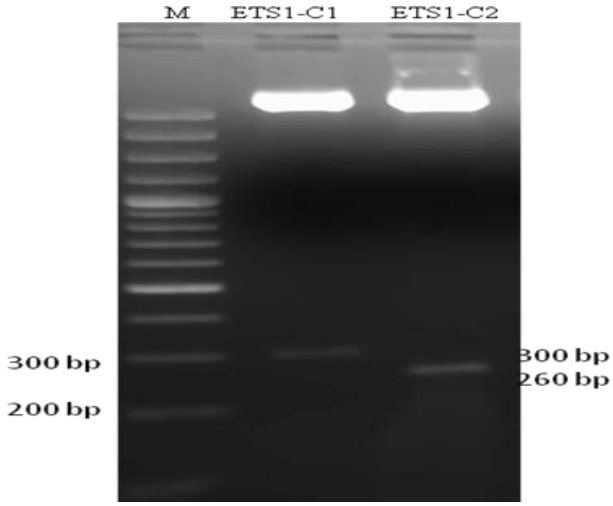

Figure 3. 40 (Continued) B. *HindIII* and *SacI* digestion for confirming the cloning of 3'-UTR of ETS1-C1 and ETS1-C2. M: MassRuler marker.

After confirming the correct constructs by restriction digestion and sequencing, they were further used in luciferase assay.

3.2.7.2 Luciferase assay for miR-125 targets

3'UTR of *ETS1*, *HOXB7* and *ZBTB7A*, three potential targets of miR-125b were cloned into pmiR vector, sequenced and dual luciferase assay was performed in MCF7 cells (MCF7-125 and MCF7-EV). In addition, luciferase assay was performed in MDA-MB-231 cells, expressing high levels of miR-125b. Data are shown in Figures 3.41, 3.42 and 3.43.

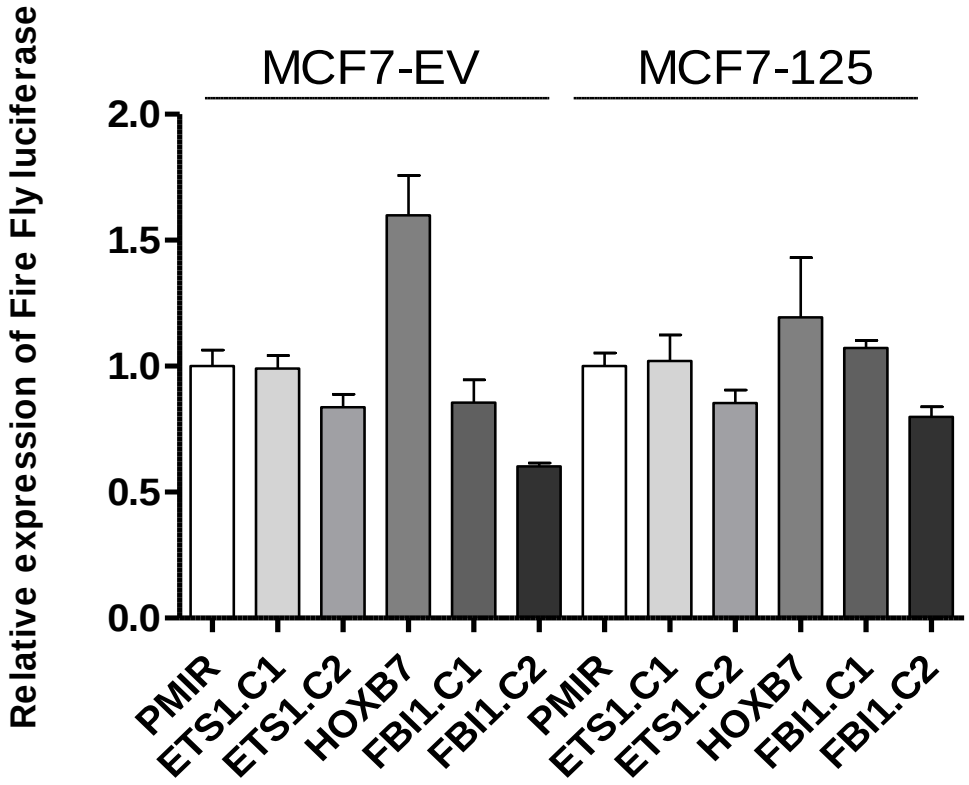

Figure 3. 41 Dual luciferase assay for predicted targets of miR-125b in MCF7 cells. Assay was performed in MCF7-EV and MCF7-125 cells for *ETS1*-C1-PMIR, *ETS1*-C2-PMIR, *HOXB7*-PMIR, *FBI1*-C1-PMIR and *FBI1*-C2-PMIR constructs. Transfection was done, using Fugene HD reagent (Fugene HD: DNA ratio was 3:2). A total of 500 ng plasmid (Firefly: Renilla ratio: 50:1) were used per each well of 24-well plate and the values for luciferase expression were detected 24 h after transfection. Renilla luciferase was used for normalization. The values were normalized to that of empty vector. The experiment was performed twice, each with 3 replicas per sample**.**

Luciferase results from Figure 3.41, for predicted targets of miR-125 in MCF7 cells revealed no decrease in luciferase expression of constructs transfected into MCF7-

125 cells, compared to MCF7-EV cells. To further confirm these results, we used MDA-MB-231 cells, expressing extremely high endogenous levels of miR-125b, compared to MCF7 cells.

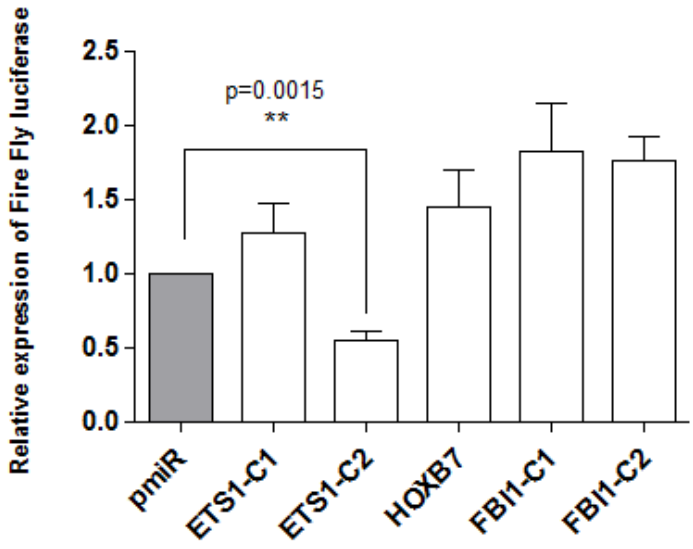

Figure 3. 42 Dual luciferase assay. Assay was performed in MDA-MB-231 cells for ETS1-C1-PMIR, ETS1-C2-PMIR, HOXB7-PMIR, FBI1-C1-PMIR and FBI1-C2-PMIR constructs. Transfection was done, using Fugene HD reagent (Fugene HD: DNA ratio was 6:2) and the values for luciferase expression were detected 24h after transfection. A total of 500 ng plasmid (Firefly:Renilla ratio: 250:1) were used per each well of 24-well plate. Renilla luciferase was used for normalization. The values were normalized to that of empty vector. The experiment was performed twice for pmiR and ETS1-C2 (3 replicas per sample were used in each experiment) and once for the rest targets (3 replicas per sample). Student t-test was used to analyze the data. **: indicates statistical significance (p:0.0015).

The differences detected in luciferase assay from MCF7 and MDA-MB-231 cells could be explained by the high level of miR-125b in MDA-MB-231 cells, make it possible to follow the microRNA- 3' UTR binding in these cells by luciferase assay.

The results from Figure 3.42 indicated a decrease in luciferase expression of *ETS1*-3'UTR-pmiR (C2), compared to pmiR alone in MDA-MB-231 cells, indicating the existence of a regulatory factor on this sequence in these cells. To confirm the results from prediction programs, indicating the possibility for binding of miR-125b to *ETS1*- 3'UTR sequence, we performed dual luciferase for pmiR and *ETS1*-3'UTR-pmiR (C2), using anti-miR-125b and control oligos in MDA-MB-231 cells (expressing high level of miR-125b, as shown in Figure 3.17). Transfection was done, using Fugene HD transfection reagent (6:2 ratio was used for Fusion HD (µl): DNA (µg) and oligos were used at final concentration of 100 nM). Renilla luciferase was used for normalization of the data. 250:1 ratio was used for Firefly: Renilla luciferase transfections (Figure 3.43).

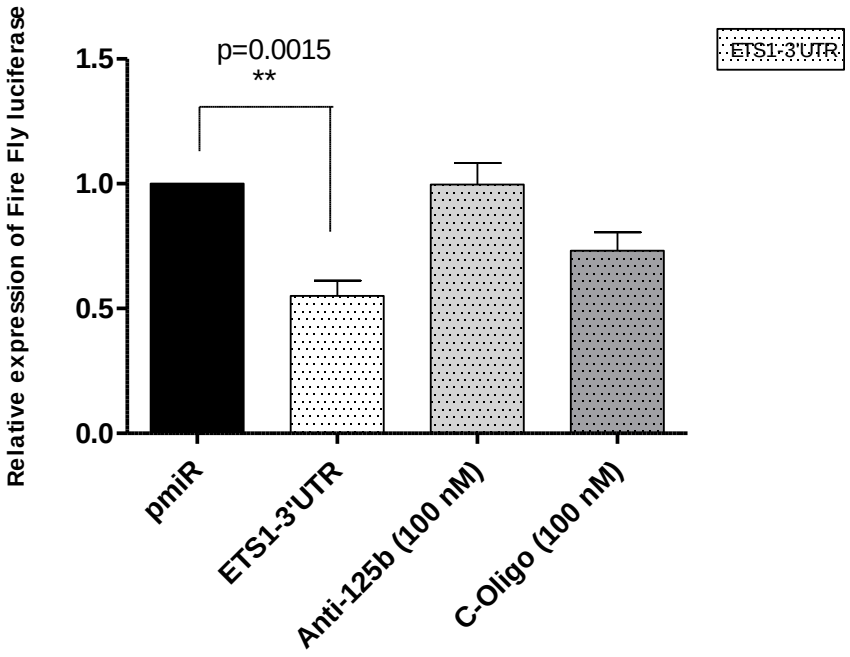

Figure 3. 43 Dual luciferase assay for miR-125b targets in MDA-MB-231 cells transfected with anti-miR-125b and control oligo. Assay was performed inMDA-MB-231 cells for empty PMIR vector and ETS1-C2-PMIR construct (containing 1 conserved predicted miR-125b binding site on ETS1-3'-UTR), with or without 100 nM Anti-125b oligo and C-Oligo. Transfection was done, using Fugene HD reagent (Fugene HD: DNA ratio was 6:2) and the values for luciferase expression were detected 24 h after transfection. Renilla luciferase was used for normalization (Firefly: Renilla is 250:1). The values were normalized to that of empty vector. The experiment was performed twice for pmiR and ETS1-C2 (3 replicas per sample were used in each experiment) and once for miR-125b inhibitor and control oligo treated samples. **: indicates statistical significance (p:0.0015).

Results, shown on Figure 3.43, indicated a miR- 125b dependent decrease (~45%) of luciferase in *ETS1*- 3'UTR-pmiR (C2), compared to pmiR alone in MDA-MB-231 cells. This decrease was ~100% recovered after anti-miR-125b oligo (but not control oligo) treatment in these cells. Recently, in agreement with our results, miR-125b was shown to target ETS1.(Zhang et al. 2011) also showed that *ETS1* in HEK293 (Human embryonic kidney) cell line was responsible for decreased proliferation rate.

Our results showed that miR-125b expression caused a decrease in proliferation and migration of MCF7 cells, independent of ERBB2 expression. Further, the localization of actin cytoskeleton was changed in MCF7 cells in response to miR-125b expression, indicating decreased cytoplasmic protrusions in MCF7-125 cells, compared to MCF7-EV control cells, possibly regulating the migration of MCF7 cells. Using bioinformatics tools, we chose *ARID3B*, as a possible potent target of miR-125b and we showed that the ARID3B protein levels had an approximately 50% decrease in MCF7-125 cells. Furthermore, *ARID3B* silenced MCF7 cells showed a decrease in their migration rates, compared to MCF7 cells, but no change in the proliferation of MCF7 cells was detected after *ARID3B* silencing. miR-125a was an already known regulator of ARID3B protein in ovarian cancer, and as miR-125a and miR-125b had the same seed, but different mature sequences, we investigated the effect of miR-125b on the ARID3B expression. We further confirmed the regulatory role of miR-125b on ARID3B expression in T47D cells expressing high levels of endogenous miR-125a, by inhibiting 125b and detected ~40% recovery for ARID3B protein levels after miR-125b inhibition in these cells, revealing a regulatory role for miR-125b in the presence of miR-125a expression.

CHAPTER 4

CONCLUSION

A. Localization of USP32, as a Potent Oncogene Candidate

USPs are members of deubiquitinating enzymes, responsible for the cleavage of Ub from ubiquitinated proteins. Deubiquitination by this group of proteases could determine the fate of target proteins. Protein degradation, cell signaling and receptor endocytosis are among the pathways regulated by protein deubiquitination. *USP32* is an ancient and highly conserved but poorly characterized gene and is a member of the USP family. *USP32* gene is located on 17q23 chromosomal band. This gene rich region undergoes amplification and overexpression in many cancers including breast, suggesting a possible oncogenic role for this gene.

The present study focused on characterization of USP32 via investigating the subcellular localization of this protein. For this purpose, the full length and partial but overlapping fragments of USP32 were fused to EGFP and constructs were tracked inside the HeLa cells. We performed FPP and confocal microscopy to determine the localization of USP32 fusion protein. Our results suggested a Golgi localization for USP32-Full (full length protein)-EGFP and USP32-I-EGFP and EGFP-USP32-II (partial fragments of USP32 protein) with a cytoplasmic localization in some cells expressing EGFP-USP32-I, however EGFP-USP32-III showed a cytoplasmic localization. These results may be interpreted by the existence of a Golgi localization signal around the overlapping sequences of

USP32-I and USP32-II, probably weakened in USP32-I fragment, as a result of dividing the full sequence. Alternatively, observations from the localization of USP32-I and USP32-II could also be a consequence of an unusual folding for partial peptides or a difference in cell cycle status of cells expressing these peptides. The results from FPP assay was also confirmed by confocal microscopy detection.

The mechanism for Golgi localization is not fully understood as a conserved Golgi localization signal has not been detected. The Golgi is a membranous organelle which receives newly synthesized lipids and proteins from the ER. Proteins in Golgi are further processed, mostly by glycosylation, in order to properly function and find their final destinations. The Golgi has a diverse range of functions such as its assembly/disassembly during mitosis, its connection to cytoskeleton organization and dynamics as well as its role in calcium homoestasis and plasma membrane receptor-initiated signaling events (Wilson et al. 2011).

Significant role of ubiquitination in protein degradation, receptor endocytosis and vesicle trafficking has already been revealed. The link between deubiquitination and Golgi was earlier demonstrated in yeast by the function of deubiquitinating enzyme Ubp3p. Ubp3p, in combination with its cofactor Bre5p is responsible for deubiquitinating the Sec23p and β'-COP subunits of ER- Golgi transport complexes COPII and COPI respectively. Deubiquitination of these components are required for the proper vesicle trafficking between ER and Golgi (Cohen et al. 2003a; Cohen et al. 2003b).

In addition to vesicular transport, Ub seems to play role in Golgi biogenesis. VCIP135 is also a deubiquitinating enzyme, localized in Golgi membrane and playing role in Golgi biogenesis and dynamics during mitosis. Deubiquitination activity of this enzyme reverses the Golgi disassembly and support Golgi membrane fusion (Totsukawa et al. 2011; Wang et al. 2004).

USP33, another deubiquiting enzyme was shown to have three endoplasmic reticulum associated isoforms, with its isoform 3, distinctly localizing to the Golgi apparatus (Thorne et al. 2011). USP33 is a ROBO1 interacting protein, causing its relocalization from the intracellular compartments to the plasma membrane to perform its anti migratory function in breast cancer (Yuasa-Kawada et al. 2009). As Robo1 (in *Drosophila*) is localized in cell membrane, ER and Golgi apparatus (Keleman et al. 2002), it may suggest a role for isoform3 of USP33 to partly regulate Robo1 l, which is localized in Golgi, beside its other possible roles to be further investigated.

All these findings reveal the importance of deubiquitinating enzymes in Golgi. The localization study of USP32, suggested an as of yet unknown possible function for this enzyme in Golgi. Further investigations to find the interacting partner proteins as well as the function of N-terminus Ca2+ and EF-hand domains may help to clarify the connection between USP32 and Golgi.

B. Functional characterization of miR-125b as potential tumor suppressor

microRNAs are 16-29 nucleotides long RNA molecules, that post-transcriptionally regulate the expression of their target mRNAs. These non-coding small RNAs play role in many key regulatory pathways such as cell proliferation, differentiation, apoptosis and migration. Deregulation of microRNAs is involved in various human diseases including cancer. miR-125b attracts attention, especially in breast cancer, due to its down regulation in cancer.

In this study, we aimed to further clarify the function of miR-125b in breast cancer. For this reason, we first investigated the expression of mature miR-125a and miR-125b, two members of miR-125 family, in 10 breast cancer cell lines. Compared to miR-125a, whose expression was available nearly in all samples, the expression of

miR-125b was found to be dramatically low or absent in 9 of 10 cell lines, compared to immortalized MCF10A cell line and normal breast tissue controls, suggesting a tumor suppressor role for this miRNA in breast cancer. These finding was also in agreement with primary tumor samples (Iorio et al. 2005; Mattie MD 2006). By performing functional assays in MCF7 cells, stably expressing miR-125b we detected a decrease of MCF7 cells' proliferation and migration.

Interestingly, an earlier study done in breast cancer showed the role of miR-125b in cell motility by targeting the well known oncogene, *ERBB2*. Our model system to study the effects of miR-125b restoration was MCF7 in this study. MCF7 cells do not overexpress ERBB2. Interestingly, we used miR-125b transfected MCF7 cells and compared them to empty vector transfected MCF7 cells, and detected ~ 50% decrease in cell motility. The migration recovery was also confirmed by miR-125b inhibition in these cells. These finding forced us to seek non ERBB2 dependent cell motility mechanisms to explore the phenotype we observed. Moreover, the lower long cytoplasmic protrusions structure in miR-125b expressing compared to control MCF7 cells after staining the actin filaments was observed.

Based on earlier experiment done in our laboratory, *ARID3B* was shown to be a target of miR-125b. In this study, we focused on ARID3B and its possible involvement in cell motility because ARID3B was shown to regulate the formation of limb buds during the embryogenesis of chick and mouse with a regulatory effect on cell motility and affecting the organization of actin cytoskeleton (Casanova et al. 2011). We hypothesized that the decreased migration and actin cytoskeleton phenotype we have seen was due to ARID3B. First we eliminated the possibility of involvement of basal levels ERBB2 in this phenotype.

ARID3B, is a member of ARID family, which are transcription factors and regulators of cell proliferation, differentiation and development (Casanova et al.

2011; Kobayashi et al. 2006) with possible roles in chromatin remodeling. ARID3B is known to be a retinoblastoma (RB)- binding protein and associated with malignant neuroblastoma. Further studies revealed its role in induction of immortalization and mesenchymal transition in mouse embryonic fibroblasts (Takebe et al. 2006). The most recent exciting findings revealed the involvement of ARID3B in regulating the formation of limb buds during the embryogenesis of chick and mouse with a regulatory effect on cell motility and the organization of actin cytoskeleton (Casanova et al. 2011).

Moreover, *ARID3B* was shown to be targeted by miR-125a in ovarian cancer (Cowden Dahl et al. 2009). miR-125a and miR-125b have the same seed but different mature sequences and for this reason further studies were performed on ARD3B, for understanding the regulatory effect of miR-125b, with frequent lost or decreased expression in breast cancer. Results from this study confirmed the down regulation effect of miR-125b on ARID3B protein levels in MCF7 cells, as its direct binding to the 3'UTR of *ARID3B* was also previously shown in our lab. This results were further confirmed by the inhibition of miR125a and miR125b in MCF7 cells, expressing miR-125b, revealing a ~20% and 30% recovery of ARID3B protein respectively and indicating the involvement of both microRNAs in the regulation of ARID3B protein in these cells. Additionally, to further confirm the regulation of *ARID3B* with miR-125b in the presence of miR-125a, miR-125b was inhibited in T47D cells expressing high levels of endogenous miR-125a and approximately 40% recovery for ARID3B protein was detected, indicating particular regulatory impact of miR-125b on ARID3B in the presence of miR-125a. The significance of this finding could be loss of miR-125b regulation on ARID3B protein level in breast cancers losing the expression of this microRNA.

Further, to find if the decrease in cell migration and proliferation of miR-125b expressing MCF7 cells is associated with ARID3B, this gene was transiently

silenced. Our findings from the silencing of *ARID3B* in MCF7 cells revealed a decrease in cell migration, suggesting that down regulation of *ARID3B* by miR-125b may play a regulatory role in the migration of cancer cells. No change in the proliferation of MCF7 cells was detected after *ARID3B* silencing. As we excluded the contribution of ERBB2 in our model system and miR-125b is shown to target mRNAs that me regulate proliferation (example: ETS1 (Zhang et al. 2011)) the possibility predicted for each microRNA to be able to target hundreds of different target mRNAs, it could be possible that the decreased of proliferation in miR-125b expressing cells was due to the regulation of target/targets other than *ARID3B* by miR-125b. Interestingly, recent studies revealed *ETS1*, as an effective target of miR-125b, affecting the proliferation property of the cells.

In summary, in this thesis we showed ability of miR-125b to alter cell migration through ARID3B, independent of ERBB2. Finally, studies for identifying 3 other potential targets of miR-125b (*ETS1, HOXB7* and *FBI1*) was performed, revealing *ETS1* as a target of miR-125b, in agreement with the results, recently published by another group (Zhang et al. 2011).

Together, growing lines of evidences suggest a general tumor suppressor role for miR-125b in breast cancer. This microRNA, is already known to target many key oncogenes such as *ERBB2*, *ERBB3*, *ETS1* and *BCL3*. Our findings revealed the ERBB2 independent effect of miR-125b on cell migration and formation of actin filaments, possibly to be in part by regulating *ARID3B*, whose regulation could be further implicated with other pathways during tumorigenesis. *ARID3B* was suggested to regulate the mesenchymal transition in mouse embryonic fibroblasts (Takebe et al. 2006), for this reason, down regulation of *ARID3B* by miR-125b may also play role in repressing mesenchymal morphology and regulating Epithelial Mesenchymal Transition (EMT). The general decrease/loss of miR-125b, detected

in many breast cancers and the possible known and potential targets of miR-125b may be further used as cues to be considered for therapeutic purposes.

REFERENCES

Adriance MC IJ, Petersen OW, Bissell MJ. (2005) Myoepithelial cells: good fences make good. Breast Cancer Res. **7**, 190-197

Akhavantabasi S, Akman HB, Sapmaz A, Keller J, Petty EM, Erson AE (2010) USP32 is an active, membrane-bound ubiquitin protease overexpressed in breast cancers. Mamm Genome 21, 388-397

Akhavantabasi S, Sapmaz A, Tuna S, Erson-Bensan AE (2012) miR-125b targets ARID3B in breast cancer cells. Cell Struct Funct 37, 27-38

Albertson DG (2006) Gene amplification in cancer. Trends Genet 22, 447-455

Ambros V, Bartel B, Bartel DP, Burge CB, Carrington JC, Chen X, Dreyfuss G, Eddy SR, Griffiths-Jones S, Marshall M, Matzke M, Ruvkun G, Tuschl T (2003) A uniform system for microRNA annotation. RNA 9, 277-279

Amerik AY, Hochstrasser M (2004) Mechanism and function of deubiquitinating enzymes.
Biochim Biophys Acta 1695, 189-207

Andersen CL, Monni O, Wagner U, Kononen J, Barlund M, Bucher C, Haas P, Nocito A, Bissig H, Sauter G, Kallioniemi A (2002) High-throughput copy number analysis of 17q23 in 3520 tissue specimens by fluorescence in situ hybridization to tissue microarrays. Am J Pathol 161, 73-79

Aoki M, Blazek E, Vogt PK (2001) A role of the kinase mTOR in cellular transformation induced by the oncoproteins P3k and Akt. Proc Natl Acad Sci U S A 98, 136-141

Barcellos-Hoff MH, Aggeler J, Ram TG, Bissell MJ (1989) Functional differentiation and alveolar morphogenesis of primary mammary cultures on reconstituted basement membrane. Development 105, 223-235

Barlund M, Forozan F, Kononen J, Bubendorf L, Chen Y, Bittner ML, Torhorst J, Haas P, Bucher C, Sauter G, Kallioniemi OP, Kallioniemi A (2000a) Detecting activation of ribosomal protein S6 kinase by complementary DNA and tissue microarray analysis. J Natl Cancer Inst 92, 1252-1259

Barlund M, Monni O, Kononen J, Cornelison R, Torhorst J, Sauter G, Kallioniemi O-P, Kallioniemi A (2000b) Multiple genes at 17q23 undergo amplification and overexpression in breast cancer. Cancer Res 60, 5340-5344

Barlund M, Tirkkonen M, Forozan F, Tanner MM, Kallioniemi O, Kallioniemi A (1997) Increased copy number at 17q22-q24 by CGH in breast cancer is due to high-level amplification of two separate regions. Genes Chromosomes Cancer 20, 372-376

Bartel DP (2004) MicroRNAs: genomics, biogenesis, mechanism, and function. Cell 116, 281-297

Beilharz TH, Humphreys DT, Clancy JL, Thermann R, Martin DI, Hentze MW, Preiss T (2009) microRNA-mediated messenger RNA deadenylation contributes to translational repression in mammalian cells. PLoS One 4, e6783

Bernstein E, Caudy AA, Hammond SM, Hannon GJ (2001) Role for a bidentate ribonuclease in the initiation step of RNA interference. Nature 409, 363-366

Bhasin M, Raghava GP (2004) ESLpred: SVM-based method for subcellular localization of eukaryotic proteins using dipeptide composition and PSI-BLAST. Nucleic Acids Res 32, W414-419

Blanchette P, Gilchrist CA, Baker RT, Gray DA (2001) Association of UNP, a ubiquitin-specific protease, with the pocket proteins pRb, p107 and p130. Oncogene 20, 5533-5537

Bohnsack MT, Czaplinski K, Gorlich D (2004) Exportin 5 is a RanGTP-dependent dsRNA-binding protein that mediates nuclear export of pre-miRNAs. RNA 10, 185-191

Borchert GM, Lanier W, Davidson BL (2006) RNA polymerase III transcribes human microRNAs. Nat Struct Mol Biol 13, 1097-1101

Bottoni A, Piccin D, Tagliati F, Luchin A, Zatelli MC, degli Uberti EC (2005) miR-15a and miR-16-1 down-regulation in pituitary adenomas. J Cell Physiol 204, 280-285

Brooks CL, Gu W (2004) Dynamics in the p53-Mdm2 ubiquitination pathway. Cell Cycle 3, 895-899

Bulavin DV, Demidov ON, Saito S, Kauraniemi P, Phillips C, Amundson SA, Ambrosino C, Sauter G, Nebreda AR, Anderson CW, Kallioniemi A, Fornace AJ,

Jr., Appella E (2002) Amplification of PPM1D in human tumors abrogates p53 tumor-suppressor activity. Nat Genet 31, 210-215

Calin GA, Croce CM (2006) MicroRNA signatures in human cancers. Nat Rev Cancer 6, 857-866

Calin GA, Dumitru CD, Shimizu M, Bichi R, Zupo S, Noch E, Aldler H, Rattan S, Keating M, Rai K, Rassenti L, Kipps T, Negrini M, Bullrich F, Croce CM (2002) Frequent deletions and down-regulation of micro- RNA genes miR15 and miR16 at 13q14 in chronic lymphocytic leukemia. Proc Natl Acad Sci U S A 99, 15524-15529

Calin GA, Ferracin M, Cimmino A, Di Leva G, Shimizu M, Wojcik SE, Iorio MV, Visone R, Sever NI, Fabbri M, Iuliano R, Palumbo T, Pichiorri F, Roldo C, Garzon R, Sevignani C, Rassenti L, Alder H, Volinia S, Liu CG, Kipps TJ, Negrini M, Croce CM (2005) A MicroRNA signature associated with prognosis and progression in chronic lymphocytic leukemia. N Engl J Med 353, 1793-1801

Calin GA, Sevignani C, Dumitru CD, Hyslop T, Noch E, Yendamuri S, Shimizu M, Rattan S, Bullrich F, Negrini M, Croce CM (2004) Human microRNA genes are frequently located at fragile sites and genomic regions involved in cancers. Proc Natl Acad Sci U S A 101, 2999-3004

Casanova JC, Uribe V, Badia-Careaga C, Giovinazzo G, Torres M, Sanz-Ezquerro JJ (2011) Apical ectodermal ridge morphogenesis in limb development is controlled by Arid3b-mediated regulation of cell movements. Development 138, 1195-1205

Chang TC, Yu D, Lee YS, Wentzel EA, Arking DE, West KM, Dang CV, Thomas-Tikhonenko A, Mendell JT (2008) Widespread microRNA repression by Myc contributes to tumorigenesis. Nat Genet 40, 43-50

Cheng Y (2009) Toward an atomic model of the 26S proteasome. Curr Opin Struct Biol 19, 203-208

Chou KC (2005) Using amphiphilic pseudo amino acid composition to predict enzyme subfamily classes. Bioinformatics 21, 10-19

Chou KC, Shen HB (2008) Cell-PLoc: a package of Web servers for predicting subcellular localization of proteins in various organisms. Nat Protoc 3, 153-162

Ciechanover A, Ben-Saadon R (2004) N-terminal ubiquitination: more protein substrates join in. Trends Cell Biol 14, 103-106

Cimmino A, Calin GA, Fabbri M, Iorio MV, Ferracin M, Shimizu M, Wojcik SE, Aqeilan RI, Zupo S, Dono M, Rassenti L, Alder H, Volinia S, Liu CG, Kipps TJ, Negrini M, Croce CM (2005) miR-15 and miR-16 induce apoptosis by targeting BCL2. Proc Natl Acad Sci U S A 102, 13944-13949

Cohen M, Stutz F, Belgareh N, Haguenauer-Tsapis R, Dargemont C (2003a) Ubp3 requires a cofactor, Bre5, to specifically de-ubiquitinate the COPII protein, Sec23. Nat Cell Biol 5, 661-667

Cohen M, Stutz F, Dargemont C (2003b) Deubiquitination, a new player in Golgi to endoplasmic reticulum retrograde transport. J Biol Chem 278, 51989-51992

Corney DC, Flesken-Nikitin A, Godwin AK, Wang W, Nikitin AY (2007) MicroRNA-34b and MicroRNA-34c are targets of p53 and cooperate in control of cell proliferation and adhesion-independent growth. Cancer Res 67, 8433-8438

Couch FJ, Wang XY, Wu GJ, Qian J, Jenkins RB, James CD (1999) Localization of PS6K to chromosomal region 17q23 and determination of its amplification in breast cancer. Cancer Res 59, 1408-1411

Cowden Dahl KD, Dahl R, Kruichak JN, Hudson LG (2009) The epidermal growth factor receptor responsive miR-125a represses mesenchymal morphology in ovarian cancer cells. Neoplasia 11, 1208-1215

Cummins JM, Vogelstein B (2004) HAUSP is required for p53 destabilization. Cell Cycle 3, 689-692

Daniel JA, Torok MS, Sun ZW, Schieltz D, Allis CD, Yates JR, 3rd, Grant PA (2004) Deubiquitination of histone H2B by a yeast acetyltransferase complex regulates transcription. J Biol Chem 279, 1867-1871

Davis E, Teng H, Bilican B, Parker MI, Liu B, Carriera S, Goding CR, Prince S (2008) Ectopic Tbx2 expression results in polyploidy and cisplatin resistance. Oncogene 27, 976-984

Deng S, Calin GA, Croce CM, Coukos G, Zhang L (2008) Mechanisms of microRNA deregulation in human cancer. Cell Cycle 7, 2643-2646

DeSalle LM, Latres E, Lin D, Graner E, Montagnoli A, Baker RT, Pagano M, Loda M (2001) The de-ubiquitinating enzyme Unp interacts with the retinoblastoma protein. Oncogene 20, 5538-5542

Deshaies RJ, Joazeiro CA (2009) RING domain E3 ubiquitin ligases. Annu Rev Biochem 78, 399-434

Dreger M (2003) Subcellular proteomics. Mass Spectrom Rev 22, 27-56

Du T, Zamore PD (2005) microPrimer: the biogenesis and function of microRNA. Development 132, 4645-4652

Dufner A, Thomas G (1999) Ribosomal S6 kinase signaling and the control of translation. Exp Cell Res 253, 100-109

Erikson E, Maller JL (1985) A protein kinase from Xenopus eggs specific for ribosomal protein S6. Proc Natl Acad Sci U S A 82, 742-746

Erson AE, Niell BL, DeMers SK, Rouillard JM, Hanash SM, Petty EM (2001) Overexpressed genes/ESTs and characterization of distinct amplicons on 17q23 in breast cancer cells. Neoplasia 3, 521-526

Erson AE, Petty EM (2009) miRNAs and cancer: New research developments and potential clinical applications. Cancer Biol Ther 8, 2317-2322

Esquela-Kerscher A, Slack FJ (2006) OncomiRs - microRNAs with a role in cancer. Nat Rev Cancer 6, 259-269

Eulalio A, Huntzinger E, Nishihara T, Rehwinkel J, Fauser M, Izaurralde E (2009) Deadenylation is a widespread effect of miRNA regulation. RNA 15, 21-32

Everett RD, Meredith M, Orr A, Cross A, Kathoria M, Parkinson J (1997) A novel ubiquitin-specific protease is dynamically associated with the PML nuclear domain and binds to a herpesvirus regulatory protein. EMBO J 16, 566-577

Feng LX, Ravindranath N, Dym M (2000) Stem cell factor/c-kit up-regulates cyclin D3 and promotes cell cycle progression via the phosphoinositide 3-kinase/p70 S6 kinase pathway in spermatogonia. J Biol Chem 275, 25572-25576

Filipowicz W, Bhattacharyya SN, Sonenberg N (2008) Mechanisms of post-transcriptional regulation by microRNAs: are the answers in sight? Nat Rev Genet 9, 102-114

Finley D, Chau V (1991) Ubiquitination. Annu Rev Cell Biol 7, 25-69

Firnberg N, Neubuser A (2002) FGF signaling regulates expression of Tbx2, Erm, Pea3, and Pax3 in the early nasal region. Dev Biol 247, 237-250

Friedman RC, Farh KK, Burge CB, Bartel DP (2009) Most mammalian mRNAs are conserved targets of microRNAs. Genome Res 19, 92-105

Garg A, Bhasin M, Raghava GP (2005) Support vector machine-based method for subcellular localization of human proteins using amino acid compositions, their order, and similarity search. J Biol Chem 280, 14427-14432

Gentile M, Olsen K, Dufmats M, Wingren S (1999) Frequent allelic losses at 11q24.1-q25 in young women with breast cancer: association with poor survival. Br J Cancer 80, 843-849

Gonzalez-Garcia A, Garrido E, Hernandez C, Alvarez B, Jimenez C, Cantrell DA, Pullen N, Carrera AC (2002) A new role for the p85-phosphatidylinositol 3-kinase regulatory subunit linking FRAP to p70 S6 kinase activation. J Biol Chem 277, 1500-1508

Gregory RI, Yan KP, Amuthan G, Chendrimada T, Doratotaj B, Cooch N, Shiekhattar R (2004) The Microprocessor complex mediates the genesis of microRNAs. Nature 432, 235-240

Grishok A, Pasquinelli AE, Conte D, Li N, Parrish S, Ha I, Baillie DL, Fire A, Ruvkun G, Mello CC (2001) Genes and mechanisms related to RNA interference regulate expression of the small temporal RNAs that control C. elegans developmental timing. Cell 106, 23-34

Guan Y, Yao H, Zheng Z, Qiu G, Sun K (2011) MiR-125b targets BCL3 and suppresses ovarian cancer proliferation. Int J Cancer 128, 2274-2283

Gumbiner BM (1997) Carcinogenesis: a balance between beta-catenin and APC. Curr Biol 7, R443-446

Guo H, Ingolia NT, Weissman JS, Bartel DP (2010) Mammalian microRNAs predominantly act to decrease target mRNA levels. Nature 466, 835-840

Guo X, Wu Y, Hartley RS (2009) MicroRNA-125a represses cell growth by targeting HuR in breast cancer. RNA Biol 6, 575-583

Gupta K, Chevrette M, Gray DA (1994) The Unp proto-oncogene encodes a nuclear protein. Oncogene 9, 1729-1731

Gupta K, Copeland NG, Gilbert DJ, Jenkins NA, Gray DA (1993) Unp, a mouse gene related to the tre oncogene. Oncogene 8, 2307-2310

Ha TY (2011) MicroRNAs in Human Diseases: From Autoimmune Diseases to Skin, Psychiatric and Neurodegenerative Diseases. Immune Netw 11, 227-244

Han J, Lee Y, Yeom KH, Kim YK, Jin H, Kim VN (2004) The Drosha-DGCR8 complex in primary microRNA processing. Genes Dev 18, 3016-3027

Han J, Lee Y, Yeom KH, Nam JW, Heo I, Rhee JK, Sohn SY, Cho Y, Zhang BT, Kim VN (2006) Molecular basis for the recognition of primary microRNAs by the Drosha-DGCR8 complex. Cell 125, 887-901

Hanahan D, Weinberg RA (2000) The hallmarks of cancer. Cell 100, 57-70

Hanahan D, Weinberg RA (2011) Hallmarks of cancer: the next generation. Cell 144, 646-674

Harper JW, Schulman BA (2006) Structural complexity in ubiquitin recognition. Cell 124, 1133-1136

Hayashita Y, Osada H, Tatematsu Y, Yamada H, Yanagisawa K, Tomida S, Yatabe Y, Kawahara K, Sekido Y, Takahashi T (2005) A polycistronic microRNA cluster, miR-17-92, is overexpressed in human lung cancers and enhances cell proliferation. Cancer Res 65, 9628-9632

He L, He X, Lim LP, de Stanchina E, Xuan Z, Liang Y, Xue W, Zender L, Magnus J, Ridzon D, Jackson AL, Linsley PS, Chen C, Lowe SW, Cleary MA, Hannon GJ

(2007) A microRNA component of the p53 tumour suppressor network. Nature 447, 1130-1134

He L, Thomson JM, Hemann MT, Hernando-Monge E, Mu D, Goodson S, Powers S, Cordon-Cardo C, Lowe SW, Hannon GJ, Hammond SM (2005) A microRNA polycistron as a potential human oncogene. Nature 435, 828-833

Henry KW, Wyce A, Lo WS, Duggan LJ, Emre NC, Kao CF, Pillus L, Shilatifard A, Osley MA, Berger SL (2003) Transcriptional activation via sequential histone H2B ubiquitylation and deubiquitylation, mediated by SAGA-associated Ubp8. Genes Dev 17, 2648-2663

Henson BJ, Bhattacharjee S, O'Dee DM, Feingold E, Gollin SM (2009) Decreased expression of miR-125b and miR-100 in oral cancer cells contributes to malignancy. Genes Chromosomes Cancer 48, 569-582

Hershko A (1991) The ubiquitin pathway for protein degradation. Trends Biochem Sci 16, 265-268

Hicke L (2001) A new ticket for entry into budding vesicles-ubiquitin. Cell 106, 527-530

Hua S, Sun Z (2001) Support vector machine approach for protein subcellular localization prediction. Bioinformatics 17, 721-728

Huang DT, Hunt HW, Zhuang M, Ohi MD, Holton JM, Schulman BA (2007a) Basis for a ubiquitin-like protein thioester switch toggling E1-E2 affinity. Nature 445, 394-398

Huang F, Goh LK, Sorkin A (2007b) EGF receptor ubiquitination is not necessary for its internalization. Proc Natl Acad Sci U S A 104, 16904-16909

Huang L, Luo J, Cai Q, Pan Q, Zeng H, Guo Z, Dong W, Huang J, Lin T (2011) MicroRNA-125b suppresses the development of bladder cancer by targeting E2F3. Int J Cancer 128, 1758-1769

Hussain S, Zhang Y, Galardy PJ (2009) DUBs and cancer: the role of deubiquitinating enzymes as oncogenes, non-oncogenes and tumor suppressors. Cell Cycle 8, 1688-1697

Hutvagner G, McLachlan J, Pasquinelli AE, Balint E, Tuschl T, Zamore PD (2001) A cellular function for the RNA-interference enzyme Dicer in the maturation of the let-7 small temporal RNA. Science 293, 834-838

Hyman E, Kauraniemi P, Hautaniemi S, Wolf M, Mousses S, Rozenblum E, Ringner M, Sauter G, Monni O, Elkahloun A, Kallioniemi OP, Kallioniemi A (2002) Impact of DNA amplification on gene expression patterns in breast cancer. Cancer Res 62, 6240-6245

Iorio MV, Ferracin M, Liu CG, Veronese A, Spizzo R, Sabbioni S, Magri E, Pedriali M, Fabbri M, Campiglio M, Menard S, Palazzo JP, Rosenberg A, Musiani P, Volinia S, Nenci I, Calin GA, Querzoli P, Negrini M, Croce CM (2005) MicroRNA gene expression deregulation in human breast cancer. In Cancer Res (United States), pp 7065-7070

Iorio MV, Piovan C, Croce CM (2010) Interplay between microRNAs and the epigenetic machinery: an intricate network. Biochim Biophys Acta 1799, 694-701

Iorio MV, Visone R, Di Leva G, Donati V, Petrocca F, Casalini P, Taccioli C, Volinia S, Liu CG, Alder H, Calin GA, Menard S, Croce CM (2007) MicroRNA signatures in human ovarian cancer. Cancer Res 67, 8699-8707

Isola JJ, Kallioniemi OP, Chu LW, Fuqua SA, Hilsenbeck SG, Osborne CK, Waldman FM (1995) Genetic aberrations detected by comparative genomic hybridization predict outcome in node-negative breast cancer. Am J Pathol 147, 905-911

Jacobs JJ, Keblusek P, Robanus-Maandag E, Kristel P, Lingbeek M, Nederlof PM, van Welsem T, van de Vijver MJ, Koh EY, Daley GQ, van Lohuizen M (2000) Senescence bypass screen identifies TBX2, which represses Cdkn2a (p19(ARF)) and is amplified in a subset of human breast cancers. Nat Genet 26, 291-299

Jiang L HQ, Zhang S, Zhang Q, Chang J, Qiu X, Wang E. (2010) Hsa-miR-125a-3p and hsa-miR-125a-5p are downregul... [BMC Cancer. 2010] - PubMed - NCBI.

Jiang L, Huang Q, Zhang S, Zhang Q, Chang J, Qiu X, Wang E (2010) Hsa-miR-125a-3p and hsa-miR-125a-5p are downregulated in non-small cell lung cancer and have inverse effects on invasion and migration of lung cancer cells. BMC Cancer 10, 318

Kallioniemi A, Kallioniemi OP, Piper J, Tanner M, Stokke T, Chen L, Smith HS, Pinkel D, Gray JW, Waldman FM (1994) Detection and mapping of amplified DNA sequences in breast cancer by comparative genomic hybridization. Proc Natl Acad Sci U S A 91, 2156-2160

Keleman K, Rajagopalan S, Cleppien D, Teis D, Paiha K, Huber LA, Technau GM, Dickson BJ (2002) Comm sorts robo to control axon guidance at the Drosophila midline. Cell 110, 415-427

Khvorova A, Reynolds A, Jayasena SD (2003) Functional siRNAs and miRNAs exhibit strand bias. Cell 115, 209-216

Kim VN (2005) MicroRNA biogenesis: coordinated cropping and dicing. Nat Rev Mol Cell Biol 6, 376-385

Kirisako T, Kamei K, Murata S, Kato M, Fukumoto H, Kanie M, Sano S, Tokunaga F, Tanaka K, Iwai K (2006) A ubiquitin ligase complex assembles linear polyubiquitin chains. EMBO J 25, 4877-4887

Knuutila S, Bjorkqvist AM, Autio K, Tarkkanen M, Wolf M, Monni O, Szymanska J, Larramendy ML, Tapper J, Pere H, El-Rifai W, Hemmer S, Wasenius VM, Vidgren V, Zhu Y (1998) DNA copy number amplifications in human neoplasms: review of comparative genomic hybridization studies. Am J Pathol 152, 1107-1123

Kobayashi K, Era T, Takebe A, Jakt LM, Nishikawa S (2006) ARID3B induces malignant transformation of mouse embryonic fibroblasts and is strongly associated with malignant neuroblastoma. Cancer Res 66, 8331-8336

Krek A, Grun D, Poy MN, Wolf R, Rosenberg L, Epstein EJ, MacMenamin P, da Piedade I, Gunsalus KC, Stoffel M, Rajewsky N (2005) Combinatorial microRNA target predictions. Nat Genet 37, 495-500

Krol J, Krzyzosiak WJ (2004) Structural aspects of microRNA biogenesis. IUBMB Life 56, 95-100

Lagos-Quintana M, Rauhut R, Meyer J, Borkhardt A, Tuschl T (2003) New microRNAs from mouse and human. RNA 9, 175-179

Lambert JM, Karnoub AE, Graves LM, Campbell SL, Der CJ (2002) Role of MLK3-mediated activation of p70 S6 kinase in Rac1 transformation. J Biol Chem 277, 4770-4777

Lambros MB, Natrajan R, Geyer FC, Lopez-Garcia MA, Dedes KJ, Savage K, Lacroix-Triki M, Jones RL, Lord CJ, Linardopoulos S, Ashworth A, Reis-Filho JS (2010) PPM1D gene amplification and overexpression in breast cancer: a qRT-PCR and chromogenic in situ hybridization study. Mod Pathol 23, 1334-1345

Lau NC, Lim LP, Weinstein EG, Bartel DP (2001) An abundant class of tiny RNAs with probable regulatory roles in Caenorhabditis elegans. Science 294, 858-862

Le MT, Teh C, Shyh-Chang N, Xie H, Zhou B, Korzh V, Lodish HF, Lim B (2009) MicroRNA-125b is a novel negative regulator of p53. In Genes Dev (United States), pp 862-876

Lee GY, Kenny PA, Lee EH, Bissell MJ (2007) Three-dimensional culture models of normal and malignant breast epithelial cells. Nat Methods 4, 359-365

Lee Y, Ahn C, Han J, Choi H, Kim J, Yim J, Lee J, Provost P, Radmark O, Kim S, Kim VN (2003) The nuclear RNase III Drosha initiates microRNA processing. Nature 425, 415-419

Lee Y, Kim M, Han J, Yeom KH, Lee S, Baek SH, Kim VN (2004) MicroRNA genes are transcribed by RNA polymerase II. EMBO J 23, 4051-4060

Lee YS, Kim HK, Chung S, Kim KS, Dutta A (2005) Depletion of human micro-RNA miR-125b reveals that it is critical for the proliferation of differentiated cells but not for the down-regulation of putative targets during differentiation. In J Biol Chem (United States), pp 16635-16641

Lei Z, Dai Y (2005) An SVM-based system for predicting protein subnuclear localizations. BMC Bioinformatics 6, 291

Lengauer C, Kinzler KW, Vogelstein B (1998) Genetic instabilities in human cancers. Nature 396, 643-649

Lewis BP, Burge CB, Bartel DP (2005) Conserved seed pairing, often flanked by adenosines, indicates that thousands of human genes are microRNA targets. In Cell (United States), pp 15-20

Li M, Brooks CL, Kon N, Gu W (2004) A dynamic role of HAUSP in the p53-Mdm2 pathway. Mol Cell 13, 879-886

Li M, Chen D, Shiloh A, Luo J, Nikolaev AY, Qin J, Gu W (2002) Deubiquitination of p53 by HAUSP is an important pathway for p53 stabilization. Nature 416, 648-653

Lingbeek ME, Jacobs JJ, van Lohuizen M (2002) The T-box repressors TBX2 and TBX3 specifically regulate the tumor suppressor gene p14ARF via a variant T-site in the initiator. J Biol Chem 277, 26120-26127

Liu F, Walters KJ (2010) Multitasking with ubiquitin through multivalent interactions. Trends Biochem Sci 35, 352-360

Livak KJ, Schmittgen TD (2001) Analysis of relative gene expression data using real-time quantitative PCR and the 2(-Delta Delta C(T)) Method. Methods 25, 402-408

Lorenz H, Hailey DW, Lippincott-Schwartz J (2006) Fluorescence protease protection of GFP chimeras to reveal protein topology and subcellular localization. Nat Methods 3, 205-210

Lu J, Getz G, Miska EA, Alvarez-Saavedra E, Lamb J, Peck D, Sweet-Cordero A, Ebert BL, Mak RH, Ferrando AA, Downing JR, Jacks T, Horvitz HR, Golub TR (2005) MicroRNA expression profiles classify human cancers. Nature 435, 834-838

Lujambio A, Lowe SW (2012) The microcosmos of cancer. Nature 482, 347-355

Lund E, Guttinger S, Calado A, Dahlberg JE, Kutay U (2004) Nuclear export of microRNA precursors. Science 303, 95-98

Marques AJ, Palanimurugan R, Matias AC, Ramos PC, Dohmen RJ (2009) Catalytic mechanism and assembly of the proteasome. Chem Rev 109, 1509-1536

Matranga C, Tomari Y, Shin C, Bartel DP, Zamore PD (2005) Passenger-strand cleavage facilitates assembly of siRNA into Ago2-containing RNAi enzyme complexes. Cell 123, 607-620

Mattie MD BC, Bowers J, Sensinger K, Wong L, Scott GK, Fedele V, Ginzinger D, Getts R, Haqq C (2006) Optimized high-throughput microRNA expression pro... [Mol Cancer. 2006] - PubMed - NCBI.

Meijer IM, van Leeuwen JE (2011) ERBB2 is a target for USP8-mediated deubiquitination. Cell Signal 23, 458-467

Mizuno Y, Yagi K, Tokuzawa Y, Kanesaki-Yatsuka Y, Suda T, Katagiri T, Fukuda T, Maruyama M, Okuda A, Amemiya T, Kondoh Y, Tashiro H, Okazaki Y (2008) miR-125b inhibits osteoblastic differentiation by down-regulation of cell proliferation. In Biochem Biophys Res Commun (United States), pp 267-272

Mohri T, Nakajima M, Takagi S, Komagata S, Yokoi T (2009) MicroRNA regulates human vitamin D receptor. Int J Cancer 125, 1328-1333

Monni O, Barlund M, Mousses S, Kononen J, Sauter G, Heiskanen M, Paavola P, Avela K, Chen Y, Bittner ML, Kallioniemi A (2001) Comprehensive copy number and gene expression profiling of the 17q23 amplicon in human breast cancer. Proc Natl Acad Sci U S A 98, 5711-5716

Mosesson Y, Mills GB, Yarden Y (2008) Derailed endocytosis: an emerging feature of cancer. Nat Rev Cancer 8, 835-850

Mourelatos Z, Dostie J, Paushkin S, Sharma A, Charroux B, Abel L, Rappsilber J, Mann M, Dreyfuss G (2002) miRNPs: a novel class of ribonucleoproteins containing numerous microRNAs. Genes Dev 16, 720-728

Mukhopadhyay D, Riezman H (2007) Proteasome-independent functions of ubiquitin in endocytosis and signaling. Science 315, 201-205

Murray RZ, Jolly LA, Wood SA (2004) The FAM deubiquitylating enzyme localizes to multiple points of protein trafficking in epithelia, where it associates with E-cadherin and beta-catenin. Mol Biol Cell 15, 1591-1599

Myllykangas S, Knuutila S (2006) Manifestation, mechanisms and mysteries of gene amplifications. Cancer Lett 232, 79-89

Nakagawa T, Kajitani T, Togo S, Masuko N, Ohdan H, Hishikawa Y, Koji T, Matsuyama T, Ikura T, Muramatsu M, Ito T (2008) Deubiquitylation of histone H2A activates transcriptional initiation via trans-histone cross-talk with H3K4 di- and trimethylation. Genes Dev 22, 37-49

Nicassio F, Corrado N, Vissers JH, Areces LB, Bergink S, Marteijn JA, Geverts B, Houtsmuller AB, Vermeulen W, Di Fiore PP, Citterio E (2007) Human USP3 is a chromatin modifier required for S phase progression and genome stability. Curr Biol 17, 1972-1977

Niendorf S, Oksche A, Kisser A, Lohler J, Prinz M, Schorle H, Feller S, Lewitzky M, Horak I, Knobeloch KP (2007) Essential role of ubiquitin-specific protease 8 for receptor tyrosine kinase stability and endocytic trafficking in vivo. Mol Cell Biol 27, 5029-5039

Nijman SM, Huang TT, Dirac AM, Brummelkamp TR, Kerkhoven RM, D'Andrea AD, Bernards R (2005a) The deubiquitinating enzyme USP1 regulates the Fanconi anemia pathway. Mol Cell 17, 331-339

Nijman SM, Luna-Vargas MP, Velds A, Brummelkamp TR, Dirac AM, Sixma TK, Bernards R (2005b) A genomic and functional inventory of deubiquitinating enzymes. Cell 123, 773-786

Numata S, Claudio PP, Dean C, Giordano A, Croce CM (1999) Bdp, a new member of a family of DNA-binding proteins, associates with the retinoblastoma gene product. Cancer Res 59, 3741-3747

O'Donnell KA, Wentzel EA, Zeller KI, Dang CV, Mendell JT (2005) c-Myc-regulated microRNAs modulate E2F1 expression. Nature 435, 839-843

Oliveira AM, Hsi BL, Weremowicz S, Rosenberg AE, Dal Cin P, Joseph N, Bridge JA, Perez-Atayde AR, Fletcher JA (2004) USP6 (Tre2) fusion oncogenes in aneurysmal bone cyst. Cancer Res 64, 1920-1923

Onno M, Nakamura T, Mariage-Samson R, Hillova J, Hill M (1993) Human TRE17 oncogene is generated from a family of homologous polymorphic sequences by single-base changes. DNA Cell Biol 12, 107-118

Ozen M, Creighton CJ, Ozdemir M, Ittmann M (2008) Widespread deregulation of microRNA expression in human prostate cancer. In Oncogene (England), pp 1788-1793

Papa FR, Hochstrasser M (1993) The yeast DOA4 gene encodes a deubiquitinating enzyme related to a product of the human tre-2 oncogene. Nature 366, 313-319

Parssinen J, Kuukasjarvi T, Karhu R, Kallioniemi A (2007) High-level amplification at 17q23 leads to coordinated overexpression of multiple adjacent genes in breast cancer. Br J Cancer 96, 1258-1264

Paulding CA, Ruvolo M, Haber DA (2003) The Tre2 (USP6) oncogene is a hominoid-specific gene. Proc Natl Acad Sci U S A 100, 2507-2511

Paxton C, Zhao H, Chin Y, Langner K, Reecy J (2002) Murine Tbx2 contains domains that activate and repress gene transcription. Gene 283, 117-124

Peng J, Schwartz D, Elias JE, Thoreen CC, Cheng D, Marsischky G, Roelofs J, Finley D, Gygi SP (2003) A proteomics approach to understanding protein ubiquitination. Nat Biotechnol 21, 921-926

Perera RJ, Ray A (2007) MicroRNAs in the search for understanding human diseases. BioDrugs 21, 97-104

Pickart CM, Eddins MJ (2004) Ubiquitin: structures, functions, mechanisms. Biochim Biophys Acta 1695, 55-72

Pickart CM, Fushman D (2004) Polyubiquitin chains: polymeric protein signals. Curr Opin Chem Biol 8, 610-616

Pierleoni A, Martelli PL, Fariselli P, Casadio R (2007) eSLDB: eukaryotic subcellular localization database. Nucleic Acids Res 35, D208-212

Popov N, Herold S, Llamazares M, Schulein C, Eilers M (2007a) Fbw7 and Usp28 regulate myc protein stability in response to DNA damage. Cell Cycle 6, 2327-2331

Popov N, Wanzel M, Madiredjo M, Zhang D, Beijersbergen R, Bernards R, Moll R, Elledge SJ, Eilers M (2007b) The ubiquitin-specific protease USP28 is required for MYC stability. Nat Cell Biol 9, 765-774

Qu H, Qu D, Chen F, Zhang Z, Liu B, Liu H (2010) ZBTB7 overexpression contributes to malignancy in breast cancer. Cancer Invest 28, 672-678

Rajabi H, Jin C, Ahmad R, McClary C, Joshi MD, Kufe D (2010) MUCIN 1 ONCOPROTEIN EXPRESSION IS SUPPRESSED BY THE miR-125b ONCOMIR. Genes Cancer 1, 62-68

Rajewsky N (2006) microRNA target predictions in animals. Nat Genet 38 Suppl, S8-13

Saito Y, Liang G, Egger G, Friedman JM, Chuang JC, Coetzee GA, Jones PA (2006) Specific activation of microRNA-127 with downregulation of the proto-oncogene BCL6 by chromatin-modifying drugs in human cancer cells. Cancer Cell 9, 435-443

Salmena L, Pandolfi PP (2007) Changing venues for tumour suppression: balancing destruction and localization by monoubiquitylation. Nat Rev Cancer 7, 409-413

Schwartz AL, Ciechanover A (1999) The ubiquitin-proteasome pathway and pathogenesis of human diseases. Annu Rev Med 50, 57-74

Schwarz DS, Hutvagner G, Du T, Xu Z, Aronin N, Zamore PD (2003) Asymmetry in the assembly of the RNAi enzyme complex. Cell 115, 199-208

Scott GK, Goga A, Bhaumik D, Berger CE, Sullivan CS, Benz CC (2007) Coordinate suppression of ERBB2 and ERBB3 by enforced expression of micro-RNA miR-125a or miR-125b. In J Biol Chem (United States), pp 1479-1486

Shen HB, Chou KC (2006) Ensemble classifier for protein fold pattern recognition. Bioinformatics 22, 1717-1722

Shen HB, Chou KC (2007) Hum-mPLoc: an ensemble classifier for large-scale human protein subcellular location prediction by incorporating samples with multiple sites. Biochem Biophys Res Commun 355, 1006-1011

Shen HB, Chou KC (2009) A top-down approach to enhance the power of predicting human protein subcellular localization: Hum-mPLoc 2.0. Anal Biochem 394, 269-274

Shi L, Zhang J, Pan T, Zhou J, Gong W, Liu N, Fu Z, You Y (2010) MiR-125b is critical for the suppression of human U251 glioma stem cell proliferation. In Brain Res (Netherlands: 2009 Elsevier B.V), pp 120-126

Shi XB, Xue L, Yang J, Ma AH, Zhao J, Xu M, Tepper CG, Evans CP, Kung HJ, deVere White RW (2007) An androgen-regulated miRNA suppresses Bak1 expression and induces androgen-independent growth of prostate cancer cells. In Proc Natl Acad Sci U S A (United States), pp 19983-19988

Sinclair CS, Rowley M, Naderi A, Couch FJ (2003) The 17q23 amplicon and breast cancer. Breast Cancer Res Treat 78, 313-322

Song MS, Salmena L, Carracedo A, Egia A, Lo-Coco F, Teruya-Feldstein J, Pandolfi PP (2008) The deubiquitinylation and localization of PTEN are regulated by a HAUSP-PML network. Nature 455, 813-817

Spencer KS, Graus-Porta D, Leng J, Hynes NE, Klemke RL (2000) ErbB2 is necessary for induction of carcinoma cell invasion by ErbB family receptor tyrosine kinases. J Cell Biol 148, 385-397

Stevenson LF, Sparks A, Allende-Vega N, Xirodimas DP, Lane DP, Saville MK (2007) The deubiquitinating enzyme USP2a regulates the p53 pathway by targeting Mdm2. EMBO J 26, 976-986

Tagawa H, Seto M (2005) A microRNA cluster as a target of genomic amplification in malignant lymphoma. In Leukemia (England), pp 2013-2016

Tagwerker C, Flick K, Cui M, Guerrero C, Dou Y, Auer B, Baldi P, Huang L, Kaiser P (2006) A tandem affinity tag for two-step purification under fully denaturing conditions: application in ubiquitin profiling and protein complex identification combined with in vivocross-linking. Mol Cell Proteomics 5, 737-748

Takebe A, Era T, Okada M, Martin Jakt L, Kuroda Y, Nishikawa S (2006) Microarray analysis of PDGFR alpha+ populations in ES cell differentiation culture identifies genes involved in differentiation of mesoderm and mesenchyme including ARID3b that is essential for development of embryonic mesenchymal cells. Dev Biol 293, 25-37

Takekawa M, Adachi M, Nakahata A, Nakayama I, Itoh F, Tsukuda H, Taya Y, Imai K (2000) p53-inducible wip1 phosphatase mediates a negative feedback regulation of p38 MAPK-p53 signaling in response to UV radiation. EMBO J 19, 6517-6526

Taya S, Yamamoto T, Kanai-Azuma M, Wood SA, Kaibuchi K (1999) The deubiquitinating enzyme Fam interacts with and stabilizes beta-catenin. Genes Cells 4, 757-767

Thien CB, Langdon WY (2001) Cbl: many adaptations to regulate protein tyrosine kinases. Nat Rev Mol Cell Biol 2, 294-307

Thorne C, Eccles RL, Coulson JM, Urbe S, Clague MJ (2011) Isoform-specific localization of the deubiquitinase USP33 to the Golgi apparatus. Traffic 12, 1563-1574

Totsukawa G, Kaneko Y, Uchiyama K, Toh H, Tamura K, Kondo H (2011) VCIP135 deubiquitinase and its binding protein, WAC, in p97ATPase-mediated membrane fusion. EMBO J 30, 3581-3593

Tsai CM, Levitzki A, Wu LH, Chang KT, Cheng CC, Gazit A, Perng RP (1996) Enhancement of chemosensitivity by tyrphostin AG825 in high-p185(neu) expressing non-small cell lung cancer cells. Cancer Res 56, 1068-1074

Volinia S, Calin GA, Liu CG, Ambs S, Cimmino A, Petrocca F, Visone R, Iorio M, Roldo C, Ferracin M, Prueitt RL, Yanaihara N, Lanza G, Scarpa A, Vecchione A, Negrini M, Harris CC, Croce CM (2006) A microRNA expression signature of human solid tumors defines cancer gene targets. Proc Natl Acad Sci U S A 103, 2257-2261

Wang Y, Satoh A, Warren G, Meyer HH (2004) VCIP135 acts as a deubiquitinating enzyme during p97-p47-mediated reassembly of mitotic Golgi fragments. J Cell Biol 164, 973-978

Weissman AM (2001) Themes and variations on ubiquitylation. Nat Rev Mol Cell Biol 2, 169-178

Wilson C, Venditti R, Rega LR, Colanzi A, D'Angelo G, De Matteis MA (2011) The Golgi apparatus: an organelle with multiple complex functions. Biochem J 433, 1-9

Winter J, Jung S, Keller S, Gregory RI, Diederichs S (2009) Many roads to maturity: microRNA biogenesis pathways and their regulation. Nat Cell Biol 11, 228-234

Wong TS, Liu XB, Wong BY, Ng RW, Yuen AP, Wei WI (2008) Mature miR-184 as Potential Oncogenic microRNA of Squamous Cell Carcinoma of Tongue. In Clin Cancer Res (United States), pp 2588-2592

Wu G, Sinclair C, Hinson S, Ingle JN, Roche PC, Couch FJ (2001) Structural analysis of the 17q22-23 amplicon identifies several independent targets of amplification in breast cancer cell lines and tumors. Cancer Res 61, 4951-4955

Wu L, Belasco JG (2005) Micro-RNA regulation of the mammalian lin-28 gene during neuronal differentiation of embryonal carcinoma cells. In Mol Cell Biol (United States), pp 9198-9208

Wu X, Chen H, Parker B, Rubin E, Zhu T, Lee JS, Argani P, Sukumar S (2006) HOXB7, a homeodomain protein, is overexpressed in breast cancer and confers epithelial-mesenchymal transition. Cancer Res 66, 9527-9534

Xia HF, He TZ, Liu CM, Cui Y, Song PP, Jin XH, Ma X (2009) MiR-125b expression affects the proliferation and apoptosis of human glioma cells by targeting Bmf. In Cell Physiol Biochem (Switzerland: 2009 S. Karger AG, Basel.), pp 347-358

Yanaihara N, Caplen N, Bowman E, Seike M, Kumamoto K, Yi M, Stephens RM, Okamoto A, Yokota J, Tanaka T, Calin GA, Liu CG, Croce CM, Harris CC (2006) Unique microRNA molecular profiles in lung cancer diagnosis and prognosis. Cancer Cell 9, 189-198

Yi R, Qin Y, Macara IG, Cullen BR (2003) Exportin-5 mediates the nuclear export of pre-microRNAs and short hairpin RNAs. Genes Dev 17, 3011-3016

Yuan Z, Teasdale RD (2002) Prediction of Golgi Type II membrane proteins based on their transmembrane domains. Bioinformatics 18, 1109-1115

Yuasa-Kawada J, Kinoshita-Kawada M, Rao Y, Wu JY (2009) Deubiquitinating enzyme USP33/VDU1 is required for Slit signaling in inhibiting breast cancer cell migration. Proc Natl Acad Sci U S A 106, 14530-14535

Zhang L, Huang J, Yang N, Greshock J, Megraw MS, Giannakakis A, Liang S, Naylor TL, Barchetti A, Ward MR, Yao G, Medina A, O'Brien-Jenkins A, Katsaros D, Hatzigeorgiou A, Gimotty PA, Weber BL, Coukos G (2006) microRNAs exhibit high frequency genomic alterations in human cancer. Proc Natl Acad Sci U S A 103, 9136-9141

Zhang L, Volinia S, Bonome T, Calin GA, Greshock J, Yang N, Liu CG, Giannakakis A, Alexiou P, Hasegawa K, Johnstone CN, Megraw MS, Adams S, Lassus H, Huang J, Kaur S, Liang S, Sethupathy P, Leminen A, Simossis VA, Sandaltzopoulos R, Naomoto Y, Katsaros D, Gimotty PA, DeMichele A, Huang Q, Butzow R, Rustgi AK, Weber BL, Birrer MJ, Hatzigeorgiou AG, Croce CM, Coukos G (2008a) Genomic and epigenetic alterations deregulate microRNA expression in human epithelial ovarian cancer. Proc Natl Acad Sci U S A 105, 7004-7009

Zhang XY, Pfeiffer HK, Thorne AW, McMahon SB (2008b) USP22, an hSAGA subunit and potential cancer stem cell marker, reverses the polycomb-catalyzed ubiquitylation of histone H2A. Cell Cycle 7, 1522-1524

Zhang Y, Gao JS, Tang X, Tucker LD, Quesenberry P, Rigoutsos I, Ramratnam B (2009) MicroRNA 125a and its regulation of the p53 tumor suppressor gene. FEBS Lett 583, 3725-3730

Zhang Y, Yan LX, Wu QN, Du ZM, Chen J, Liao DZ, Huang MY, Hou JH, Wu QL, Zeng MS, Huang WL, Zeng YX, Shao JY (2011) miR-125b is methylated and functions as a tumor suppressor by regulating the ETS1 proto-oncogene in human invasive breast cancer. In Cancer Res (United States: 2011 Aacr), pp 3552-3562

Zhou M, Liu Z, Zhao Y, Ding Y, Liu H, Xi Y, Xiong W, Li G, Lu J, Fodstad O, Riker AI, Tan M (2010) MicroRNA-125b confers the resistance of breast cancer cells to paclitaxel through suppression of pro-apoptotic Bcl-2 antagonist killer 1 (Bak1) expression. In J Biol Chem (United States), pp 21496-21507

APPENDIX A

PRIMERS

Table A.1 List of primers.

NAME	SEQUENCE
F1	5’-CCGCTCGAGATGGGTGCCAAGGAGTCAC-3'
R1	5’-GGGCCCGCTGTAACACACAGTACTTTTTGTAATCAG-3'
F2	5’-ACGCGTCGACTAATAACAACCAGTGTTTGCT-3’
R2	5’-ATAAGAATGCGGCCGCTTAGAGGCTGGGGCGATTCTT-3’
F3	5’-ACGCGTCGACTCCTGTGTCTCCAATTTCAGCT-3’
R3	5’-GGGCCCTGGCTCCCTTTTCTGTGGGAAC-3’
R4	5’ATAAGAATGCGGCCGCTTACTGTAACACACAGTACTTT-3’
7F-CDS	5’- CCTGTCCCTGTGTCTCCAAT-3’
SC1-F	5’-ACATGGTCCTGCTGGAGTTC-3’
SC1-R	5’-TTCAGGTTCAGGGGGAGGT-3’
HOXB7-F	5’-CGAGCTCGGGCAGAGGAAGAGACAT-3'
HOXB7-R	5’-CCCAAGCTTGCGTTTTATTTTTCCATCCTTTAGAT-3'
FBI1-C1-F	5’-GAGCTCGACTGGGGTGGGCTTTTAAT-3'
FBI1-C1-R	5’-CTCAAGCTTTGCTTTAAAAATTTGGGAGA-3'
FBI1-C2-F	5’-GAGCTCTTGGTTCTGACGTGAAGAGG--3'
FBI1-C2-R	5’-CTCAAGCTTCATCCAAGGTCCAGCTCCT-3'
ETS1-C1-F	5’-GAGCTCTTGGAAAAGCAAAACGCTCT-3'
ETS1-C1-R	5’-CTCAAGCTTTCTCCCTTCCAGGACTTCAA-3'

Table A.1 (Continued) List of primers.

NAME	SEQUENCE
ETS1-C2-F	5’-GAGCTCTGATCTTTTGGATGCAGGTG-3'
ETS1-C2-R	5’-CTCAAGCTTTTTCAGCTGCAGTTTTGCAT-3'

APPENDIX B

VECTORS

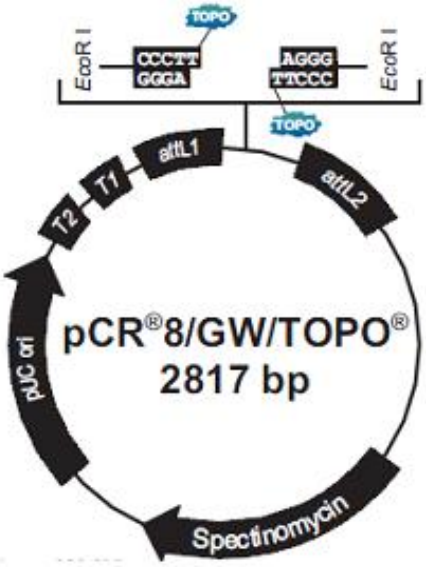

Multiple Cloning Site:

Figure B. 1 The map and multiple cloning site of PCR ® 8/GW/TOPO®TA (Invitrogen) vector.

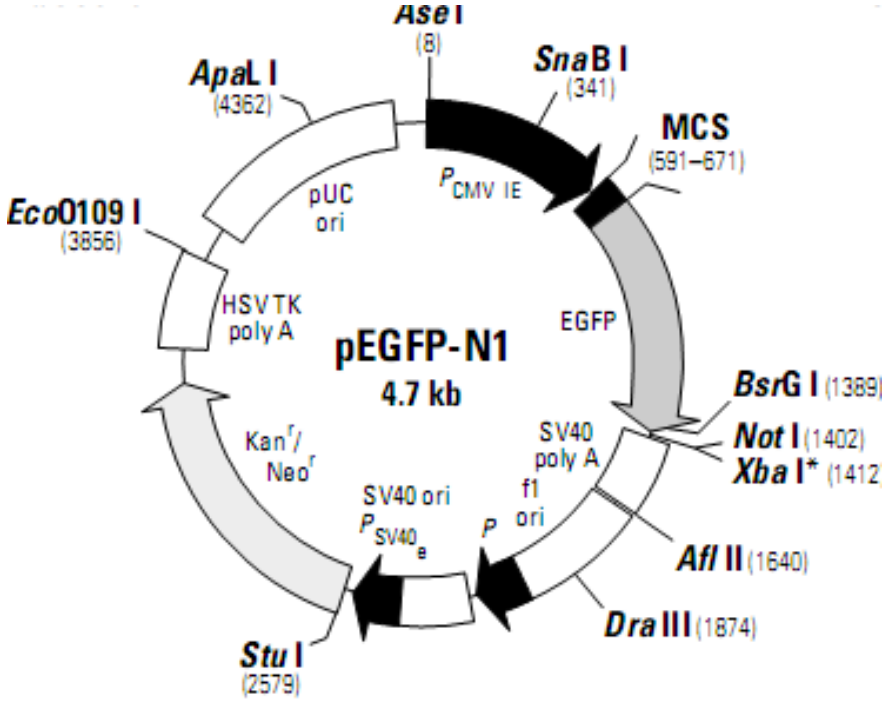

Multiple Cloning Site (MCS):

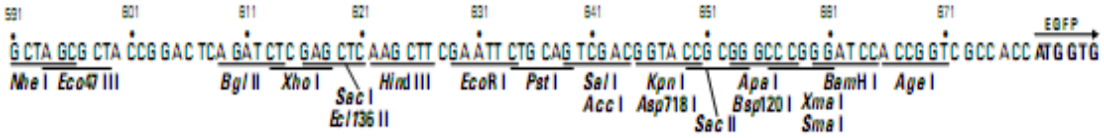

Figure B. 2 The map and multiple cloning site of pEGFPN1(Clontech) vector.

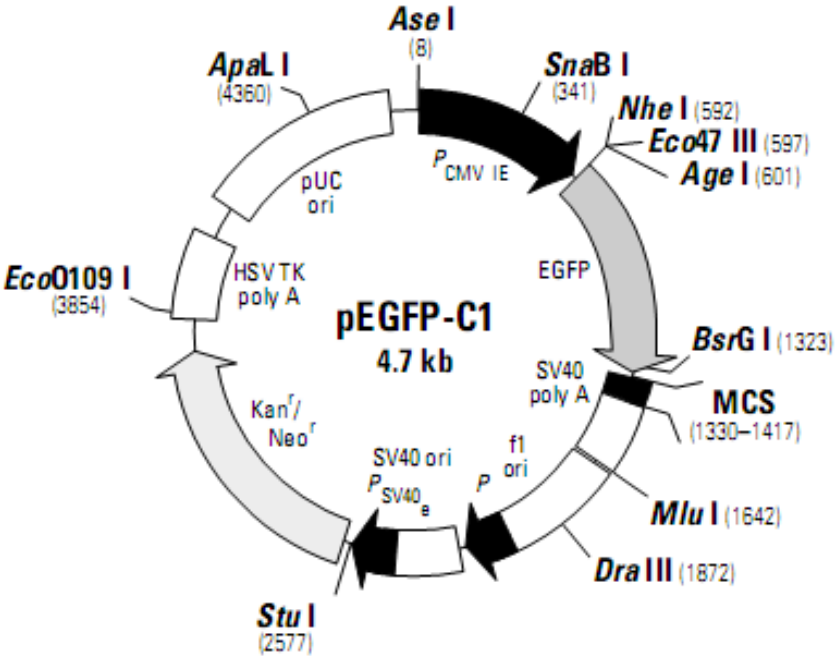

MCS:

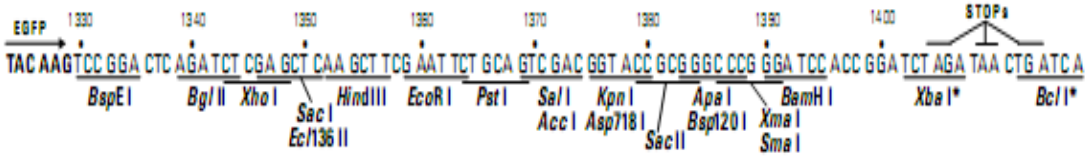

Figure B. 3 The map and multiple cloning site of pEGFPC1(Clontech) vector.

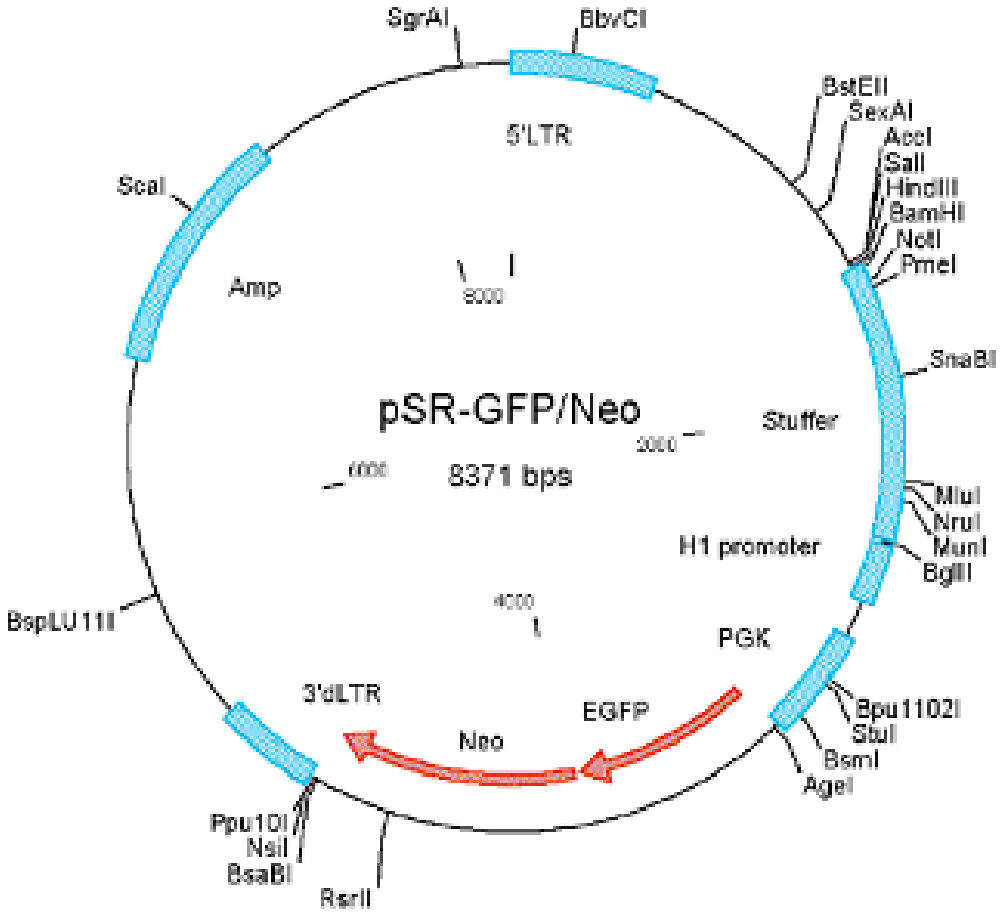

Figure B. 4 The map of pSUPER.retro.neo+GFP (Invitrogen) vector.

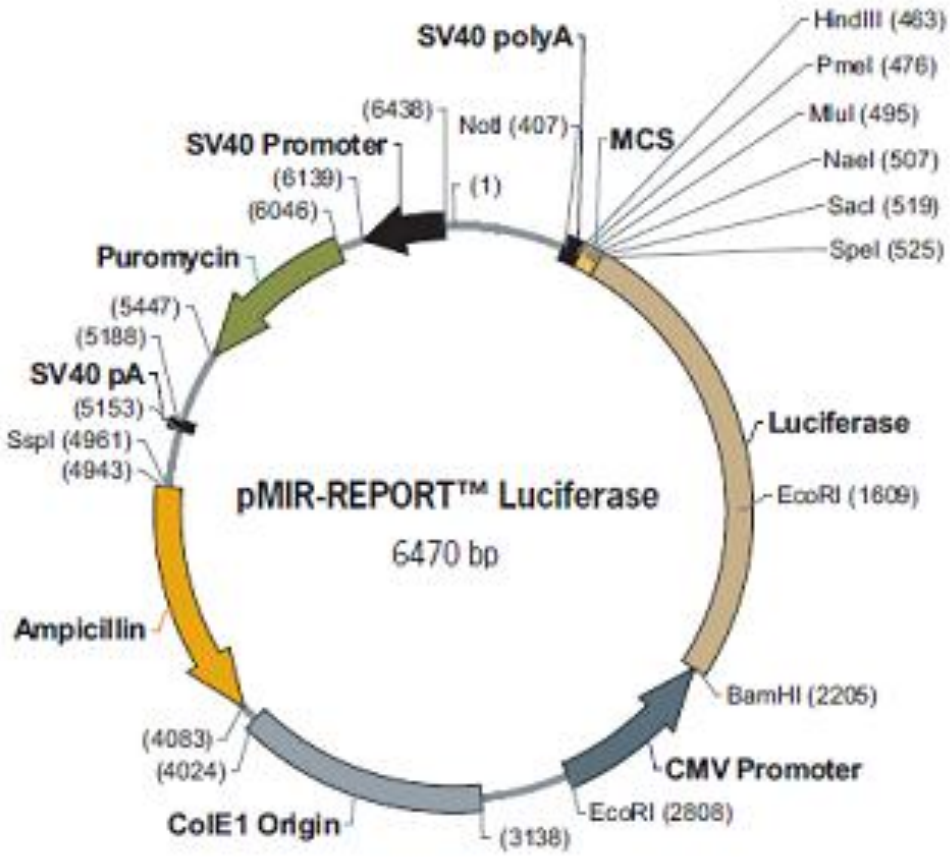

Figure B. 5 The map of pMIR-REPORT Luciferase (Ambion) vector.

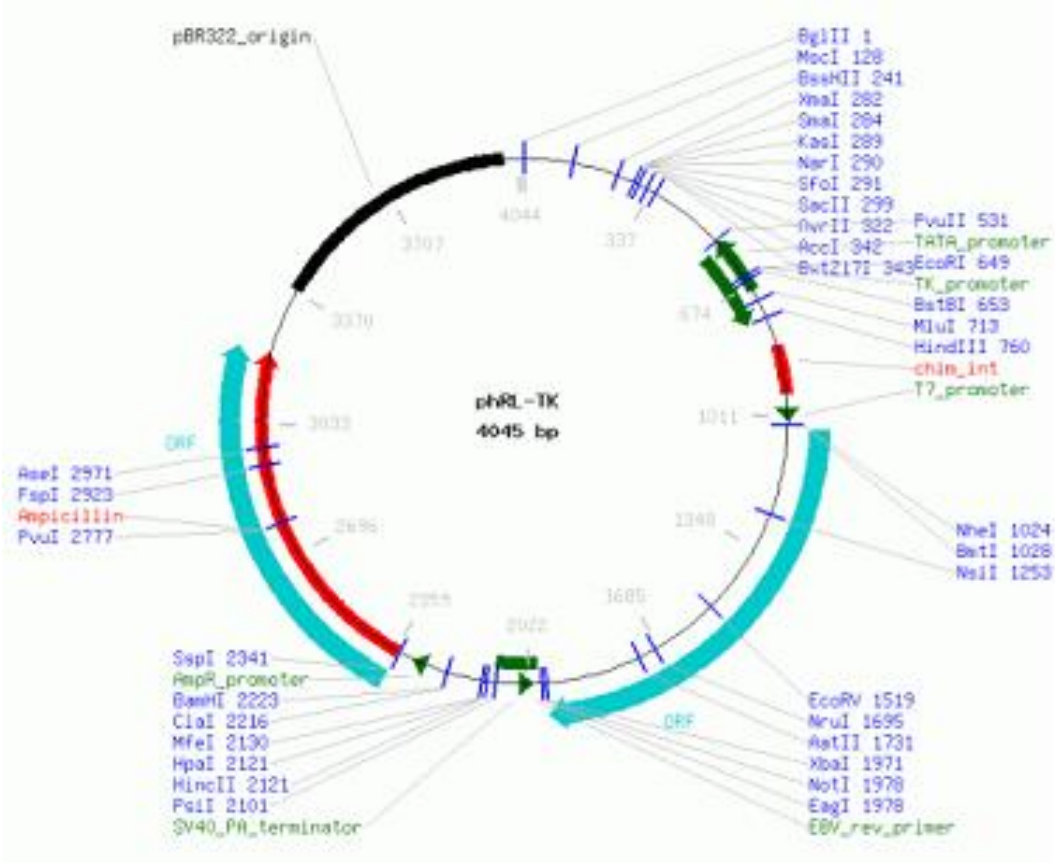

Figure B. 6 The map of PhRL-TK (Promega) vector.

APPENDIX C

BACTERIAL CULTURE MEDIA

LB-Medium (Luria-Bertani Medium)

Component:	
Tryptone	10 g
Yeast Extract	5 g
NaCl	10 g

The volume was reached to 1 liter and the medium was sterilized by autoclaving for 20 minutes at 15 Psi.

LB-Agar

Component:	
Bacto Agar	15 g
Tryptone	10 g
Yeast Extract	5 g
NaCl	10 g

The volume was adjusted to 1 liter. The medium was sterilized by autoclaving for 20 minutes at 15 Psi. The pH was adjusted to 7 with using NaOH (5 N).

S.O.C Medium

Component:	
Tryptone	20 g
Yeast Extract	5 g
NaCl	0.5 g
250 mM KCl	10 ml

The volume was adjusted to 1 liter. The pH was adjusted to 7, using NaOH (5 N). The medium was sterilized by autoclaving for 20 minutes at 15 Psi. 20 ml of sterile 1M solution of glucose was added to the cooled medium. Just before use, 5 ml of a sterile solution of $MgCl_2$ (2M) was added to the medium.

APPENDIX D

DNA AND PROTEIN MARKERS

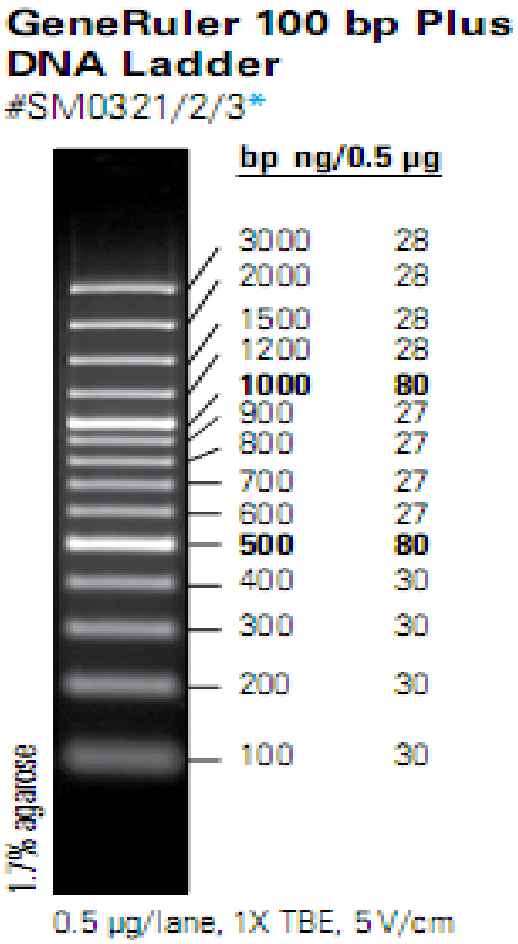

Figure D. 1 GeneRuler 100 bp Plus DNA Ladder (Fermentas, catalog #: SM0321/2/3).

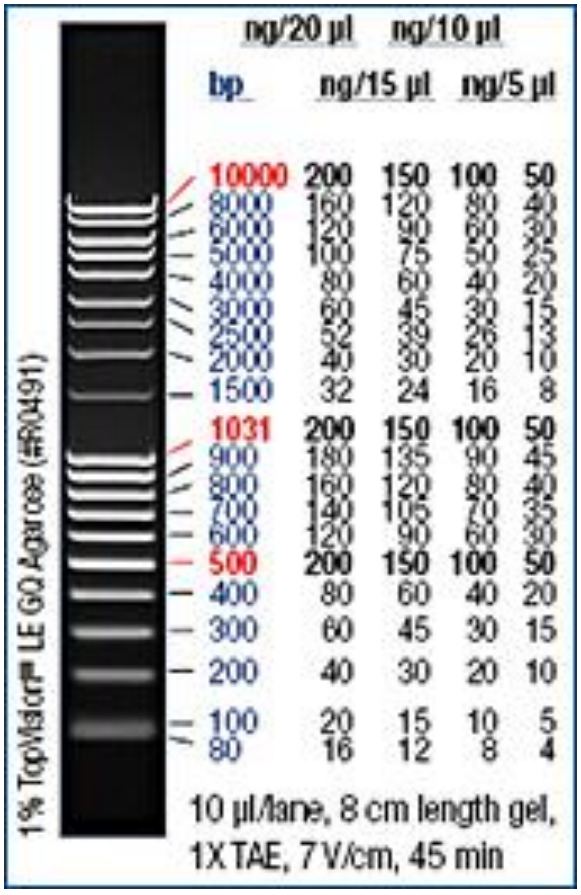

Figure D. 2 MassRuler DNA Ladder Mix, ready-to-use, 80-10,000 bp (Fermentas, catalog #: R0491).

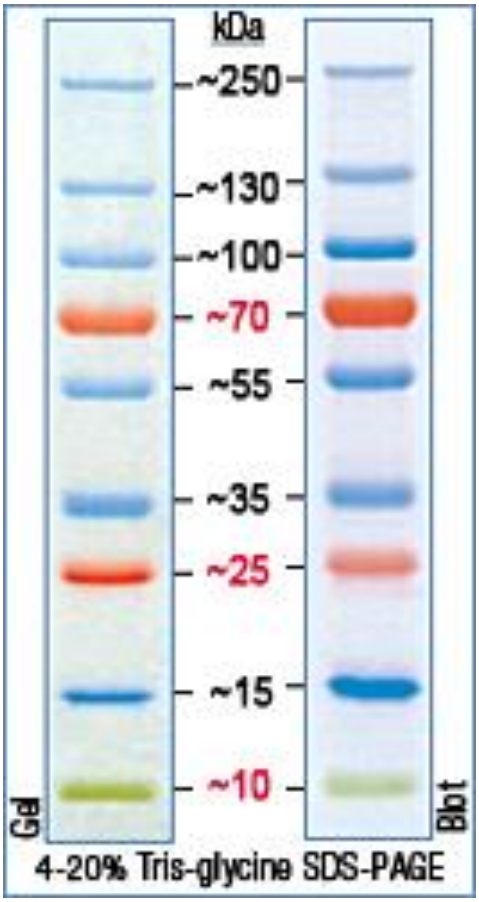

Figure D. 3 PageRuler™ Plus Prestained Protein Ladder, (Fermentas, catalog # SM1811).

CURRICULUM VITAE

Personal Information:

Surname, Name: Akhavantabasi, Shiva
Date and Place of Birth: 9 September 1980, Mashhad, IRAN

Education:

PhD, 2007- 2012

Department of Biological Sciences,
Middle East Technical University, Ankara, Turkey

MSc, 2005-2007

Department of Biological Sciences,
Middle East Technical University, Ankara, Turkey

BS, 1998-2002

Department of Microbiology,

University of Jahrom, Iran

Peer Reviewed Publications:

Akhavantabasi S*, Akman HB*, Sapmaz A*, Keller J, Petty EM, Erson AE, USP32 is an active, membrane-bound ubiquitin protease overexpressed in breast cancers. Mamm Genome. 2010, 21(7-8):388-97.*; equal contribution.

Shiva Akhavantabasi, Aysegul Sapmaz, Serkan Tuna, Ayse Elif Erson-Bensan. Phenotypical and functional changes due to miR-125b expression in MCF7 breast cancer cells. Cell Structure and Function (CSF). 2012, 37(1):27-38.

Peer Reviewed Electronic Publications:

Tabasi SA, Erson AE . MIRN221 (microRNA 221). Atlas Genet Cytogenet Oncol Haematol. September 2008.URL : http://AtlasGenetics Oncology.org/Genes /MIRN 221 ID44277chXp11. html

Tabasi SA, Erson AE . MIRN222 (microRNA 222). Atlas Genet Cytogenet Oncol Haematol. September 2008.URL : http://AtlasGeneticsOncology.org/Genes/ MIRN 222 ID44278chXp11. html

Presentations/Conference Papers:

2011

S. Akhavantabasi, A.E. Erson. Investigating the Regulation of CHFR Protein Expression by miRNAs in Breast Cancer (poster presentation). Department of Biological Sciences, METU, Ankara, Turkey, March 26. 2011, Ankara, Turkey.

S.Akhavantabasi. Investigating the Involvement of relevant miRNAs in Breast Tumorigenesis (oral presentation). "MicroRNA-profiling: From in-situ

hybridization to next-generation sequencing" practical course, Galway, Ireland, May 26.

2010

S. Akhavantabasi, H.B. Akman Tuncer, A. Sapmaz, A.E. Erson. Characterization of a ubiquitin specific protease in the 17q23 amplicon (poster presentation). The European Association for Cancer Research 21st meeting, June 26-29 2010, Oslo, Norway.

Şimşek Özek N., **Tabasi S.A.**, Erson A.E., Severcan F, Metastatik ve Nonmetastatik Meme Kanseri Hücre Hatlarında Makromoleküler Düzeydeki Farklılıklar. "II. Multidisipliner Kanser Araştırma Sempozyumu, Uludağ, Bursa,", , (2010).

2009

Ozek NS, **Akhavantabasi S**, Erson AE, Severcan F., Analysis of Metastatic and Non-metastatic Breast Cancer Cell Lines (poster presentation). II. International Biophysics Conference, Diyarbakir, Turkey, Oct 5-9, 2009.

S. Akhavantabasi, A. E. Erson. Subcellular Localization of Ubiquitin Specific Protease 32 (USP32). Int. Symposium on Biotechnology, Ankara, Turkey, Sept. 27-30, 2009.

S. Akhavantabasi, A. Sapmaz, E. M. Petty, A. E. Erson, Characterization of an Oncogene Candidate, USP32, on 17q23, European Human Genetics Conference ,Austria Center Vienna, May 23 - 26, 2009.

S. Akhavantabasi and A. E. Erson, "Investigating the subcellular localization of an oncogene candidate". HIBIT'09 Ankara, Turkey April 16-17, 2009.

2006

Akhavan S, Ekim B, Erson AE, Characterization of two ubiquitin specific proteases in cancer, International Symposium on Health Informatics and Bioinformatics, Antalya, Turkey, April 30- May 2, 2006.

Projects involved:

Scientific and Technical Research Council of Turkey (TUBITAK) 1001 Project: 108S381: Expression and Functional Analysis of Two microRNA Genes Mapping to Breast Cancer Genomic Instability Region (2009-2012).

Scientific and Technical Research Council of Turkey (TUBITAK) 1002 Project: 108S408: Cellular Localization of USP32. (2009- 2010).

Scientific and Technical Research Council of Turkey (TUBITAK) Career Project: 104S241: "Structural and functional characterization of USP32 and revealing its role in mammary tumorigenesis" (2005-2008).

Experiences:

Graduate student research assistant 2005-2012

Teaching assistant 2008-2011
Experimental Techniques in Molecular Biology course,
(Basic bioinformatics on gene identification section).

Awards:

Travel grant from European Molecular Biology Organization (EMBO) for participating in "MicroRNA-profiling: From in-situ hybridization to next-generation sequencing" practical course (May 21-27, 2011).

Travel grant from European Association of Cancer Research (EACR) for annual meeting poster presentation (2009).

International Courses Participated:

European Molecular Biology Organization (EMBO "MicroRNA-profiling: From in-situ hybridization to next-generation sequencing" practical course (May 21-27, 2011), based on the following techniques: quantitative PCR for microRNAs, microRNA microarray and in situ Hybridization for microRNAs.

Memberships:

The European Association of Cancer Research (EACR).